2013

EFFECTS OF ACUTE STRETCH ON CARDIAC ELECTRICAL PROPERTIES IN SWINE

Anuj Agarwal
University of Kentucky, bindaasanuj@gmail.com

Recommended Citation

EFFECTS OF ACUTE STRETCH ON CARDIAC ELECTRICAL PROPERTIES IN
SWINE

DISSERTATION

A dissertation submitted in partial fulfillment of the requirements for the degree of
Doctor of Philosophy in the College of Engineering at the University of Kentucky

By
Anuj Agarwal
Lexington, Kentucky

Director: Dr. Abhijit Patwardhan, Professor of Biomedical Engineering
Lexington, Kentucky
2013

ABSTRACT OF DISSERTATION

EFFECTS OF ACUTE STRETCH ON CARDIAC ELECTRICAL PROPERTIES IN SWINE

Stretch is known to result in an electrically less stable ventricular substrate, yet the reported effects of stretch on measured electrophysiological parameters have been inconsistent and even contradictory. The goal of this study was to evaluate the effects of acute mechanical stretch on cardiac electrical features thought to be key in generation of arrhythmia, namely restitution of action potential duration (APD), electrical memory, and onset of alternans.

Microelectrodes were used to record intracellular potentials pre, during, and post-stretch from isolated right ventricular tissues from swine. In separate experiments, the effects of two levels of stretch were quantified. Pacing protocols employing explicit diastolic interval (DI) control and cycle length (CL) control were used to obtain measures of restitution of APD, memory, and alternans of APD. Stretching the tissue had varying effects on APD, restitution and memory. Stretch increased APD, restitution slopes and memory by as much as 24, 30 and 53 % in some cases, while it decreased these by up to 18, 37 and 81 % in others. During stretch, alternans of APD were observed in some cases, which occurred at slower rates of activation than before stretch. Histology of tissue samples showed localized changes in orientation of cells relative to the direction of stretch.

Our results show that among individual trials, stretch altered the measured electrophysiological properties, sometimes markedly. However, when pooled together, these changes cancelled each other and the averages showed no statistically significant difference after stretch. A potential mechanism that explains this divergent and inconsistent response to stretch is the presence of local, micron level, variation in orientation of myocytes. Upon stretch, these divergent effects likely increase dispersion of repolarization diffusely and might thus be the reason behind the consistently observed increase in arrhythmic substrate after stretch.

Anuj Agarwal

July 25, 2013

EFFECTS OF ACUTE STRETCH ON CARDIAC ELECTRICAL PROPERTIES IN SWINE

By

Anuj Agarwal

Dr. Abhijit Patwardhan
Director of Dissertation

Dr. Abhijit Patwardhan
Director of Graduate Studies

July 25, 2013
Date

DEDICATION

I dedicate this dissertation to my parents, especially to my mother, who at most times had more faith in my abilities than me, and who never let me give up on this sometimes distant dream of getting a doctorate. I could not have achieved this without my parents' endless support and encouragement.

ACKNOWLEDGEMENTS

With utmost sincerity I would like to thank my advisor and mentor Dr. Abhijit Patwardhan for his continued guidance and patience over the course of this doctorate. His two success mantra's; namely "test everything beforehand" and "think simple" have been forever imbibed in my work ethic. He has been a mentor in the true sense and I have learned a lot from him over these years.

I would also like to acknowledge the members of my dissertation committee; Dr. Randall, Dr. Shin, and Dr. Knapp for their support and guidance. I would also like to thank Dr. Bummer for agreeing to serve as an external examiner.

TABLE OF CONTENTS

LIST OF FIGURES

LIST OF TABLES

Chapter I BACKGROUND

1.1 Role of electrical conduction in function of the heart

Heart as an organ functions to pump blood to the body and requires electrical stimulation to perform the mechanical function (of contraction). The electrical impulse in the heart originates from the sinoatrial (SA) node present in the right atria and then moves across to the left atria and then down to the atrioventricular (AV) node. After a brief delay it propagates through the bundle of His to the Purkinje fibers to stimulate the ventricles. The myocardium (cardiac muscle) contracts in response to electrical stimulation owing to a complex series of ion movements across the cell membrane of cardiac myocytes. An electrical impulse propagates through the ventricles very rapidly making the cells contract nearly simultaneously. This synchronous contraction optimizes the systolic pressure required to force blood through the circulation.

1.2 Morphology of intracellular potentials

When an electrical impulse arrives at a myocyte, the intracellular potential (ICP) of the cell rises and falls in a specific trajectory called the cardiac action potential. In general, the action potentials are divided into 5 distinct phases (0- 4) as shown in figure 1.1. When a cell is at rest (i.e. not stimulated), the membrane potential (V), that is the difference V_{in}-V_{out}, is negative and between -85 mV to -95 mV. This potential is termed as the resting membrane potential and forms the phase 4 of the cardiac action potential. At this potential the membrane is most permeable to K^+ ions. When a sufficient amount of electrical charge arrives at a cell, the voltage dependent fast sodium channels are activated and Na^+ (I_{Na}) rushes into the cell very quickly to make the membrane potential positive. This forms the phase 0 and is called the depolarization phase. This phase is the shortest in duration of all phases. Phase 1 occurs with the inactivation of the fast sodium channels. The membrane potential becomes slightly less positive due to the outward movement of K^+ and the inward movement of the Cl^-, carried by the I_{to}

currents. Phase 1 is also short and lasts only a few milliseconds. Following phase 1 the membrane potential plateaus around 0 mV for a few hundred milliseconds forming the phase 2. This phase is sustained by a balance between the inward movement of Ca^{2+} (I_{Ca}) through the L-type calcium channels and the outward movement of K^+ through the slow delayed rectifier potassium channels (I_{Ks}). The sodium-calcium exchanger current (I_{NaCa}) and the sodium potassium pump current (I_{NaK}) also play minor roles in maintaining this phase. The muscle contraction takes place during phase 2. In phase 3, the membrane potential starts to go down (become negative) because the L-type Ca^{2+} channels close, while the slow delayed rectifier K^+ channels are still open. Decreasing membrane potential also leads to opening of the rapid delayed rectifier K^+ channels (I_{Kr}) and the inwardly rectifying K^+ current (I_{K1}). This net outward positive current repolarizes the membrane back to the resting membrane potential. The delayed rectifier K^+ channels close upon reaching the resting membrane potential, while the inwardly rectifying K^+ channels remain open to maintain the phase 4 of the cardiac action potential.

- K^+ (out), Cl^- (in)
- $I_{to1,2}$ (transient outward)
- Early repolarization

- Ca^{2+} (in), K^+ (out)
- I_{Ca-L} (L-type calcium)
- I_{Ks} (slow delayed rectifier)
- I_{NaCa}, I_{NaK}
- Plateau phase

- Na^+ (in)
- I_{Na} (rapid inward)
- Depolarization phase

- K^+ (out)
- I_{Kr} (rapid delayed rectifier)
- I_{Ks} (slow delayed rectifier)
- I_{K1} (inward rectifier)
- Repolarization phase

- K^+
- I_{K1} (inward rectifier)
- Resting membrane potential
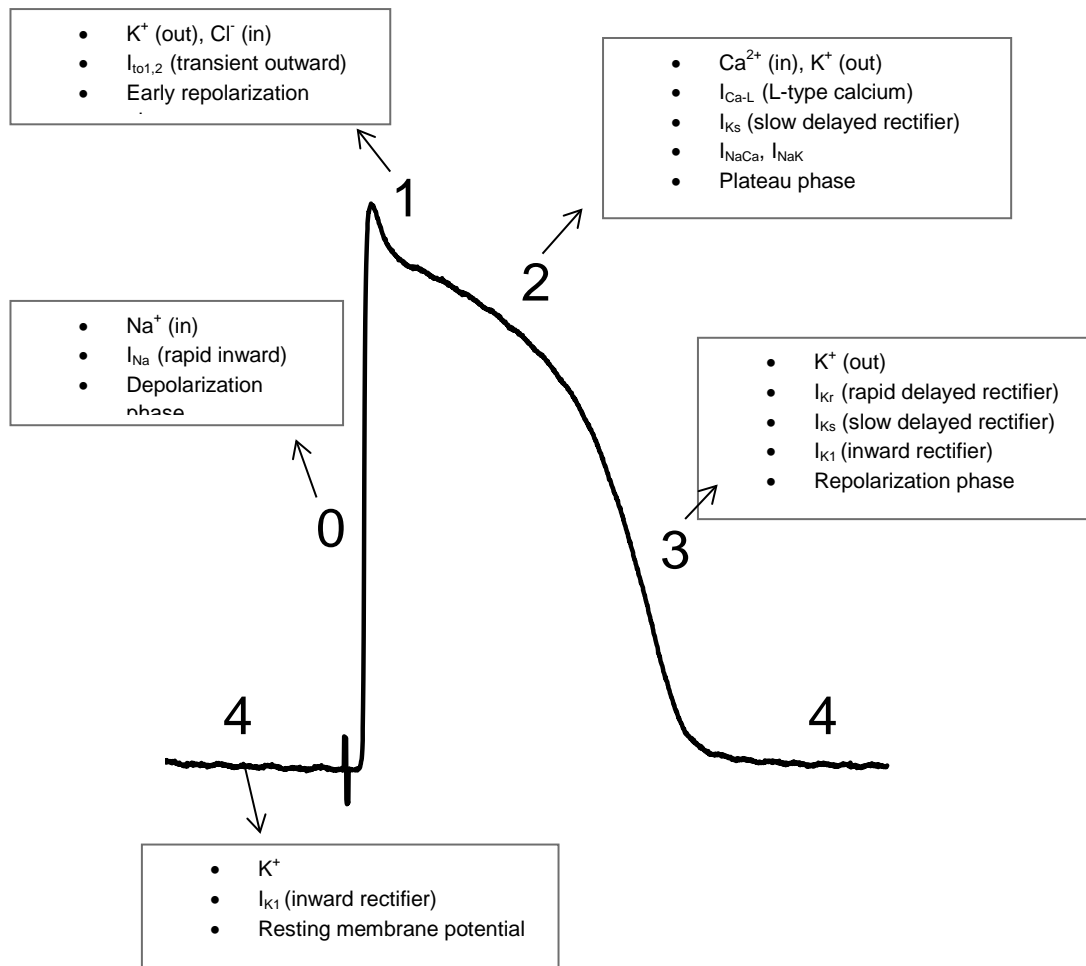
Figure 1.1 Morphology of cardiac action potential. Example of a cardiac action potential obtained from the swine right ventricle. The different phases and dominant currents in each phase are marked.

1.3 Electrical dysfunction of the heart

According to the NIH National Heart, Lung, and Blood Institute; "an arrhythmia is a problem with the rate or rhythm of the heartbeat." [3]. During an arrhythmia, the heart can beat too fast, too slow, or erratically because the electrical impulses come about too fast, too slow, or get disrupted locally along propagation. Arrhythmias occurring in the ventricles are very dangerous and mostly require immediate medical attention. Ventricular arrhythmias (VA) such as ventricular

3

tachycardia and ventricular fibrillation (VF) are the end cause of a majority of cardiac deaths. Degeneration of only a few electrical impulses, out of the approximately two billion impulses occurring during a normal lifespan, can trigger the process leading up to ventricular fibrillation. During VF the ventricular muscle contracts in an uncoordinated manner which makes the muscle quiver and it stops pumping blood to the body and to the heart. Death results if VF is not treated within minutes.

1.4 Electrical properties of the heart

Stability in the heart, apart from its electrical properties, depends on a lot of other factors. An inadequate coronary blood supply leads to ischemia, which can lead to damage or death of part of the heart muscle called myocardial infarction (MI) or heart attack. Heart attacks can lead to cardiac arrests which are caused by arrhythmias like VF. Other factors like hypertrophy (enlargement of the heart muscle), fibrosis, and heterogeneity also affect heart's stability. According to the Centers for Disease Control and Prevention, nearly 600,000 people die every year of heart disease in the United States [4]. Out of those 600,000 nearly 270,000 die because of out-of-hospital cardiac arrests [5]. Two important electrical properties which affect the stability in the heart are restitution of action potential duration and cardiac memory.

1.4.1 Restitution of action potential duration

Restitution of action potential duration (APD) is defined as the dependence of an APD on the preceding diastolic interval (DI). The word restitution means "the act of compensating for loss" [6]. Normal resting heart rates range from 60-90 beats a minute. Within this range the heart has sufficient time for both diastole (filling) and systole (contraction). The heart rate increases when the body needs to absorb oxygen and excrete carbon dioxide at a faster rate, such as during exercise or illness. At higher heart rates the APD (i.e. systole) restitutes by becoming smaller so that there is enough time for the heart to refill with blood

4

(diastole), preventing it from running empty and causing vasovagal syncope [7]. When the heart rate is restored to normal resting levels, the APD also increases back. Figure 1.2 shows an example of restitution of APD. When the interactivation interval, i.e. the cycle length (CL), is decreased the APD restitutes and becomes smaller to preserve the DIs.
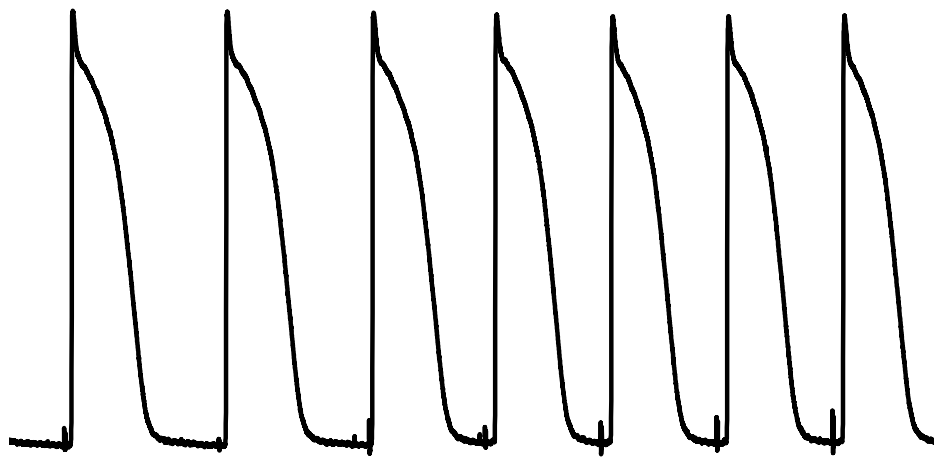
Figure 1.2 Example of restitution of APD. When the interactivation interval, i.e. the cycle length, is decreased the APD restitutes to become smaller to accommodate enough filling time (diastole).

1.4.2 Cardiac memory

In the context of this dissertation, cardiac electrical memory is defined as the dependence of an APD on duration of previous action potentials over a scale of several seconds. Figure 1.3 shows an example of memory. The APD values (B) were obtained in response to a pacing protocol (A) where the DIs were explicitly controlled to vary sinusoidally. In figure 1.3B, note that at a given value of DI (marked by the red star), the APD can have two values (marked by the blue stars) depending on whether the APDs preceding it were increasing or decreasing. This adaptability of APD, owing to memory, theoretically tends to buffer activation instability.
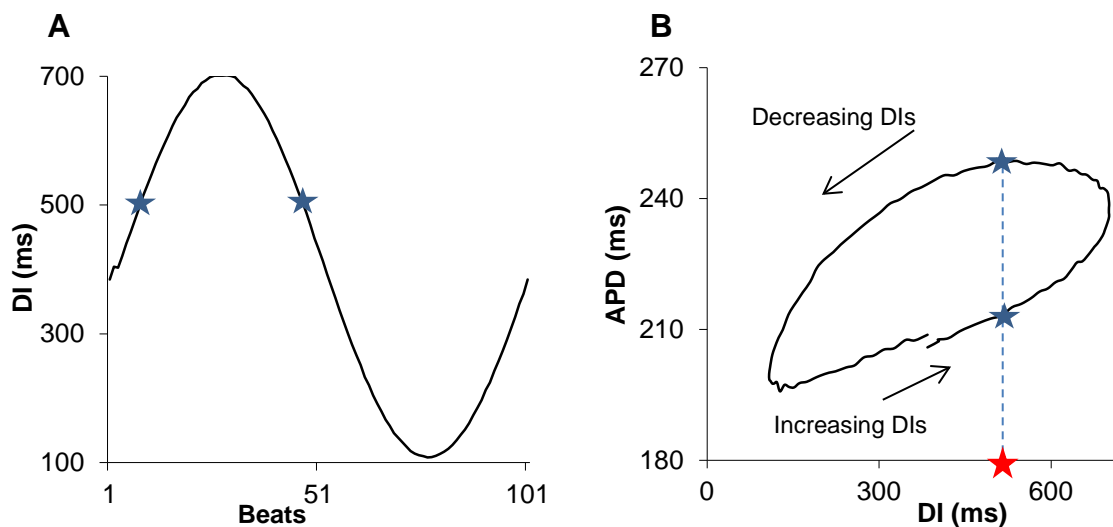
Figure 1.3 Example depicting cardiac memory. The APD values (B) are obtained in response to a sinusoidal DI pacing protocol (A). In panel B note that at a given value of DI (marked by the red star) the APD can have two values (blue stars) depending on whether the APDs preceding it were increasing or decreasing.

Electrical restitution is thought to play an important role in determining whether an electrical perturbation disintegrates into a reentrant activation [8]. The hypothesized link between restitution of APD and stability of electrical activation is the slope of the restitution function [9-16]. Slopes of greater than or equal to one can lead to alternans of APD and increase in their amplitude leads to localized block of electrical propagation. Block can cause reentry and further spiral wave breakup can lead to arrhythmia such as ventricular fibrillation (VF). On the other hand, restitution slopes of less than one decrease the disturbances in APD and returns it to a stable activation. It is also hypothesized that memory impacts stability [17-19] and is required, in addition to restitution, to explain the fate of electrical disturbances. Figure 8 of Wu et al [19] and figure 7 of Guzman et al [20] theoretically demonstrate that memory tends to buffer activation instability. Chialvo et al [21] were the first to demonstrate that memory can gradually decrease chaotic dynamics by flattening restitution.

1.5 Tools for investigating the dynamics of cardiac electrical properties

Ventricular arrhythmias (VA) like VF are often fatal and most people don't survive past the first episode [22, 23]. The only way of preventing an episode of lethal arrhythmia like VF is to develop robust predictors of the heart's electrical substrate. The most contemporary non-invasive clinical measure to assess patients at risk of lethal electrical instability (or VA) is microvolt T wave alternans (MTWA) testing [24]. T wave alternans is a periodic beat-to-beat alternation in the T wave shape, amplitude, or timing in an electrocardiogram (ECG). MTWA can be measured during low-level exercise stress test, a pharmacological stress test, or via pacing. For patients with reduced systolic function (i.e. left ventricular ejection fraction), MTWA testing has been suggested to be used to identify patients who are at an increased risk of sudden cardiac death (SCD) and need an implantable cardiac defibrillator (ICD) [25]. The main problem associated with MTWA testing is its low specificity. Gehi et al [24] preformed a meta-analysis of the predictive value of MTWA testing in a wide variety of population and showed

that the positive predictive value (PPV) expressed in percentage was 19.3 while the negative predictive value (NPV) was 97.2. This means that for a patient who tests negative in MTWA testing has only a 3% risk of having an arrhythmic event. On the other hand, the presence of MTWA predicts an arrhythmic event in only 19% of subjects. Considering the cost of surgically implanting an ICD and the risk and stress associated with false shocks [26-28], MTWA testing is not a very specific tool to assess risk of arrhythmias. There still remains a need to develop robust predictors of electrical instability which could be used in addition to MTWA testing for risk stratification.

At a tissue level, T wave alternans are manifested as repolarization alternans also known as APD alternans. It has been recently shown that mechanism of alternans has two components: DI dependent and DI independent [29]. The DI dependent component can be investigated using pacing protocols employing CL control and has been well established over the past few decades. The more recently discovered DI independent component of restitution is investigated using novel pacing protocols employing DI control and is still under exploration. Techniques using CL control and DI control to investigate electrical stability are elaborated below.

1.5.1 Cycle length control

Pacing protocols employing cycle length control are mostly used to quantify the APD restitution function. The two most widely used pacing schemes are the standard protocol and the dynamic protocol. In the standard protocol the tissue is paced for several tens of activations at a constant cycle length (S_1) followed by a stimulus (S_2) delivered at progressively shorter or longer intervals. The APD resulting from S_2 is plotted against the preceding DI. Several such DI-APD pairs are obtained by repeating the process to form the standard restitution curve. In the dynamic restitution protocol the tissue is paced at S_1 for several tens of activations, then, instead of using a perturbation S_2, another sequence of S_1 stimuli are repeated at a progressively shortened S_1-S_1 interval. The value of the

8

first APD at the start of a new S_1 train is plotted against the last DI value of the preceding S_1-S_1 interval train. The standard restitution curve is a measure of the APD response to an abrupt change in the cycle length, whereas the dynamic restitution curve is a measure of the steady-state response. To incorporate the memory-dependent effects in restitution, a new protocol called the "perturbed downsweep protocol" (PDP) was developed [30]. The PDP starts with a long basic cycle length (BCL), typically 1000 ms and then the BCL is decreased (downswept) in six distinct steps. At each step the APD and DI are recorded. Then, the BCL is decreased (by 50-100 ms), and the six steps are repeated until a 2:1 response occurs. The PDP allows investigators to obtain restitution portraits which simultaneously incorporate the steady-state response, the transient response and the long-term accommodation of the response.

1.5.2 Diastolic interval control

The link between restitution and stability of activation is thought to occur as follows: an operating point (see, for example, figure 8 of Wu et al [19]) is produced by the intersection of the restitution relationship and a line which describes constant cycle length. Depending upon the slope of the restitution relationship near operating point, a perturbation (e.g. abrupt shortening) in DI, can lead to stable oscillation between APD and DI for successive beats if the slope is equal to 1, could lead to an activation block if slope >1 or a return to a stable point if slope <1. Thus the prediction of APD for beats that occur after a perturbation is based on DIs that change sequentially in time. In protocols using CL control the functional relationship between DI and APD, however, is not quantified during sequential changes in DI. In the standard protocol, several constant cycle length beats separate two perturbations, where the values of DIs are recorded as data points for the restitution plot. Similarly in the dynamic protocol, the DI for beat n+1 results from the last beat of a sequence of several tens of beats at constant cycle lengths. Likewise, in the PDP, successive values of the restitution relationship are not obtained sequentially in time. To get a better

prediction of changes in APD following changes in DI occurring over successive beats, a protocol was developed that explicitly controlled DIs, permitting the exploration of restitution characteristics when DI change sequentially in time [19, 29, 31]. For explicit control of DI, the location of APD repolarization to 90% (APD_{90}) is identified in real time and a pacing stimulus is given after waiting for a predefined interval DI.

Several protocols employing DI control have been developed [1, 19, 29, 31] and are listed below with their respective utilities in predicting electrical stability.

1. Sinusoidal DI protocol: in this protocol the DI change sequentially and in an oscillatory pattern as shown in figure 1.3A. The restitution relationship shows two trajectories, i.e. hysteresis, as shown in figure 1.3B. For a given DI, the resulting value of APD differs, based on prior activation history. This behavior accounts for the memory-dependent restitution effects on APD and provides the only quantifiable measure of memory reported thus far. Sinusoidal DI pacing protocols are very useful in studying the effects of drug induced ion-channel modifications [32] on electrical stability in the heart. Figure 1.4, for example, shows the effect of blocking the rapid component of the delayed rectifier current (I_{Kr}) in swine right ventricular tissue using the drug E-4031 [2]. Most new drugs are tested by the Food and Drug Administration to see if they block I_{Kr} [33], which can cause drug induced *acquired long QT syndrome* and lead to SCD [34]. Figure 1.4A shows that blocking I_{Kr} increased the APDs significantly. Figure 1.4B and C show the average restitution curves obtained pre and post block of I_{Kr} for two different sinusoidal DI protocols; with central DI values equal to 400 ms (n=5, B) and 150 ms (n=3, C). The restitution curves in B and C show hysteresis. Further details about this study are given in appendix A. The parameters of hysteresis, normalized with the changes in baseline APD, such as loop thickness, area, and tilt help in estimating the effect of the ionic modification on electrical stability [2].
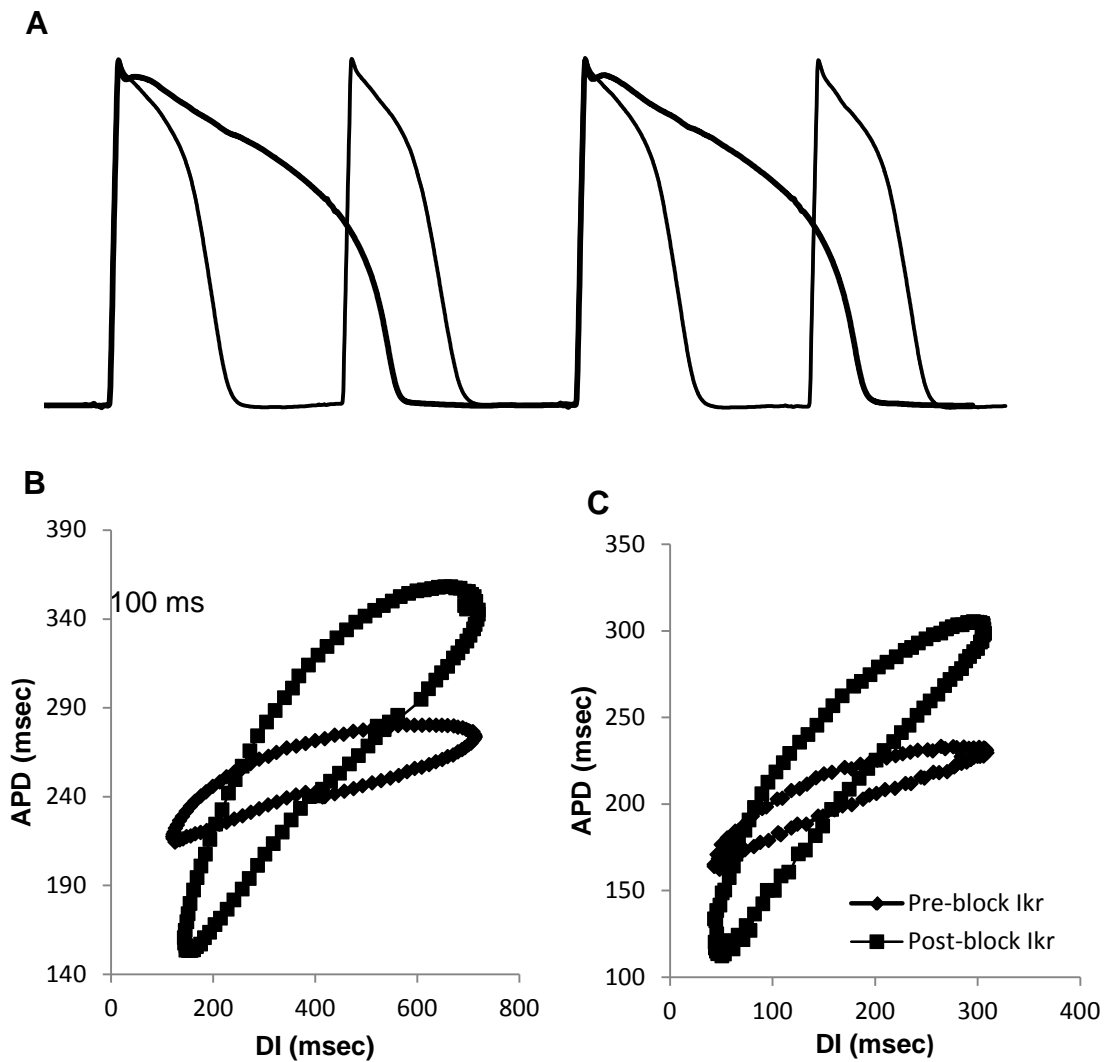
Figure 1.4 Effects of blocking the rapid component of the delayed rectifier current (I_{Kr}) in swine [2]. E-4031 was used to block I_{Kr}. (A) Blocking I_{Kr} increased the APDs significantly. (B, C) Average restitution curves obtained pre and post-block of I_{Kr} for two different sinusoidal DI protocols.

2. Constant DI protocol: in this protocol the DIs are held constant at short values for several beats. At short constant DI, the APDs show alternans, thus revealing the DI independent component [29]. Spatially, if the DIs at one end of the tissue are held constant and the progression of alternans is captured at a distal end, the rate of change in alternans amplitude as a function of distance provides a measure of the contribution of DI dependent restitution to alternans [1]. Figure 1.5 shows the intracellular potential traces recorded from the two ends of a right ventricular swine tissue. The DIs were held constant at the pacing site and thus the alternans were DI independent. As the activation reaches the other end, the alternans amplitude grows larger because of the contribution from the DI dependent restitution effects. Further details about this study are given in appendix B.
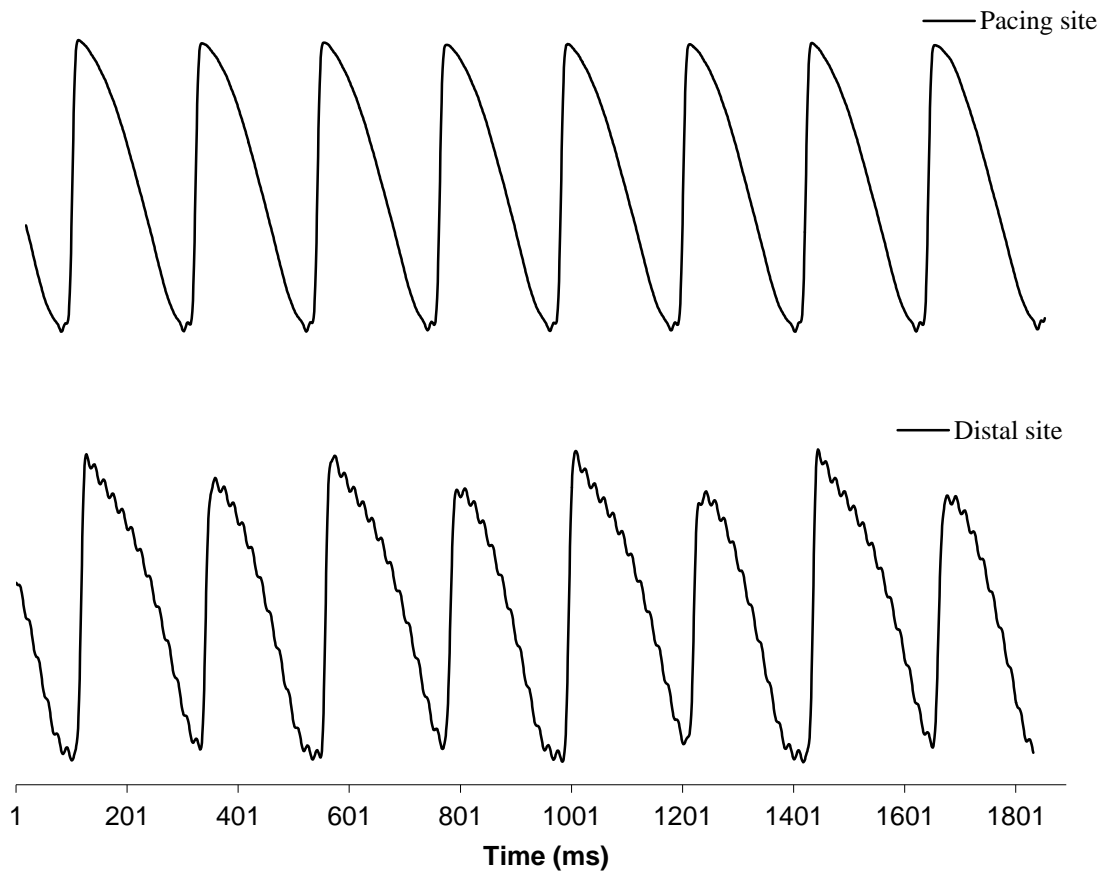
Figure 1.5 Intracellular potentials recorded from the two ends of a strand of right ventricular tissue [1]. The DIs were made nearly invariant for successive beats at the pacing site. Alternans of larger amplitude are clearly seen at the distal site because of the contribution from the DI dependent restitution effects.

1.5.3 Phase relation between early and late phases of action potentials

Apart from DI control and CL control, another tool useful for exploring the fate of an electrical activation is to study the phase relation between depolarization and repolarization alternans of ventricular action potentials. Alternans of APD occur in two major forms; concordant and discordant. Figure 1.6A, B show an example of spatially concordant alternans, where all cells in a given area alternate in the same phase. Figure 1.6C, D show an example of discordant alternans, where cells of neighboring regions alternate in opposite phases. Transition of

concordant alternans to discordant alternans increases the dispersion of repolarization and makes the electrical substrate more conducive to arrhythmias like VF [10]. APD alternans, i.e. repolarization alternans, are frequently accompanied by alternans of depolarization, and mostly occur in phase with each other. However, the in phase relation sometimes switches to out of phase spontaneously [2]. As presented in figure 1.7, results from simulation show that the switch from in phase to out of phase (1.7D-1.7F) progressively removed the discordant alternans and prevented the further transition from concordant to discordant alternans. This prevention of a transition to discord may have a stabilizing effect on conduction of electrical impulses [2]. Further details about this study are given in appendix C.
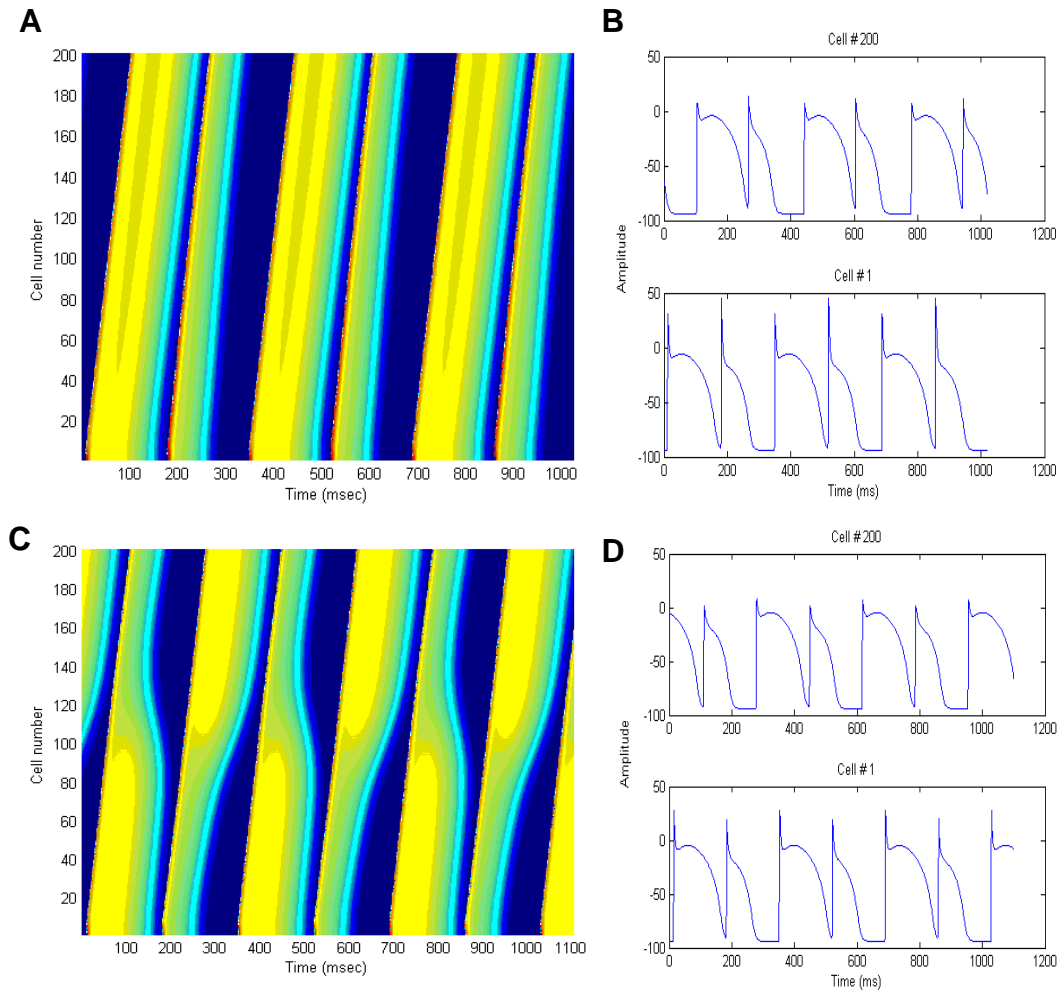
Figure 1.6 Examples of spatially concordant (A, B) and discordant (C, D) alternans of APD. The pseudo colored images and TMPs were obtained from simulation. Areas in blue are completely repolarized. Colors orange to light blue in panels A and C represent a gradient from depolarization until repolarization. Alternans are considered concordant if all cells in an area alternate in the same phase (B). Discordant alternans occur when cells of neighboring regions alternate in opposite phases (D).
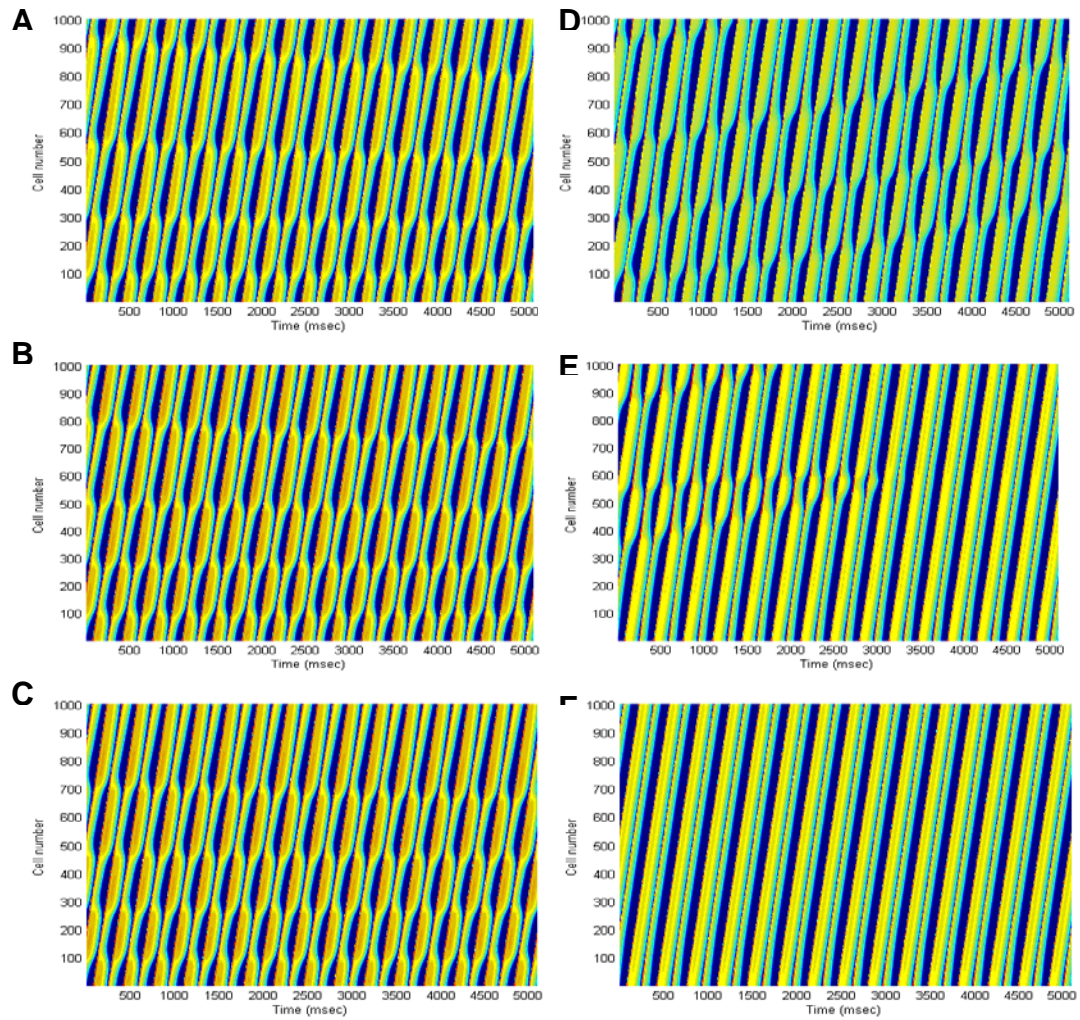
Figure 1.7 Effects of in phase and out of phase relationship on electrical stability. Simulated time space plots showing effects of in phase and out of phase relationship between alternans of repolarization and depolarization on electrical stability. (A-C) Ninety beats of in phase alternans, shown in three sections (30 beats for each panel), where concordant alternans transitioned into discordant alternans several times. (D-F) Ninety beats of out of phase alternans. The switch to out of phase relationship progressively removes the discordant alternans and then maintains consistent in phase alternans in all regions of the simulated tissue.

Chapter II   INTRODUCTION

After the onset of VF, the arterial and venous pressures begin to equilibrate [35]. Complete equilibration takes about 4-5 minutes [36] and is associated with shift of blood from the high-pressure arterial system to the lower-pressure venous system. This shift in blood causes a marked increase in the RV volume over the first few minutes of untreated VF [36, 37]. Berg et al [37] showed that the mean RV volume increased by 29% within one minute of untreated VF in swine. Over-distension of the RV reduces the success of a defibrillation shock and may result in asystole or pulseless electrical activity in response to a defibrillation shock. Clinical studies show that patients with increased ventricular volume [38] and end-diastolic diameter [39] have higher defibrillation threshold (DFT). Acute ventricular dilatation and volume overload also increases the DFT [40, 41]. Cardiac compression (or heart massage), which results in reduced cardiac preload and size, significantly decreases the DFT [42, 43] and increases the chances of return to normal circulation post defibrillation [36]. Ventricular stretch is thought to increase the DFT by changing electrical properties of the heart [44]. This transduction of mechanical stimuli into electrical signals is known as mechanoelectric feedback (MEF). Commotio cordis is an excellent example of MEF; whereby a blow directly above the area of the heart, given at a critical time during the cycle of a heartbeat (i.e. during T wave), disrupts the heart rhythm and causes cardiac arrest. Mechanical perturbation activates stretch activated channels (SACs), which leads to changes in electrical parameters such as action potential duration (APD), conduction velocity, and resting membrane potential [45, 46]. Changes in cardiac electrical properties (via stretch) in turn affect the electrical stability in the heart.

Myocardial stretch, via alterations in cellular electrophysiological properties, is pro-arrhythmic [47]; a concept that has been known for over three decades now. However, when the ventricular electrical properties have been investigated under mechanical stretch the results have been inconsistent and even contradictory in some cases. For example, Zabel et al [48] showed that sustained ventricular load

17

decreased APD in a rabbit model, whereas Sung et al [49], using the same animal model and a similar experimental loading protocol, reported an increase in APD during load. Stretch also produces varying results on conduction velocity. Conduction velocities have been shown to have increased [50], decreased [49] and not change at all [51] after stretch. Investigation of effects of stretch on electrical properties at a tissue level, have been conducted several decades ago, however, these studies concluded that acute stretch does not affect the electrophysiological properties [50, 52]. An inconsistent effect of stretch on electrophysiology of myocytes seems to be puzzling, considering the clear demonstration of its destabilizing effect on the heart's electrical stability. We hypothesized that these variant observations in electrophysiology, in response to stretch, are due to the presence of a local, micron level, heterogeneity in the tissue architecture. Note that this micron level heterogeneity, that is referred to here, is different than the more widely known heterogeneity in electrophysiology which is in terms of different regions of the heart such as LV, RV, epi, endo, mid myocardium, basal, and apical regions or even in terms of trans-mural fiber orientation [53-55].

Effects of stretch on electrical properties have been previously investigated at different scales; that is in intact ventricles, isolated myocytes, and at a tissue level. Although the isolated myocyte studies [56-58] are insightful, the lack of connectivity between myocytes eliminates the effects of source and sink related electrical factors. For studies done using the intact ventricles, the measurement either relies on electrical mapping for in-vivo [59-61] preparations or electrical or optical mapping for in-vitro preparations [48, 49, 62]. Electrical mapping can provide fairly reasonable estimates of conduction velocities via activation times, but cannot faithfully measure repolarization times. Optical mapping permits measurement of action potential durations; however, the optical signal is an integrated measure, proportional to the averaged activity from regions underlying a transmural depth equal to several layers of myocytes. Thus in an electrically coupled native environment, the techniques discussed above are not suitable to determine effects of acute stretch on myocytes. Previous studies done using

preparations containing an electrically coupled environment did not investigate the effects of stretch on dynamical properties such as restitution, and memory. The electrophysiological properties measured by them however showed discrepant results as discussed before.

These results, taken together, indicate that the discrepant effects of acute stretch, which is clearly arrhythmogenic, on basic electrophysiology of myocytes needs further clarification. This need was the motivation for our study to reexamine the effects of acute stretch in tissues. We recorded intracellular potentials before, during, and after stretch in ventricular tissues from pigs and determined the effects of stretch on restitution of APD, memory, and onset and amplitude of alternans; electrophysiological properties that are considered critical in cardiac electrical stability. Our results showed that stretch produced considerable difference in electrical properties when compared within individual recordings. However, when averaged, our results showed no statistical significance in these properties after stretch, as has been reported before. We think that looking at the average results, leads one to a wrong interpretation that stretch does not affect these properties. It is likely that stretch does affect electrical properties, although differentially, as suggested by our results and those from previous comparable studies. A potential mechanism, as stated above, that explains these divergent effects of acute stretch on electrophysiology is local, micron level, tissue heterogeneity in orientation of myocytes relative to the direction of stretch. It is also likely that this same mechanism tends to make the myocardium inherently electrically vulnerable during the T wave.

Chapter III   METHODS

3.1 Sample preparation

All animal studies were conducted after approval from and in accordance with guidelines set by the Institutional Animal Care and Use Committee (IACUC) at the University of Kentucky. Farm pigs were sedated using a combination of Telazol (4-8 mg/kg), Ketamine (2-4 mg/kg), and Xylazine (2-4 mg/kg). Anesthesia was induced by sodium pentobarbital (40-60 mg/kg, IV), following which the hearts were rapidly excised and placed in a chilled Tyrode's solution. A piece of tissue, approximately 10 mm x 20 mm was cut from the right ventricular (RV) free wall along the gross endocardial fiber direction between the apex and the base. Sutures were tied at both ends of the tissue and a waterproof permanent ink marker (MarketLab Inc.) was used to put landmarks (dots) on the endocardial side of the tissue for local strain measurement

3.2 Setup

The tissue was placed horizontally in a plastic chamber with the endocardial side up and was superfused with Tyrode's solution which was continuously gassed with 95% O_2 and 5% CO_2. The temperature of the solution was maintained at 36 $\pm 1^\circ$ C with a pH of 7.3 ± 0.05. The composition of the solution was (mmol/L): 0.5 $MgCl_2$, 0.9 NaH_2PO_4, 137.0 NaCl, 4.0 KCl, 5.5 glucose, and 2.0 $CaCl_2$. To this mixture $NaHCO_3$ was added until the desired pH level was achieved. The tissue was clamped at one end by tying one of the sutures to a plastic rod affixed in the chamber as shown in figure 3.1. The suture at the other end was looped over a steel rod and tied to a fixed weight resting on a platform. Stretch was applied by lowering the platform on which the weight was resting to let the weight hang freely.
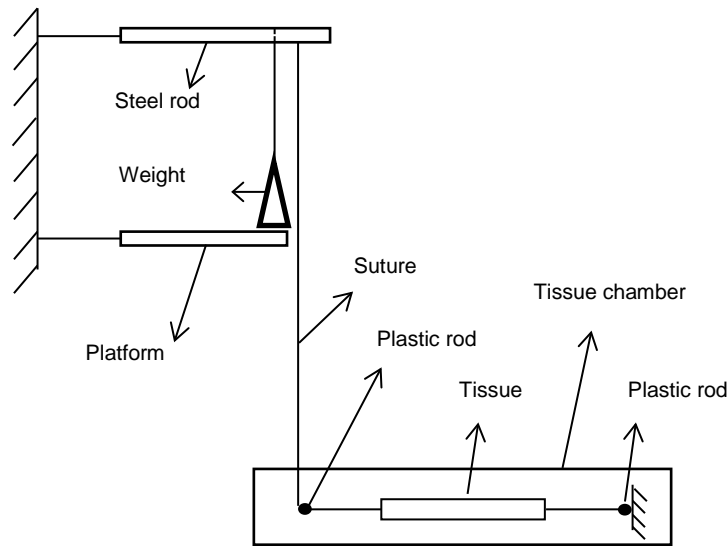
Figure 3.1 Schematic of experimental setup showing application of stretch.

A bi-polar platinum-iridium electrode was used to deliver biphasic pacing stimuli of 3 ms pulse width. The stimulus intensity was 3 - 4 times the diastolic threshold for stimulus related activation of an action potential. The tissue was acclimated for about an hour, during this time, it was paced at a constant CL of 500 ms. Glass micropipettes filled with 3 M KCl were used to record ICP from the endocardial side. For protocols that required DI control, the ICPs were used for real-time control of DI using a custom code written in LabVIEW. The details of control of DI have been provided elsewhere [20], briefly, the program determined the end of an action potential (at a given repolarization level) in real time and the next pacing stimuli were delivered after predefined intervals, which were the desired DIs. Simultaneously, ICPs were digitized and stored using a commercial data acquisition system (WinDaq) at a rate of 50,000 samples/sec. These simultaneously recorded data were used in further analysis, which was conducted offline.

3.3 Pacing protocols

The following pacing protocols were used to record data pre, during, and post-stretch: 1) Two protocols in which the DIs changed in a sinusoidal fashion. In these protocols, the tissue was paced for 220 beats, with first 20 beats at a constant level of DI equal to 400 (150) ms, followed by an oscillatory change in DI for 2 periods of 100 beats each. The mean value of oscillatory DI was equal to 400 (150) ms and the amplitude of oscillation was 300 (140) ms from the mean. Figure 3.2 shows an example of a sinusoidal DI protocol and the resultant hysteresis in restitution of APD. 2) Dynamic restitution protocol [63] with 50 beats at each CL, starting at CL=800 ms and decrementing it in steps of 100 until 400 ms, then in steps of 50 until 250 ms, and in steps of 20 until block of activation occurred. 3) Standard restitution protocol [63] (S_1-S_2) with one recurrent beat at S_1-S_2 interval occurring between trains of 20 beats of S_1 at a CL of 500 ms. The S_1-S_2 interval started at 800 ms and was decreased in steps of 100 ms until 400 ms, then in steps of 50 until 250 ms, and in steps of 20 until the S_2 failed to produce an AP. In addition to the above protocols, in some experiments, the tissue was paced at short constant CLs or constant DIs to explore occurrence of alternans of APD.
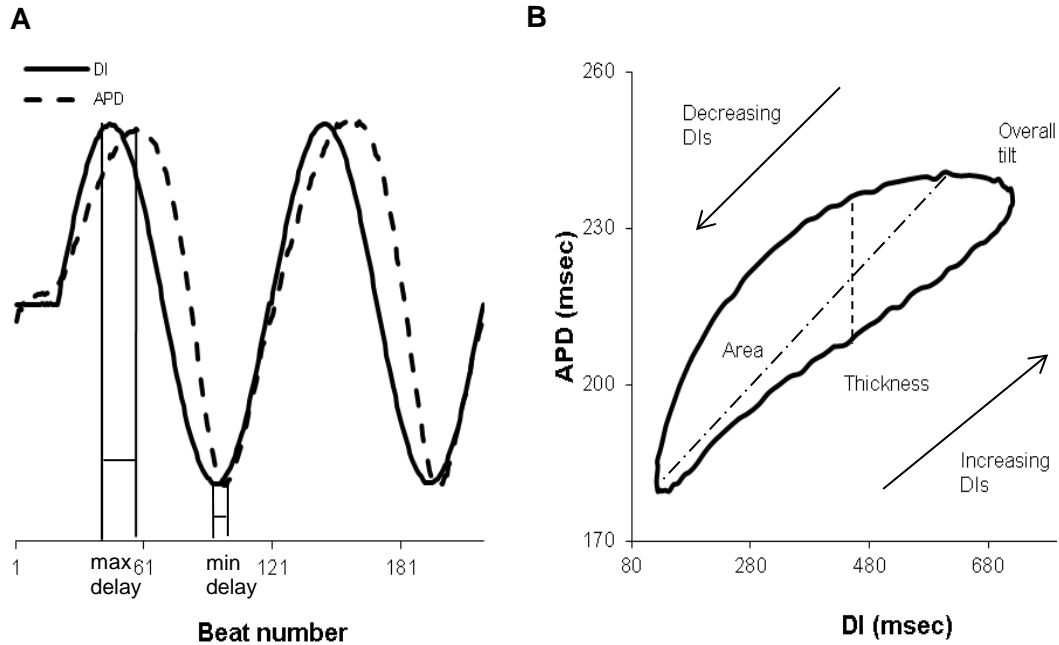
Figure 3.2 Sinusoidal DI pacing protocol and resultant hysteresis in restitution of APD. (A) Example of a sinusoidal oscillating DI protocol and the resultant APDs. The APDs have been scaled and shifted vertically to better visualize the delays between DI and APD peaks. (B) Hysteresis in restitution of APD in response to DI values in panel A. Memory was quantified by using parameters of loop thickness, overall tilt, maximum delay, minimum delay, and area.

3.4 Data collection and post-processing

Two levels of stretch, referred to as st-level I and st-level II, were applied by using two weights in separate experiments, i.e. in separate tissues that were cut adjacent to each other from the same animals. A weight of 200 grams (st-level I) produced local strains ranging between 15%-40%, 400 grams (st-level II) produced local strains ranging between 28%-49%. Digital images of the tissue strip, obtained pre, during and post stretch, were used to quantify the induced local strain and residual strain.

23

3.4.1 Local strain measurement

A custom code developed in Matlab was used for tracking of landmarks (dots marked on tissue) to approximate the local strain induced during stretch and the residual strain post release of stretch. The image obtained before stretching the tissue was used as the reference image. All image processing was done using Matlab's built-in functions. Briefly, a rectangular area enclosing the two dots surrounding the region of impalement was manually selected, the contrast of the image was enhanced and a threshold applied to highlight the boundaries of the two dots. These boundaries were smoothened and their centroids were determined. The distance V_1 between the two centroids along the direction of the stretch was computed. The procedure was repeated for the same two dots in the image taken during stretch and post-stretch, to obtain the differences V_2 and V_3 respectively. Local strain (during stretch) and the residual strain (post-stretch) were computed as the differences between V_2 and V_1, and V_3 and V_2.

3.4.2 Histology

To determine if orientation of cells relative to the direction of stretch could change, we conducted histology on two tissue samples, one each from st-level I and st-level II. A small piece of tissue from approximately the area where the microelectrode impaled the tissue was fixed, embedded and sliced into 5 µm thick sections, parallel to the endocardial surface. These sections were stained with hematoxylin and eosin and imaged using a camera attached to a microscope.

3.4.3 Intracellular Potential Analysis

The recorded ICPs were lowpass filtered (cutoff 5000 Hz) and analyzed offline to determine APDs and DIs using custom code developed in Matlab. Start of each AP was marked as the instant at which the slope of ICP became positive. End of an AP was marked when the ICP repolarized to 90%. The difference, in time, between the end and start of a given AP was quantified as the APD and the time difference between the start of an AP and the end of previous AP was quantified as the DI. Markings for every action potential were visually inspected to ensure correct quantification of APD and DI.

Restitution of APD during oscillatory changes in DI displayed hysteresis. The restitution curves were used to calculate the following parameters of hysteresis: thickness of the loop, overall tilt, maximum delay, minimum delay, and area under loop. As defined previously [20], loop thickness was measured as the difference between APDs at mean values of oscillatory DI during increasing and decreasing DI trajectories. Tilt was measured as the ratio of differences of maximum and minimum APD and their corresponding DI values. Maximum (minimum) delay was measured as the delay, in beats, between the maximum (minimum) values of APD and DI during the sinusoidal change. Area under loop was quantified as the area under the hysteresis curve. We used the second cycle of the DI protocol to calculate the hysteresis parameters to minimize the effects of APD adaptation, caused due to a switch to constant DI pacing from cycle length pacing. In some cases the control of DI in the second cycle was not as effective as the first one, in these cases, the data from the first cycle was used to calculate hysteresis parameters. A Student's paired t-test was used to test differences between the control and the stretched groups. Differences were considered significant at $p \leq 0.05$.

Pacing at short CLs can cause the duration of APs to oscillate on a beat-by-beat basis, i.e. cause alternans of APD. Absolute differences between successive

APDs of ≥ 4 ms, occurring over at least 5 consecutive beats was considered as alternans of APD. The 4 ms threshold for determining alternans is the same as that used by Pruvot et al [64]. The slopes of the dynamic and the standard restitution curves were computed as a ratio of the difference between successive APDs divided by the difference between successive preceding DIs.

Figure 4.1 shows images of a strip of tissue pre-stretch (A) and during st-level II stretch (B). The tissue strip shows marked landmarks; displacement of these upon stretch was used to measure the local strain near the site of impalement. Figure 4.1C shows a pseudo-colored map depicting the local strain distribution (in %) in the strip during stretch.
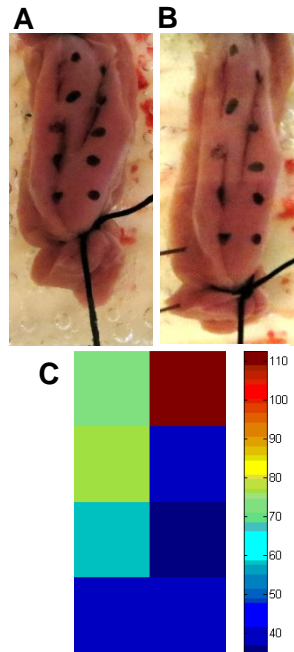
Figure 4.1 Application of stretch to a strip of tissue and the resultant strain distributions. Example showing the images of a strip of tissue pre-stretch (A) and during st-level II (B). (C) Pseudo-colored image depicting local strain (in %) distributions after stretch.

In all experiments, the stretch phase lasted for at least an hour and this sustained stretch left a permanent residual strain in the tissue. Upon stretch it became difficult to maintain a stable impalement for long periods in some samples; therefore all protocols could not be completed in all tissue samples.

For both groups, stretching the tissue produced divergent changes in baseline APD. Figure 4.2 shows examples of ICPs pre and during-stretch (st-level I) recorded during baseline CL of 500 ms. Stretching increased the APD in some cases (A) while decreased it in others (B).
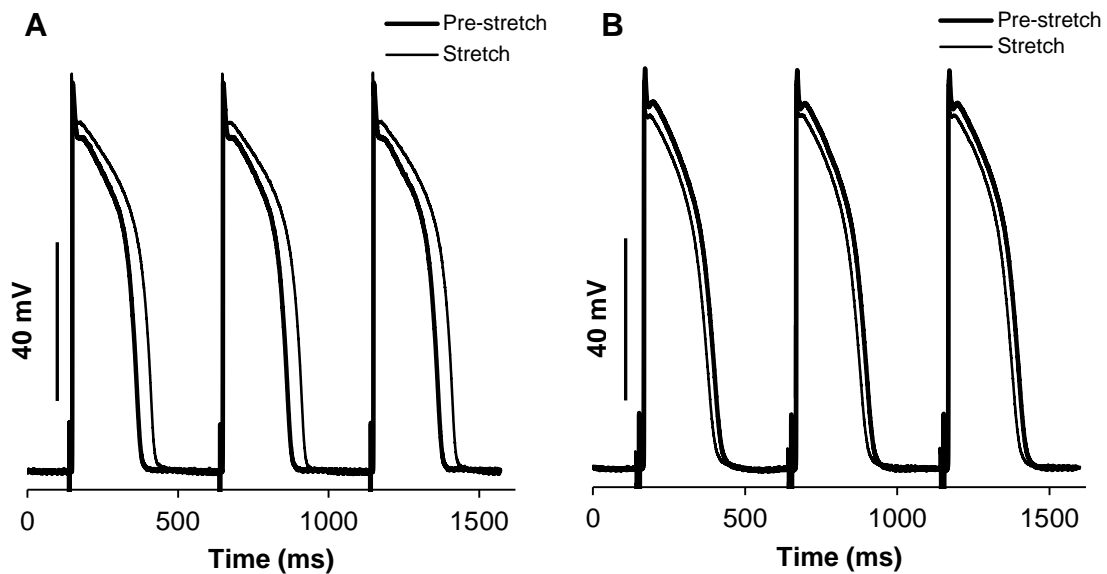
Figure 4.2 Example of varying effects of stretch on APD. Shown are ICPs recorded at baseline CL of 500 ms pre-stretch and during stretch (st-level I), during two separate experiments. Stretching increased the APD (A) in some cases while it decreased it (B) in others.

Figure 4.3 shows the values of baseline APD (± standard deviation) pre-stretch and during stretch for both groups. Figure 4.3A shows the changes in APD (n=5) in the st-level I group. After stretch, APD increased in 3 cases and decreased in 2. Figure 4.3B shows the changes in APD (n=5) in the st-level II group. After stretch, APD increased in 2 and decreased in 3 cases.
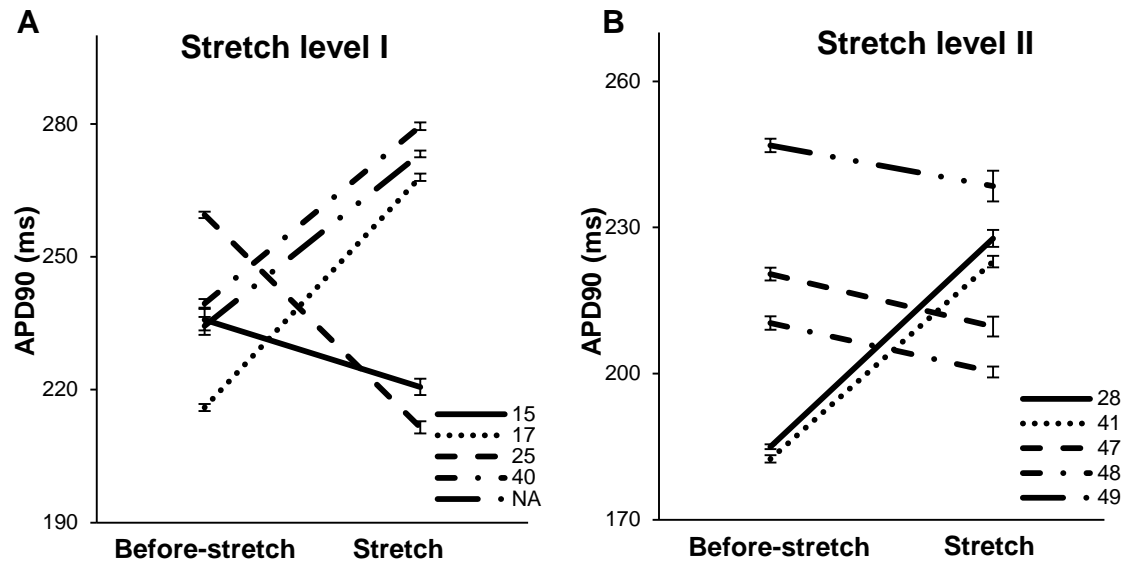
Figure 4.3 Values of baseline APDs, pre and during-stretch, for the st-level I and st-level II groups. Shown are the APD values (± standard deviation) obtained at a CL of 500 ms for the st-level I group (A, n=5) and the st-level II group (B, n=5). The numbers in the legends represent the local strain (in %) experienced near the site of impalement. After stretch, APD increased in 3 and decreased in 2 cases in the st-level I (A) group and increased in 2 and decreased in 3 in the st-level II (B) group. Due to technical difficulties, the strain information from one experiment was not available (NA) in the st-level I group.

Table 4.1 lists the percentage change in baseline APD and the local (or remnant) strain during and post-stretch of tissue.

Table 4.1 Percentage change in baseline APD90 and the local strain produced (or remnant) during and post-stretch of tissue.

Group	n	Pre-stretch - Stretch		Stretch - Post-stretch	
		APD_{90} change (%)	Strain (%)	APD_{90} change (%)	Strain (%)
St-level I	1	-6.4	15	-1.5	-4
	2	24	17	-3.2	NA
	3	-18.5	25	-9.2	-5
	4	16.7	40	-21.2	-14
	5	16.6	NA	-2.1	NA
St-level II	1	23	28	0.8	-9
	2	22.2	41	4.3	-6
	3	-4.9	47	32.7	-5
	4	-4.8	48	16.7	-10
	5	-3.4	49	NA	NA

In order to explore the effects of stretch on ionic mechanisms dominant during different phases of an AP, we computed AP durations at varying degrees of repolarization. Table 4.2 lists the during-stretch change in APD at different repolarization levels. For the st-level I group, APDs at all computed repolarization levels followed the same direction of change during stretch. That is, if APD_{90} reduced after stretch, so did APD_{50} and APD_{20}. In the st-level II group, APD_{90} and APD_{50} had the same direction of change (during stretch) in all cases, but APD_{20} changed in the opposite direction in 2 cases. Disappearance of the notch in the APs caused the relatively large changes in APD_{20} seen during st-level II.

Table 4.2 During-stretch change in baseline APD at different repolarization levels.

Group	Local strain (%)	% change in APD during stretch at CL of 500ms		
		APD_{90}	APD_{50}	APD_{20}
St-level I	15	-6.4	-6.2	-4.9
	17	24.1	23.8	6.1
	25	-18.5	-22.4	-26.8
	40	16.7	15.1	7.8
	NA	16.6	16.4	19.3
St-level II	28	23.1	29.3	15.0
	41	22.2	22.3	39.1
	47	-4.9	-9.8	120.9
	48	-4.8	-8.8	92.8
	49	-3.4	-12.0	-13.3

Figure 4.4 shows the hysteresis parameters, pre and during-stretch, for the st-level I group. As shown in the figure, for both sinusoidal protocols, differences between pre and during-stretch and those between during and post-stretch (data not shown) were present in individual trials. However, when pooled together, the averages were not statistically significantly different as the increases cancelled the decreases.
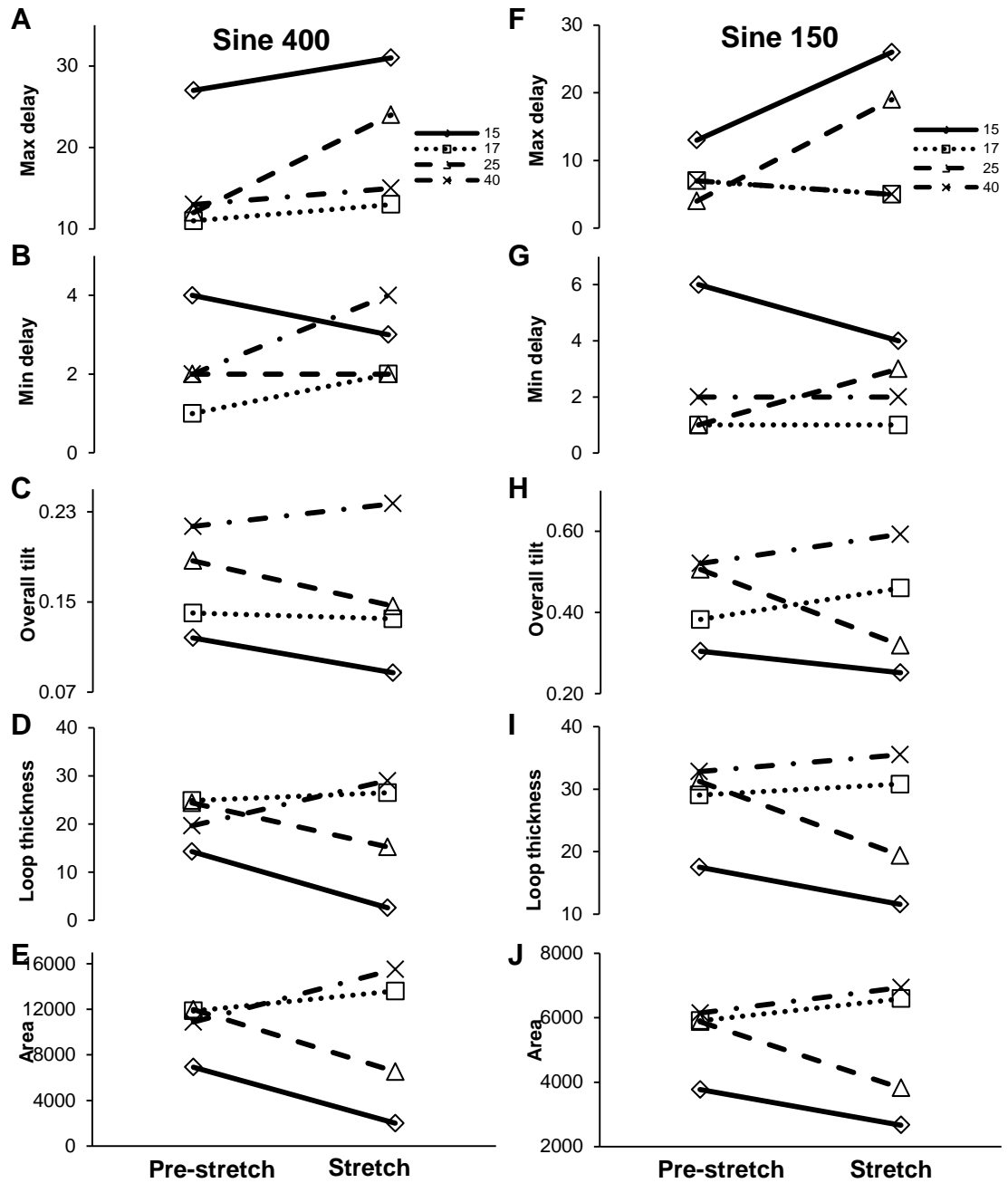
Figure 4.4 Hysteresis parameters, pre and during-stretch, for the st-level I group. The parameters were computed from 2 sinusoidal DI protocols; where the mean values of oscillatory DI were equal to 400 ms (A-E) and 150 ms (F-J) respectively. The numbers in the legend represent the local strain (in %) experienced near the site of impalement. Data from only four animals could be obtained for both sinusoidal DI protocols.

Figure 4.5 shows the hysteresis parameters pre and during-stretch for the st-level II group. Similar to st-level I results, for both sinusoidal protocols, differences between pre and during-stretch and those between during and post-stretch (data not shown) were present in individual trials, which, when combined, were not significantly different.
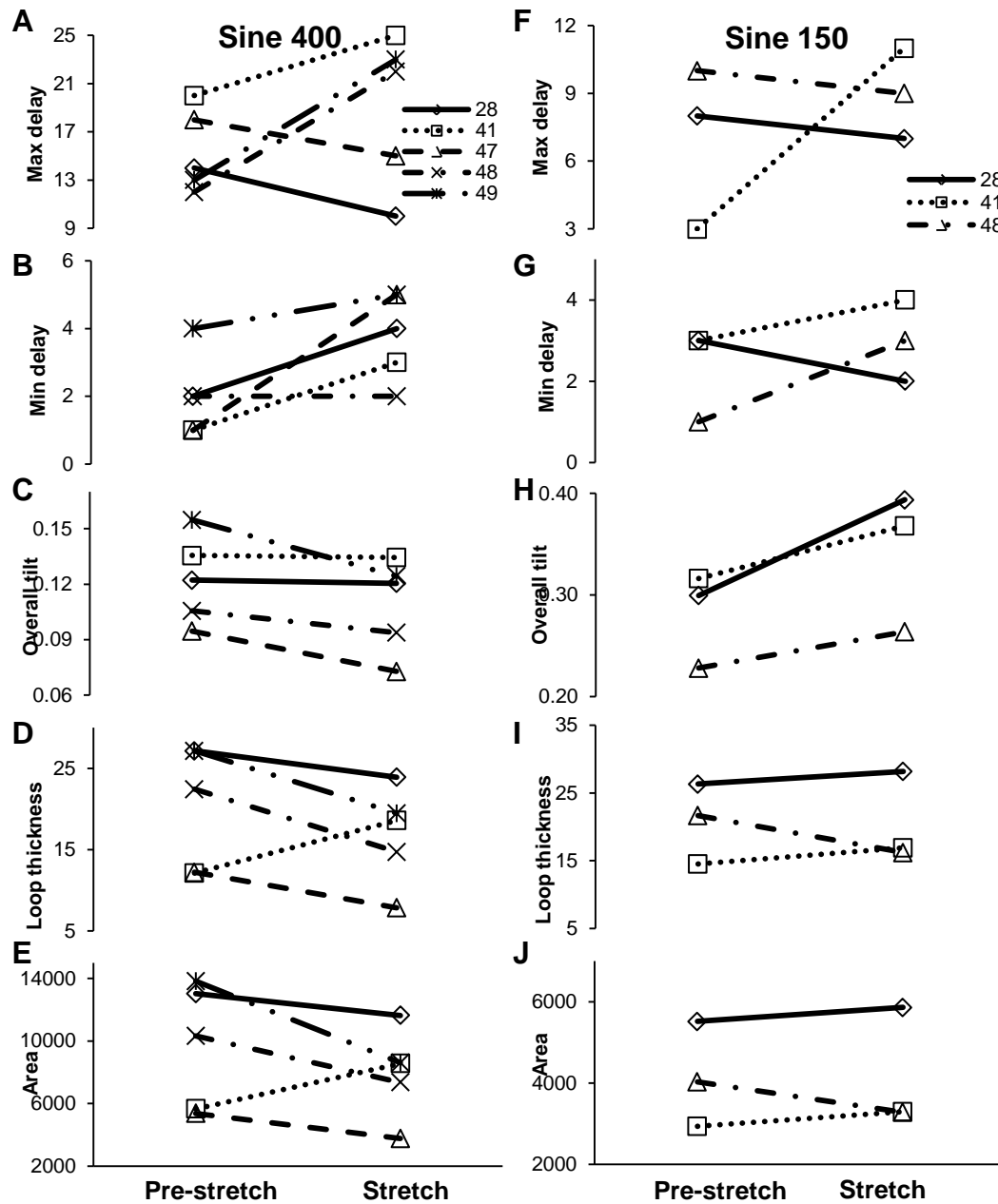
Figure 4.5 Hysteresis parameters, pre and during-stretch, for the st-level II group. The parameters were computed from 2 sinusoidal DI protocols; where the mean values of oscillatory DI were equal to 400 ms (A-E) and 150 ms (F-J) respectively. The numbers in the legends represent the local strain (in %) experienced near the site of impalement. Data from only three animals could be obtained for the sinusoidal DI

Table 4.3 shows the maximal slopes (i.e. maximum of the local slopes) pre, during, and post-stretch, resulting from the standard and dynamic restitution curves. In most individual trials, changes in maximal slopes, between pre and during-stretch and those between during and post-stretch were substantial for both restitutions, but when averaged together, were not statistically significant. Figure 4.6 shows an example of the standard and the dynamic restitution curves from the st-level II group. In this particular example, the APD increased by 22% during stretch and changed little (i.e. < 5%) post release of stretch. Figure 4.7 shows the average (± standard error) standard and dynamic restitution curves for st-level I (n=4) and st-level II (n=5) groups. To take account of the differences in baseline APDs, the maximum APDs were normalized to a value of 1 before averaging the restitution curves. Despite the average restitution curves being similar for both groups, the curves in individual trials were different during stretch.

Table 4.3 Maximal slopes computed from the standard and dynamic restitutions pre, during, and post-stretch for both groups. Pre: pre-stretch, D: during-stretch, Post: post-stretch, NA: not available.

St-level I	% Strain		Slopes, Standard protocol			Slopes, Dynamic protocol		
n	*Pre:D*	*Pre:Post*	*Pre*	*D*	*Post*	*Pre*	*D*	*Post*
1	15	10	0.73	0.79	0.34	1.16	1.85	6.80
2	17	NA	0.95	0.39	NA	1.39	NA	NA
3	25	19	0.69	2.48	NA	1.75	1.59	NA
4	40	20	2.20	1.21	2.90	1.61	1.96	NA
5	NA	21	0.32	NA	0.48	1.85	NA	3.52
St-level II	% Strain		Standard protocol			Dynamic protocol		
n	*Pre:D*	*Pre:Post*	*Pre*	*D*	*Post*	*Pre*	*D*	*Post*
1	28	17	0.34	2.00	0.85	1.93	1.34	1.30
2	41	32	0.74	1.72	1.62	0.93	1.38	1.85
3	47	39	0.39	0.75	0.61	2.13	1.66	1.88
4	48	33	0.38	1.33	0.83	1.48	1.70	1.18
5	49	NA	0.30	0.13	NA	1.55	1.17	NA
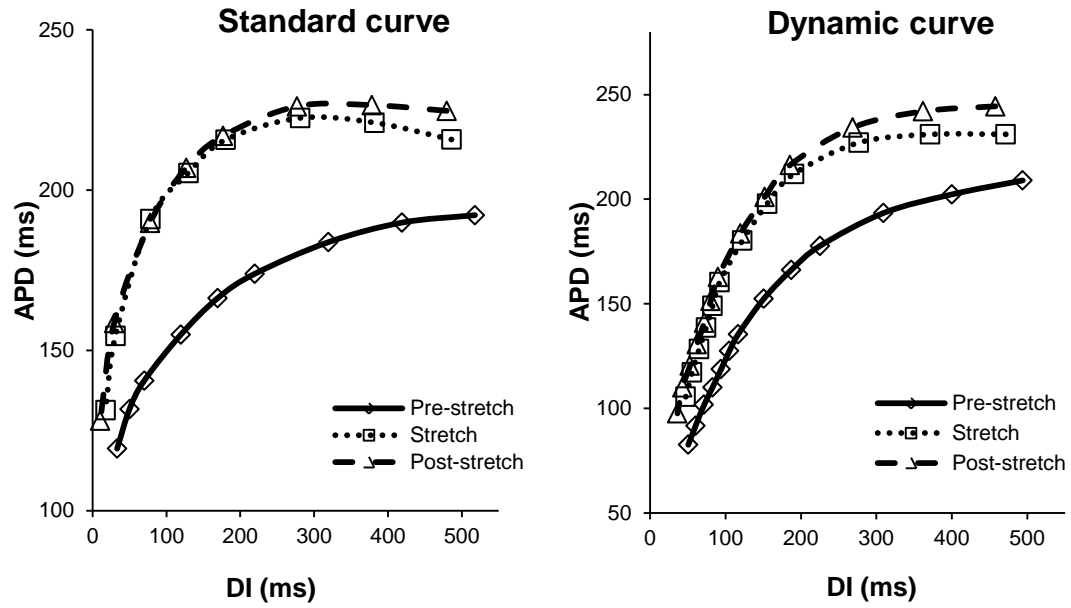
Figure 4.6 Example of standard (A) and dynamic (B) restitution curves obtained from one experiment. Shown are the restitution curves obtained pre, during, and post-stretch from one experiment from the st-level II group. In this particular case the APD increased by 22% during stretch and changed little post release of stretch.
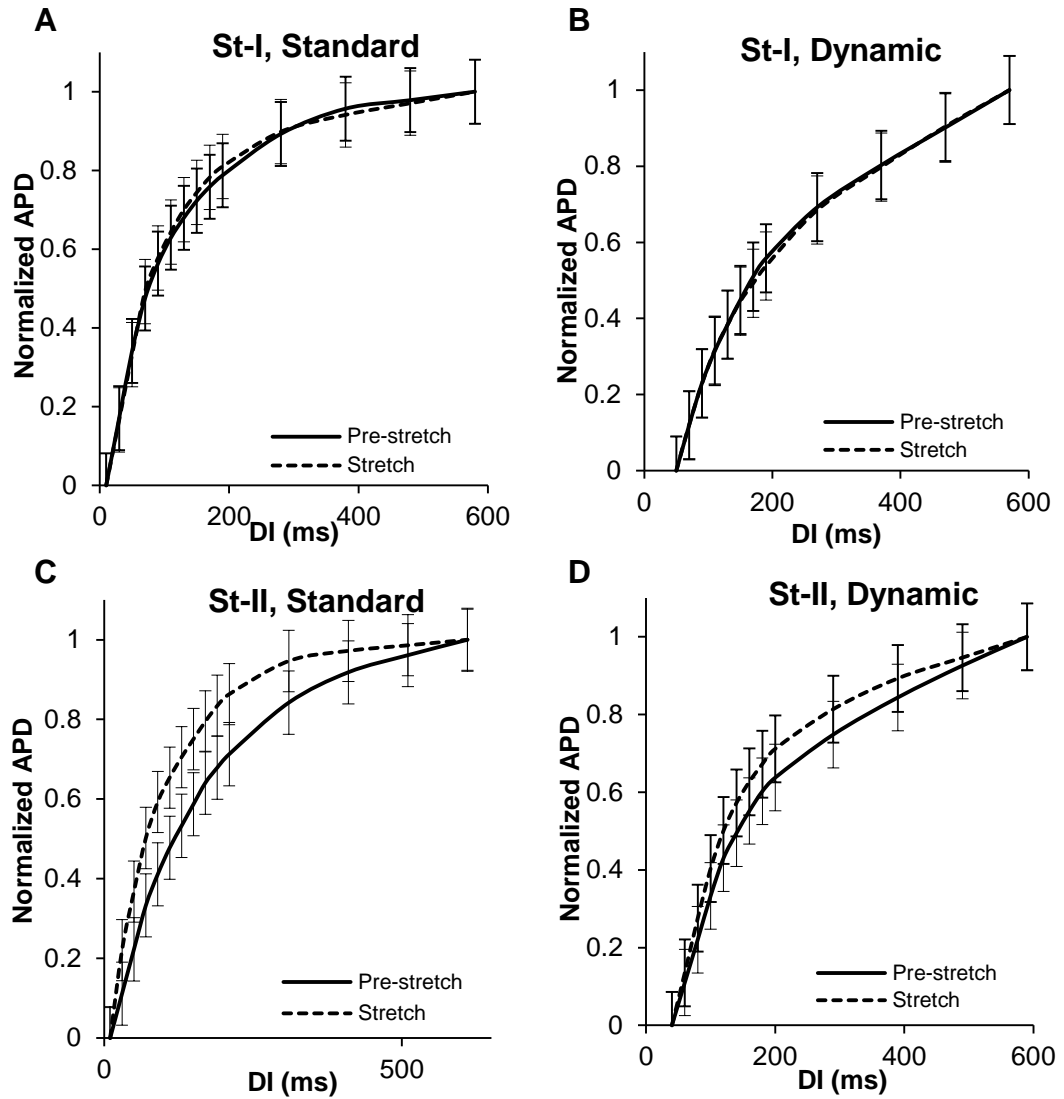
Figure 4.7: Average standard (A, C) and dynamic (B, D) restitution curves (with standard error bars), for both groups. The APDs were normalized to a maximum value of 1. For both groups, there were differences between individual trials although the average restitution curves

At short constant CLs and constant DIs, stretching the tissue produced alternans of APD in three tissues. Table 4.4 shows the alternans amplitude and the respective CLs at which alternans started during-stretch. The table also includes, for comparison, the lowest pre-stretch CLs at which the tissue exhibited a 1:1 (stimulus: activation) pattern without block. Stretching the tissue induced alternans at longer CLs as compared to pre-stretch CLs at which no alternans was seen. In one case, the alternans also persisted post-stretch, while in another, the alternans went away after release of stretch.

Table 4.4 Amplitude of APD alternans and CL of occurrence during-stretch of tissue. Listed are the lowest pre-stretch CLs at which the tissue showed a 1:1 activation. Pre: pre-stretch, D: during-stretch, Post: post-stretch.

	Alternans amplitude [cycle length] (ms)			% Strain	
Group	Pre	D	Post	Pre: D	D: Post
St-level I	0 [130]	7 [173]	11 [160]	NA	NA
	0 [130]	13 [150]	NA	25	-5
St-level II	0 [90]	9 [117]	0 [100]	28	-9

Chapter V   DISCUSSION

Acute mechanical stretch is known to produce an electrically less stable cardiac substrate. However, the direct effects of stretch on electrophysiological properties of the heart have been inconsistent and even contradictory. To reexamine the effects of stretch in tissues, we used microelectrodes to record ICPs from swine RV tissues during two levels of mechanical stretch. These studies are technically very challenging; thus we focused on tissues from the RV, because stretch seems to have a more pronounced effect on RV [65]. We quantified the effect of stretch on a variety of electrical properties that are thought to be key in development of arrhythmia, namely; restitution of APD, electrical memory, and onset threshold of alternans. Individual trials showed substantial differences in the measured electrical properties after stretch. However, when the results from individual trials were averaged over all tissue samples, no change was seen in the properties that we measured. We think that in this circumstance, averaging, i.e. pooling, all the changes together leads to a potentially wrong conclusion that stretch has no effect on these properties. It is likely that at a tissue level, stretch does affect the electrical properties of individual myocytes, although differentially. A potential mechanism of this discrepant effect of stretch, discussed in detail below, is a local, micron to mm scale heterogeneity in arrangement of myocytes. In response to stretch, local differences in orientation of myocytes relative to the axis of stretch can increase the local dispersion of repolarization throughout the tissue. This local increase in the dispersion of repolarization upon acute stretch, leads to an increased susceptibility to arrhythmia, and is possibly the reason for the heart's vulnerability during the T wave as well.

Previous studies using microelectrode based measurements from ventricular tissues have shown that stretch has an inconsistent effect on APD. Results from these studies led to a general conclusion that stretch does not affect electrical properties. Dominguez et al [50] reported that stretching cardiac purkinje fibers (up to 50%) of sheep did not change the APD significantly. Penefsky et al [52]

41

reported similar results by stretching the cat papillary muscle. Penefsky et al attributed the inconsistency in APDs to the specialized conduction fibers that ran along the papillary muscle and merged with myocardial fibers at various points. Dominguez et al concluded that AP parameters did not change after stretch. In this study, in addition to the morphology of action potentials, the dynamic electrophysiological properties of restitution, memory and alternans were also investigated. When averaged, our results also show that the mean values of these parameters were not different during stretch. However, using these results to conclude that stretch does not affect these properties misses a finer picture. We note that the studies by Dominguez and Penefsky included more trials (16, and 18) than reported in this study. However, all these three studies are qualitatively very similar, in which all show substantial changes in individual trials while the averages show no consistent change. Making these electrophysiological measurements is technically challenging, especially with precise control of DIs using real-time control, more so in a pig model. Conducting more experiments, in our prediction, will not show significant differences in average results, due to the cancellation of effects; similar to what was observed by Dominguez and Penefsky.

In order to determine if heterogeneity in local cell orientation exists, which may then contribute to heterogeneous responses upon stretch, we used histology to visualize the arrangement of myofibers relative to the direction of stretch. In particular we wanted to see if there exist regions, within a given small area of impalement, where groups of cells are arranged at an angle to the neighboring groups. The schematic in figure 5.1A depicts the effect of orientation in response to stretch. Upon stretch, shown in figure 5.1B, cells oriented along the pull direction will experience tension along the long axis and cells at an angle (perpendicular in this case) will experience compression along the long axis (plus circumferential tension). The transduction of force to cells can vary depending on their orientation. It depends upon the overall lengths of the T tubules in the rete structure [66] on the cells and the localization of the SACs on them. Variable

42

transduction of force may lead to variable activation of the SACs and thus a regionally variable effect on electrophysiology. In certain cells, the T tubules would experience tension and lengthen, while those in others can experience compression and shorten due to membrane unfolding and folding [67, 68]. It has been shown that SACs likely reside in the T tubules [69]. Thus, based on the orientation of cells relative to the direction of stretch, it is possible that stretch can have widely different effects. This effect is shown schematically in figure 5.1A.
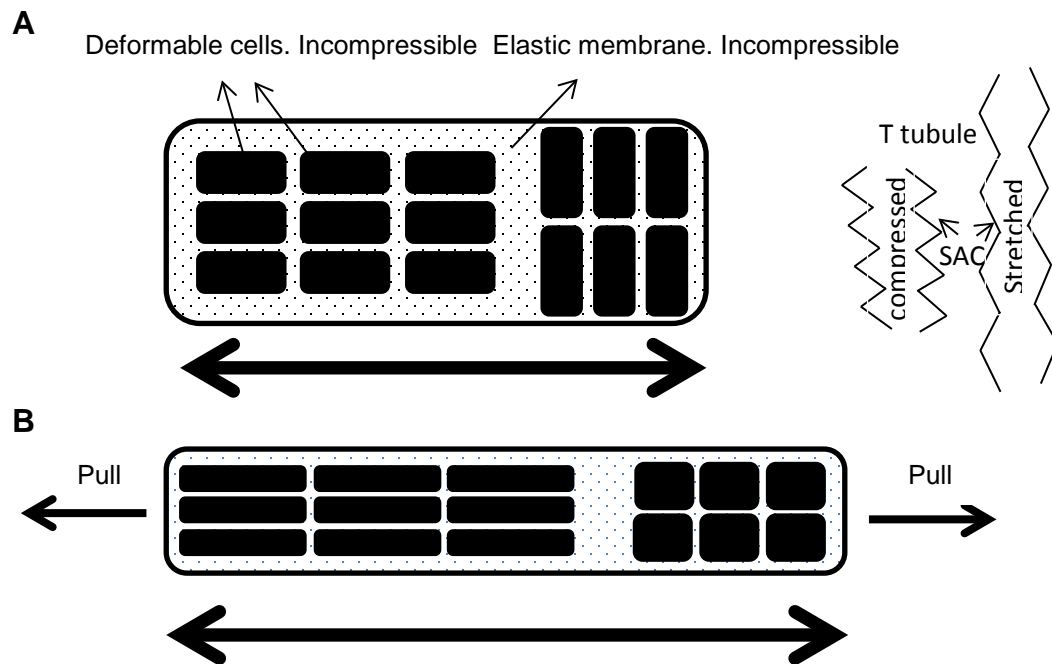
Figure 5.1 Schematic showing the hypothesized orientation of groups of cells within a tissue (A). Both the cells and membrane assumed incompressible. Upon stretching the tissue horizontally (B), cells oriented parallel to the pull direction (with long axis parallel to the pull direction) will experience tension along the long axis and cells oriented at an angle (perpendicular in this case) to the pull direction will experience compression plus tension (circumferential) along the long axis. Schematic in panel A shows the effect of this pull on T tubules.

Figure 5.2 shows three montages which were compiled from multiple images. Each montage was obtained from one slice cut from a section of tissue obtained from a region where the impalement was subjected to st-level II (A), st-level I (B) stretch, and no stretch (C). The histology images were not used to determine or correlate levels of stretch. These images just show examples of changes in local orientation of cells in tissue samples used for the two levels of stretch. The montage in figure 5.2A spans a length of about 4 mm and in B and C spans 3 mm. The images in figure 5.2, while supporting the possibility that differential orientation is the cause of heterogeneous responses, do not serve as a conclusive proof. We note that this difference in orientation is at a local scale and within a 5 micro meter thick section. This difference is distinct from the more widely considered macro level heterogeneity existing between different regions of the ventricles (LV, RV, endo, epi, etc) and also different from the trans-mural fiber rotation. It is very difficult to exactly visualize which myocyte was impaled by the tip of the microelectrode. Considering the micron to mm scale differences that exist in orientation of cells, it is likely that impalements would find myocytes at different orientation relative to the stretch direction, consistent with the mechanism shown in figure 5.1 A and B.
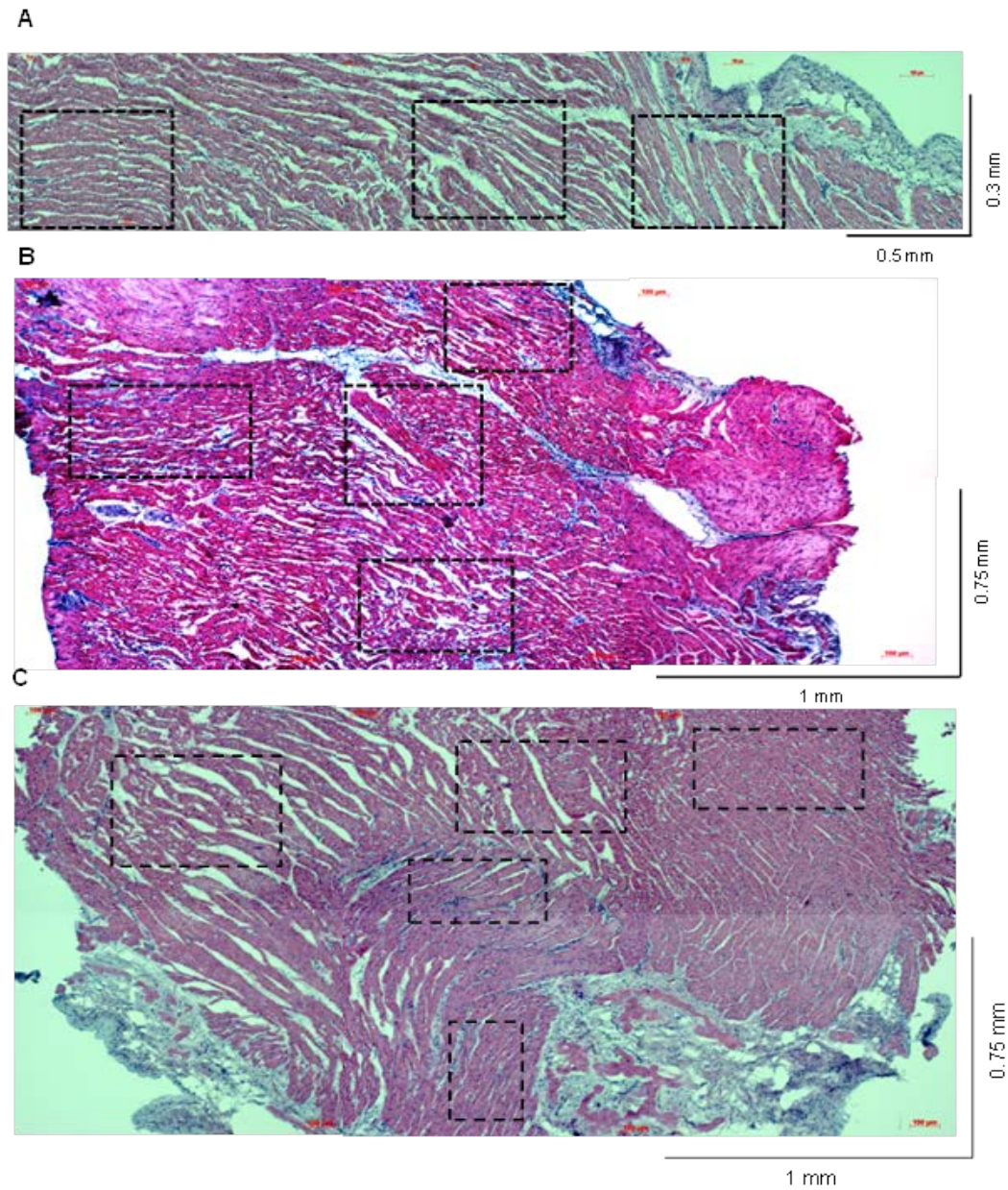
Figure 5.2 Montages showing histological data obtained from tissue slices subjected to st-level-I, st-level-II, and no stretch. The montages were obtained from a slice near to the endocardial side cut from a section of tissue subjected to st-level II (A), st-level I (B), and no stretch (C). The montage in A spans a length of about 4 mm and in B, C spans 3 mm. The boxes placed on the images show regions where cell orientation is considerably different than other locations

Alternans of APD is seen in the swine [2, 70], although it is much less frequent than other species such as canines or humans. Consistently, we did observe alternans only in a small number of trials. The limited alternans observation that we have, however, suggests that the tissue was slightly more prone to developing alternans during stretch, which may reflect the known increase in electrical stability after stretch. The changes in slopes of restitution were not consistent upon stretch, except a slight tendency for the maximum slopes of the standard restitution during st Level II to increase, likely reflecting the poor correlation that exists between slopes and alternans [71, 72]. We note that the use of constant DI pacing to explore alternans was not germane to the objectives of our study, we looked for alternans in all situations when the activation rates were high.

The maximum stress that a healthy myocardium experiences during normal physiologic conditions, lies in the range of 30-40 Kpa (or KN/m^2), occurring at the end of systole [73, 74]. Patients with severe left ventricular dysfunction have been reported [75] to have a mean ventricular systolic wall stress of about 42.1 Kpa to 50.8 Kpa and the mean diastolic wall stress to be about 10.1 Kpa to 15.4 Kpa. In patients with myocardial infarction, the end-systolic stress, in the infarct regions, is reported to be in the range of 50-60 Kpa [73]. The average tissue cross-sectional area in our study was between 24- 40 mm^2. The stress exerted by 200 gm (i.e. 1.96 N) of force on a cross-sectional area of 24- 40 mm^2 lies in the range of 50- 80 Kpa whereas the stress exerted by 400 gm (i.e. 3.92 N) of force lies in the range of 100-160 Kpa. While the experimental arrangement of our setup does not allow all of the applied force to be transduced to the tissue, these numbers resemble the stress experienced by the functioning ventricles in disease and in normal states. Therefore, the stress exerted by 200 gm of force resembles the clinical range as stated above, while the stress exerted by 400 gm of force would represent a more severe dilatation, as would be seen during distension of the RV during fibrillation.

Chapter VI LIMITATIONS

Our data was collected from the endocardial side of the right ventricular tissue from swine. In healthy patients, the longitudinal deformation in regions of RV free wall is greater and more heterogeneous than the LV free wall [65], and thus we focused on RV. During acute ventricular dilatation, it is likely that the RV will be more sensitive to MEF and will contribute significantly to the higher DFT. Given the macro level electrophysiological heterogeneity that exists in the heart, it is unclear whether other regions of the heart would also show similar results. It is possible that the un-stretched tissue may have curled a little which then straightened upon stretch, leading to a slight overestimation of the induced and residual strain values. Data from complete set of protocols could not be obtained in some experiments, because stretching of tissue makes it difficult to obtain a stable impalement for long periods of time.

APPENDIX A

Effect of Rapid Delayed Rectifier Current on Hysteresis in Restitution of Action Potential Duration in Swine *

Anuj Agarwal, Linyuan Jing, Abhijit Patwardhan, Member, IEEE

ABSTRACT

Electrical stability in the heart depends on two important factors; restitution of action potential duration (APD) and memory. Repolarization currents play an important role in determining APD and also affect memory. We determined the effects of blocking the rapid component of the delayed rectifier (I_{Kr}) on a quantifiable measure of memory, i.e. hysteresis in restitution of APD, in swine. Transmembrane potentials were recorded from right ventricular endocardial tissues. Two pacing protocols with explicit control of diastolic interval (DI) were used to change DIs in a sequential and sinusoidal pattern to quantify hysteresis in restitution of APD. E-4031 (5 μM/L) was used to block I_{Kr}. Measures of memory and restitution were quantified by calculating hysteresis loop thickness, area, overall tilt, and maximum and minimum delays between DIs and APDs. Blocking I_{Kr} with E-4031 increased the baseline APD, loop thickness, area, and tilt ($p<0.05$). However, loop thickness did not increase beyond what could be predicted by the increase in baseline APD after block of I_{Kr}. The substantial change in APD after blocking I_{Kr} suggests that this current plays a major role in repolarization in the swine. Loop thickness is a measure of memory, an increase in which is predicted by theory to reduce instability in activation. In our study, the substantial increase in loop thickness could be accounted for by an equally substantial increase in APD and therefore does not necessarily indicate

increased memory after blocking I_{Kr}. Our results also suggest that factors based on restitution and memory need to be considered in the context of operating point, i.e. baseline APD, when they are used to explore mechanisms that affect electrical stability in the heart.

INTRODUCTION

Restitution of action potential duration (APD) and memory are known to play a critical role in stability of electrical activation and predisposition to arrhythmia. Restitution here refers to dependence of an APD on its preceding diastolic interval (DI) and memory refers to dependence of an APD on previous APDs occurring over several seconds. Restitution in APD shows hysteresis when the DI changes in a sequential oscillatory pattern [1]. The parameters of hysteresis provide a quantifiable measure of memory, which theoretically has been shown to dampen activation instability [2]. Drug induced reduction or block of repolarization currents, manifested as QT interval prolongation of the electrocardiogram, increases the risk of ventricular tachyarrhythmia which can lead to sudden cardiac death [3]. Drug related prolongation of QT interval is also known as acquired long QT syndrome (LQTS). The Food and Drug Administration (FDA) places great emphasis on pre-clinical testing of many new drugs for potential proarrhythmic effects. Their criteria mainly include in vitro Human ether-a- go-go-related gene product (hERG) testing [4]. The hERG channel mediates I_{Kr} and is mostly the cause of drug induced acquired LQTS [4]. In this study, therefore, we explored the effects of this key repolarization current, I_{Kr}, on hysteresis in restitution of APD in swine, which is a widely used animal model to study the link between restitution and arrhythmia [2, 5, 6].

Our results showed that blocking I_{Kr} increased the loop thickness but this increase could be accounted by an equally large increase in baseline APD. We have previously shown that a change in loop thickness can be used as a measure of memory [2]. Therefore, our results also suggest that indexes that

predict stability dynamics, such as the loop thickness, need to be considered in the context of baseline APD, if substantial changes in baseline APD are observed such as that seen after blocking I_{Kr}.

METHODS

Experiments were approved by the Institutional Animal Care and Use Committee (IACUC) at the University of Kentucky. Narrow strips of tissues, obtained from the right ventricle of swine, were placed in a plastic chamber and superfused with modified Tyrode's solution bubbled with 95% O2 and 5% CO2 gas mixture [2]. The temperature and pH of the perfusate were maintained at 36 ± 1°C and 7.3 ± 0.05. Transmembrane potentials (TMP) from the endocardial side of tissue were recorded using glass microelectrodes filled with 3M KCl solution. A stand-alone computer with a commercial data acquisition system was used to digitize and record the TMP at a sampling rate of 10,000 samples / sec. A custom made program in LABVIEW was used to explicitly control the DIs using a feedback-based pacing protocol [1]. To determine hysteresis in restitution, the tissues were paced using two protocols. Both protocols consisted of DI control lasting 220 beats. The first 20 beats consisted of constant DI followed by 2 cycles of a sinusoidal pattern of DI with a period of 100 beats. In both protocols, the constant DI values were equal to the mean values of the sinusoidal oscillation. In the first protocol, the DI sequence had 400 ms as central value of DI with ±300 ms oscillation around the central value. The second protocol had 150 ms as central value of DI with a ±140 ms oscillation around the center. An example of one of the DI protocol is shown in Figure 1. We waited about 5 minutes between protocols; the tissue was paced at constant cycle lengths during this period. After obtaining the control recordings, we used 5 µM/L of E-4031 (TOCRIS bioscience) to block the rapidly activating delayed rectifier channel, IKr. Analyses of data were performed offline using Matlab (MathWorks, Natick, MA, USA). Before analyses, all data were digitally filtered by using a low-pass filter with a cutoff

frequency of 500 Hz. The APDs and DIs were calculated from the recorded TMP, using a constant threshold defined at 90% repolarization of action potential.

Figure 1 shows an example of the sinusoidal DI protocol used and the obtained hysteresis in restitution of APD. From the APD versus DI curve, we quantified the following parameters of hysteresis: thickness of loop, overall tilt, maximum delay, minimum delay and area under loop. As defined previously [2], loop thickness was measured as the difference between APDs at mean values of oscillatory DI during increasing and decreasing DI trajectories. Tilt was measured as the ratio of differences of maximum and minimum APD and their corresponding DI values. Maximum delay was measured as the delay in beats, between the maximum values of APD and DI during the sinusoidal change. Minimum delay was measured as the delay in beats, between the minimum values of APD and DI during the sinusoidal change. Area under loop was defined as the area under the hysteresis curves. We used the second cycle of the DI protocol to calculate the hysteresis parameters to minimize the effects of APD adaptation, caused due to a switch to constant DI pacing from cycle length pacing. However in some cases, where the control of DI during the second cycle was not as effective as that during the first cycle, the data from first cycle were used to calculate the hysteresis parameters. Data obtained from multiple trials of the same protocol were first averaged within each animal before averaging across animals. To test the statistical significance between the control and the drug groups, we used the student's paired t-test. Differences were considered significant at $p \leq 0.05$.

Hysteresis parameters were normalized to baseline APD based on results obtained from simulations using the Iyer- Mazhari-Winslow (IMW) model developed for the human ventricular myocyte [7].
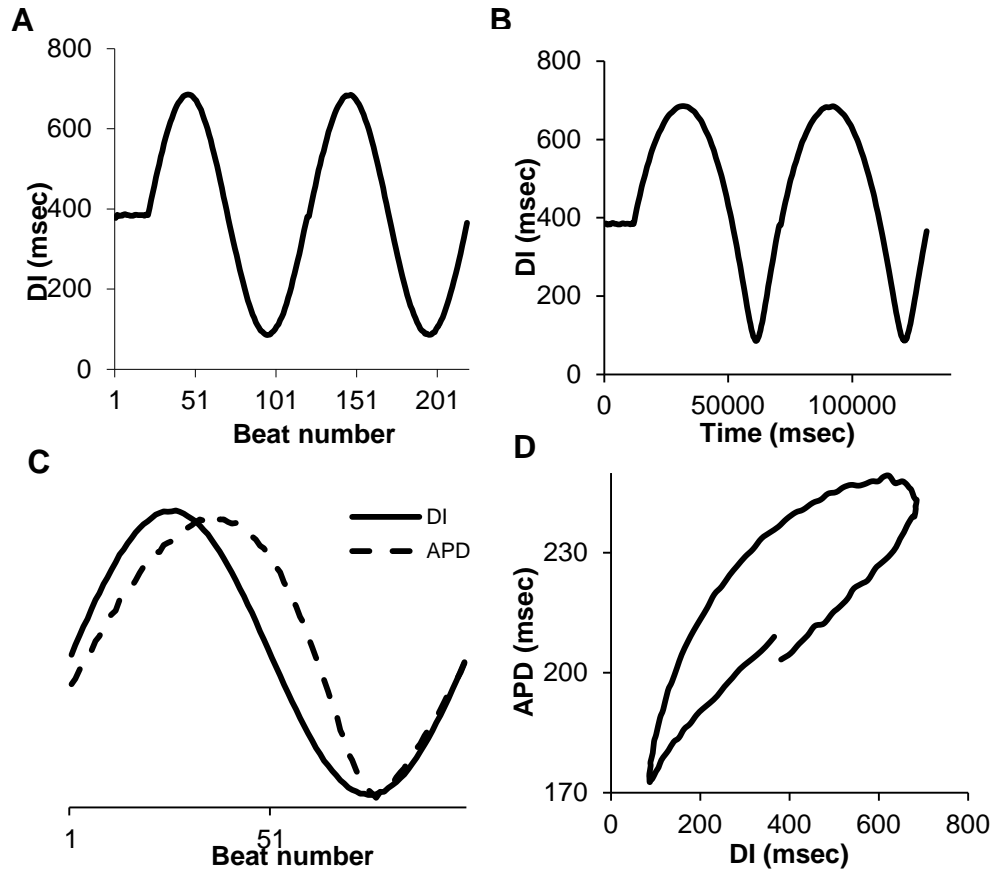
Figure 1. (A) Example of a sinusoidal DI protocol of 220 beats with central DI value of 400 ms and a ±300 ms oscillation around the central value. (B) Variation of DI with time. (C) The second cycle of the sinusoidal DI protocol (solid line) shown in (A) with the corresponding APDs (dashed line). The APDs are scaled and offset vertically to clearly show the measures of max delay and min delay. (D) The restitution relationship obtained from DI sequence in (A), shown for the second cycle of the sinusoidal DI protocol.

RESULTS

After administrating E-4031, the average APDs (n=5) changed from 213 ms to 522 ms, a 145% increase. Figure 2 shows examples of action potentials recorded during constant cycle length pacing, pre and post-block I_{Kr}. The two traces in figure 2 are aligned to better show the differences between them. Figure 3 shows the average restitution curves obtained from pre and post-block I_{Kr} for oscillatory DI trials with central DI value at 400 ms (n=5, 3A), and 150 ms (n=3, 3B). Due to difficulties in obtaining 1:1 control for the smaller values of DI in the 150 ms central DI protocols, especially post block, we were able to obtain data from only three animals for that protocol. In both cases, the restitution curves obtained post-block were shifted vertically to facilitate comparison with the pre-block curves. The shift was equal to the difference in the APD (produced by the block of I_{Kr}) at the central value of DI for each oscillatory protocol.

100 ms
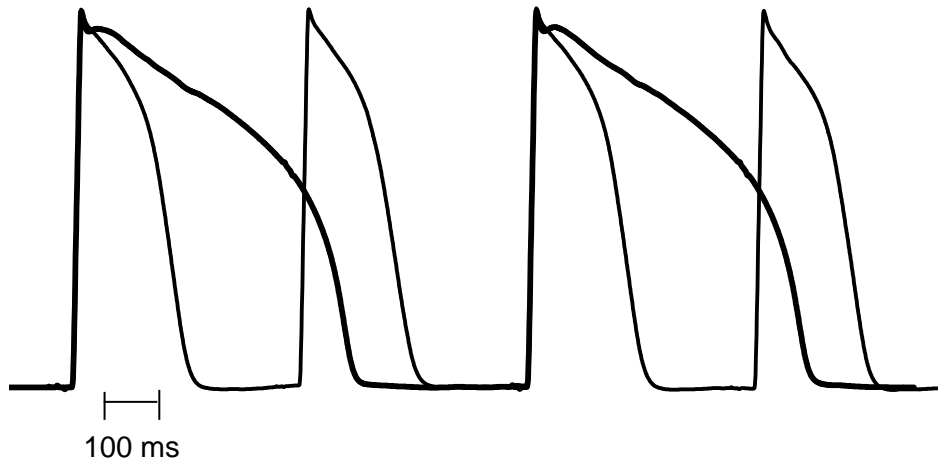
Figure 2. Example of action potentials recorded, pre-block (thin line) and post- block (thick line) of I_{Kr}. The traces are aligned to better show the differences between them.
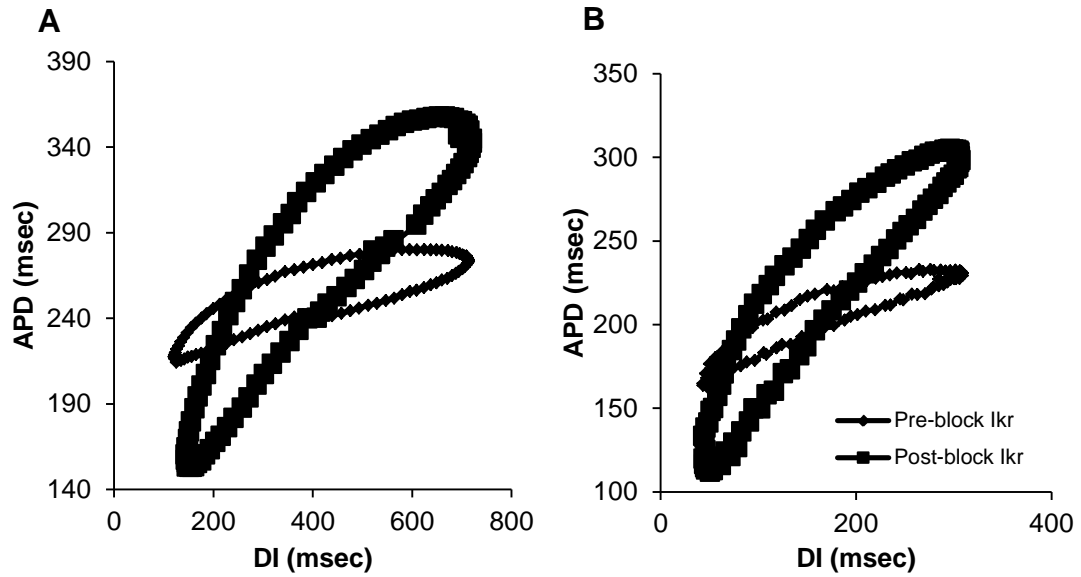
Figure 3. Effects of blocking I_{Kr}. Shown are average restitution curves obtained pre and post block of I_{Kr} for central DI values equal to (A) 400 ms (n=5) and (B) 150 ms (n=3). The restitution curves post block of I_{Kr} were shifted vertically to facilitate comparison between the two curves.

Table 1 lists the average hysteresis parameters, and percentage changes before and after the administration of E- 4031. The table shows that except maximum delay, all other parameters increased after blocking I_{Kr}. In both protocols, the most pronounced and statistically significant changes were seen in overall tilt, loop thickness, and the area under the loop.

Table1. Changes in maximum delay, minimum delay, tilt, loop thickness and area under loop of hysteresis in restitution, pre and post block of I_{Kr}. Measures for both, the 400 ms central DI value protocol and the 150 ms central DI value protocol are shown.

I_{kr}	Central DI 400 ms			Central DI 150 ms		
	Pre block	Post block	%	Pre block	Post block	%
Parameters	Mean±SEM	Mean±SEM	change	Mean±SEM	Mean±SEM	change
Max delay (beats)	12.93 ±0.91	11.66±0.53	-9.8	10.33±2.19	6.5±0.29	-37.1
Min delay (beats)	2.83±0.4	3.6±0.24	27.2	3.5±2.36	4.67±1.01	33.4
Tilt	0.137**±0.005	0.414**±0.034	202.2	0.314*±0.032	0.786*±0.029	150.3
Loop thickness (msec)	31.87±3.48	81.07*±8.11	154.4	23.58**±7.37	72.67**±6.78	208.2
Area under loop (msec^2)	14865.43**± 1172.71	39058.73**± 3567.35	162.7	4519.2**±1351.92	13199.33**± 624.83	192.1

*p<0.05, **p<0.01

We have previously reported that loop thickness is larger when baseline APDs are longer [2]. Table 2 shows control, i.e. pre block, values of the average APDs at center DI values of 400 and 150 ms and the corresponding loop thickness. The increase in loop thickness of 8.29 and in APD of 43 in going from center DI 150 ms to center DI 400 ms, gives a gain of 0.19 (8.29 / 43) in units of loop thickness per unit increase in APD. Post-block of I_{Kr}, APDs increased from 213 ms to 522 ms, a 309 ms increase. Using linear extrapolation, the expected increase in loop thickness, post- block I_{Kr}, is about 59 ms (309 * 0.19). Results in Table 1 show that the increase in loop thickness post-block I_{Kr}, for both 150 ms

center DI and 400 ms DI protocol was approximately 49 ms. Thus the loop thickness that was observed was less than that predicted by the increased APD.

Table 2. Average values of APDs and loop thickness at center DI values of 150 ms and 400 ms during control condition (i.e. pre block of I_{Kr}).

	Value at Center DI 150 ms	Value at Center DI 400 ms	Difference
Average APD (ms)	196.6	239.7	43.1
Loop thickness	23.58	31.87	8.29
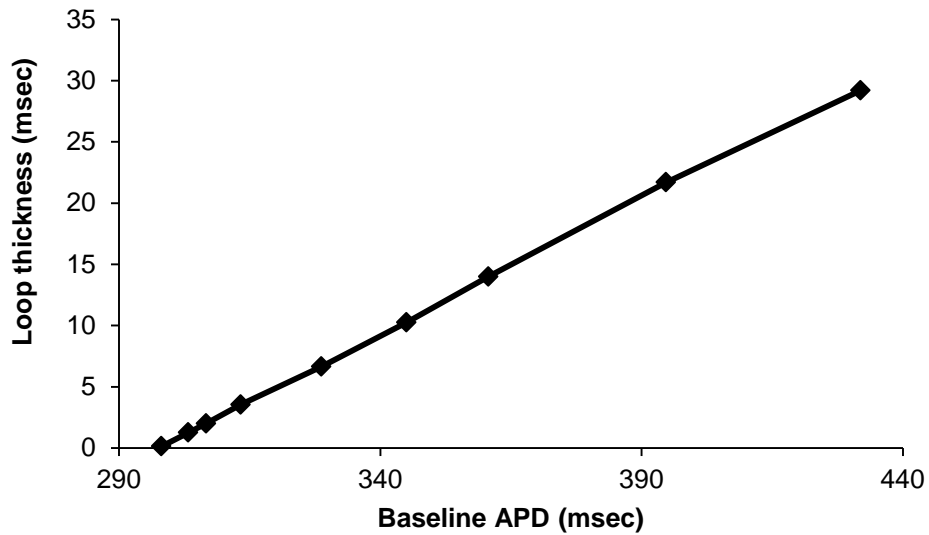
Figure 4. Simulation results from the IMW model based on human ventricular myocyte [7]. Shown is a graph of loop thickness versus baseline APD, obtained at center DI values, from several sinusoidal DI protocols with increasing center DI values and ranges. Note that the first three points, at lowest values of DI, are extrapolated from those at the right.

The assumption of a linear dependence of loop thickness on APD was supported by simulation results shown in figure 4, obtained using the IMW model [7]. We used this model because of a lack of adequate swine model. Figure 4 shows a graph of loop thickness versus baseline APD, obtained at the center DI values, from several sinusoidal DI protocols with increasing center DI values and ranges. The first three data points in the graph were extrapolated backwards because the human model, as compared to swine, has higher steady state APD values and does not exhibit hysteresis at lower ranges of sinusoidally varying DI. The graph in figure 4 shows a linear increase in loop thickness with increasing APD values.

DISCUSSION

The main objective of this study was to determine the effects of blocking repolarization current I_{Kr} on hysteresis in restitution of APD and thus on memory in electrical restitution in swine. E-4031 was used to block I_{Kr} in swine and the block of this current caused a marked increase in the baseline APD, and parameters of hysteresis such as tilt and loop thickness. However, the increase in loop thickness was less than that predicted by increase in baseline APD resulting from block of I_{Kr}. While the large change in baseline APDs make interpretation of the results difficult since the operating points are dramatically different, the less than predicted increase in loop thickness suggest that blocking the rapidly activating delayed rectifier channel I_{Kr} in swine does not affect memory substantially or may decrease it slightly.

Effect of Ikr manipulation on APD and measures of memory

Ionic manipulations, for example, blocking an ion channel current, often have an impact on APD. It is important to consider the effects of change in baseline APD (post manipulation) on measures of memory, such as loop thickness, because these measures are used to iterate a disturbance around an operating point and

58

large changes in APD indicate large changes in operating point. In our study the increase in baseline APD, after adding E-4031, was substantial (about 145%) and thus the loop thickness was normalized with the change in baseline APD.

LIMITATIONS

We obtained data only from the endocardium of right ventricle in swine. Given the heterogeneity that exists within a heart, based on these results it is difficult to predict whether other regions in the heart would also behave similarly in response to E-4031. The concentration of E4031 that we used was based on previously reported studies in canines by Hua et al. [8] and Fish et al. [9] in which the change in the baseline APD, post E-4031, was less than 30%. However, in swine, this same concentration of I_{Kr} blocker resulted in increase in APD much larger than that reported by the studies in canines. Thus, our study also points out critical differences in expression of this current between these two widely used species. As stated above, the substantial increase in APD made interpretation of changes in loop thickness, in terms of changes in memory, difficult. Studies using lower concentrations of E4031 where the changes in APD are modest are required to better determine the effects of the block of this repolarization current on measures of memory.

REFERENCES

[1] R. Wu and A. Patwardhan, "Restitution of action potential duration during sequential changes in diastolic intervals shows multimodal behavior," Circulation Research, vol. 94, pp. 634-641, Mar 19 2004.

[2] K. M. Guzman, L. Y. Jing, and A. Patwardhan, "Effects of Changes in the L-Type Calcium Current on Hysteresis in Restitution of Action Potential Duration," Pace-Pacing and Clinical Electrophysiology, vol. 33, pp. 451-459, Apr 2010.

[3] A. J. Moss, P. J. Schwartz, R. S. Crampton, D. Tzivoni, E. H. Locati, J. Maccluer, W. J. Hall, L. Weitkamp, G. M. Vincent, A. Garson, J. L. Robinson, J. Benhorin, and S. S. Choi, "The Long Qt Syndrome - Prospective Longitudinal-Study of 328 Families," Circulation, vol. 84, pp. 1136-1144, Sep 1991.

[4] J. P. Piccini, D. J. Whellan, B. R. Berridge, J. K. Finkle, S. D. Pettit, N. Stockbridge, J. P. Valentin, H. M. Vargas, M.W. Krucoff, and C. H. W. Grp, "Current challenges in the evaluation of cardiac safety during drug development: Translational medicine meets the Critical Path Initiative," American Heart Journal, vol. 158, pp. 317-326, Sep 2009.

[5] I. Banville, N. Chattipakorn, and R. A. Gray, "Restitution dynamics during pacing and arrhythmias in isolated pig hearts," J Cardiovasc Electrophysiol, vol. 15, pp. 455-63, Apr 2004.

[6] T. D. Nielsen, J. Huang, J. M. Rogers, C. R. Killingsworth, and R. E. Ideker, "Epicardial mapping of ventricular fibrillation over the posterior descending artery and left posterior papillary muscle of the swine heart," Journal of Interventional Cardiac Electrophysiology, vol. 24, pp. 11-17, Jan 2009.

[7] V. Iyer, R. Mazhari, and R. L. Winslow, "A computational model of the human left-ventricular epicardial myocyte," Biophysical Journal, vol. 87, pp. 1507-1525, Sep 2004.

[8] F. Hua and R. F. Gilmour, "Contribution of I-Kr to rate- dependent action potential dynamics in canine endocardium," Circulation Research, vol. 94, pp. 810-819, Apr 2 2004.

[9] J. M. Fish, J. M. Di Diego, V. Nesterenko, and C. Antzelevitch, "Epicardial activation of left ventricular wall prolongs QT interval and transmural dispersion of repolarization: implications for biventricular pacing," Circulation, vol. 109, pp. 2136-42, May 4 2004.

APPENDIX B

A new approach to measure the contribution of restitution to repolarization alternans *

Anuj Agarwal, and Abhijit Patwardhan

ABSTRACT

Several studies suggest link between repolarization alternans and arrhythmia. A potential target for minimization of alternans amplitude is pharmacological flattening of restitution function, which links a diastolic interval (DI) and subsequent action potential duration (APD). While our recent studies have shown that DI dependent restitution is not a necessary mechanism for alternans, in circumstances of nearly invariant activation intervals, restitution contributes to alternans. Determination of the degree to which restitution contributes to alternans during stable alternans, which requires determination of the gain between DI and APD, is not possible because it always is unity. We propose that the rate of change of alternans along the length of the tissue may provide an estimate of the degree to which restitution contributes to alternans amplitude. We conducted experiments with swine to demonstrate the above approach. In a linear strand of tissue, we paced such that DIs for successive activations were invariant at one end, which eliminates the restitution dependent mechanism of alternans at this end. Due to conduction delays, at the distal end, both restitution dependent and independent mechanisms manifest. Action potentials recorded from right ventricular endocardial tissue from swine (n=3) showed an average difference in amplitudes of alternans between the two ends to be 11.99, 25.49, and 39.37 msec. Rates of change of alternans amplitude as a function of

distance, computed using linear interpolation, were 0.36, 1.69 and 0.97. We propose that this rate of change may provide an indirect measure of degree of contribution of restitution to alternans and thus may be useful in evaluating therapeutic approaches to minimize its amplitude.

INTRODUCTION

Sudden cardiac death is caused by lethal arrhythmias. Despite extensive investigation, the mechanisms that lead to destabilizing of the rhythm into these arrhythmia remain unclear. A peculiar observation is that beat by beat alteration in action potential characteristics, which is manifest in the ECG as beat by beat alteration of T wave shape, is associated with incidence of sudden cardiac death, especially in those with systolic dysfunction, and possibly in other situations as well (1). This beat by beat change in shape of T wave is referred to as the T wave alternans (TWA), the cellular level origin of which is alternans of action potential duration (APD). The mechanisms underlying this behavior, which is period doubling bifurcation, have been the subject of extensive investigation.

A putative mechanism is restitution of APD. Restitution, in its widely defined sense, is a function that relates an APD to the interval preceding this action potential when the cells are at resting potential, which is referred to as the diastolic interval (DI). A hypothesized predictor of alternans is a steep slope of the restitution function (2-4). Decreasing the slope of this restitution function has been proposed as an anti-arrhythmic target (2). Although the theory behind the predicted role of restitution in alternans of APD and in arrhythmia has received extensive attention, there have been studies which show that this link is not always observed in experiments. For example a recent study by Narayan et al (1) found that the slope of restitution was not predictive in terms of TWA and arrhythmia. We have previously shown that the mechanisms by which alternans of APD occur have restitution dependent and independent components, the

restitution independent component can be separated and, importantly, the DI dependent restitution is not a necessary condition for alternans to exist (5). However, a change in DI does cause a change in APD, and thus it becomes important to determine the extent to which restitution contributes to alternans. One way to determine the contribution of DI dependent restitution to a change in APD is to use the slope, i.e. gain, of the function that relates an APD to preceding DI at the operating point. Virtually all previous investigations of stable alternans used protocols that employed constant cycle length pacing or combination thereof. Because the cycle lengths are constant, determination of the slope of restitution during stable alternans does not produce meaningful quantities because this slope is always equal to 1. We propose a new approach to determine the contribution of restitution to alternans of APD. We have previously developed a pacing protocol which allows one to explicitly control DI during pacing (6, 7). When this protocol is used to pace such that DIs for successive beats are invariant, the restitution dependent mechanism is eliminated. If a linear strand of tissue is paced such that at one end the DIs are maintained invariant, then the train of activations that travel from the pacing site to the other end, i.e., distal site, will experience effects of conduction delay which will bring about a graded change in DI as a function of increasing distance from the pacing site. Thus the DI dependent component of restitution will contribute to the amplitude of alternans in a graded fashion, with being eliminated at the pacing end and maximal at a location where alternans have the maximal amplitude. We consider that the rate of change of alternans amplitude as a function of distance, therefore, should provide a measure of the degree to which restitution contributes to alternans. In the present study, we demonstrate the feasibility of the proposed approach.

METHODS

A. Diastolic Interval Control:

We implemented a previously developed DI control protocol in a custom program written in LabVIEW. Details of the control protocol are described elsewhere (6, 7), briefly: the transmembrane potentials were sampled on-line and using a threshold crossing method, end of an action potential was determined on-line in real-time. Upon detection of end of an action potential (defined as recovery to 90% of total depolarizing potential), a timer was started to wait a pre-defined interval, at the end of which the next stimulating pulse was delivered. Thus, these pre-defined intervals become the DI for the subsequent activations.

B. Experimental Setup

Animal experiments were conducted after obtaining approval from the Institutional Animal Care and Use Committee (IACUC) at the University of Kentucky. A narrow strip of right ventricular tissue from swine (n=3) was placed in a tissue chamber and superfused with modified Tyrodes solution bubbled with 95% O_2 + 5% CO_2 gas mixture (7). Standard glass microelectrodes were used to record transmembrane potentials (TMP) from the endocardial side of the tissue. Two micro-electrodes were impaled at the two ends of the tissue. Figure 1 shows a schematic of the experiment. In each trial, the tissue was electrically stimulated from one end and DI control was engaged using a feed-back based pacing protocol using the TMP recorded from that end. The DI was controlled to be beat by beat invariant for 150 beats, while TMPs were recorded from both electrodes. In subsequent trials, stimulation was switched to pace the tissue from the other end with the TMP from the electrode closest to the stimulating electrode used in feedback control. The DI control protocol was then repeated. The TMP from both electrodes were continuously digitized at a rate of 10000 samples/second using a commercial data acquisition system. All data were digitally filtered by using a low-pass filter with a cut-off frequency of 500 Hz. From the digitized and filtered data APD were calculated as the duration within which

the membrane potential returned to 90% (i.e. APD_{90}) of the maximal change in potential from the start of that action potential using a fixed threshold. Amplitude of alternans was computed as the absolute difference between APD_n and APD_{n-1}. A digital image was used to quantify approximate distance between impalements.
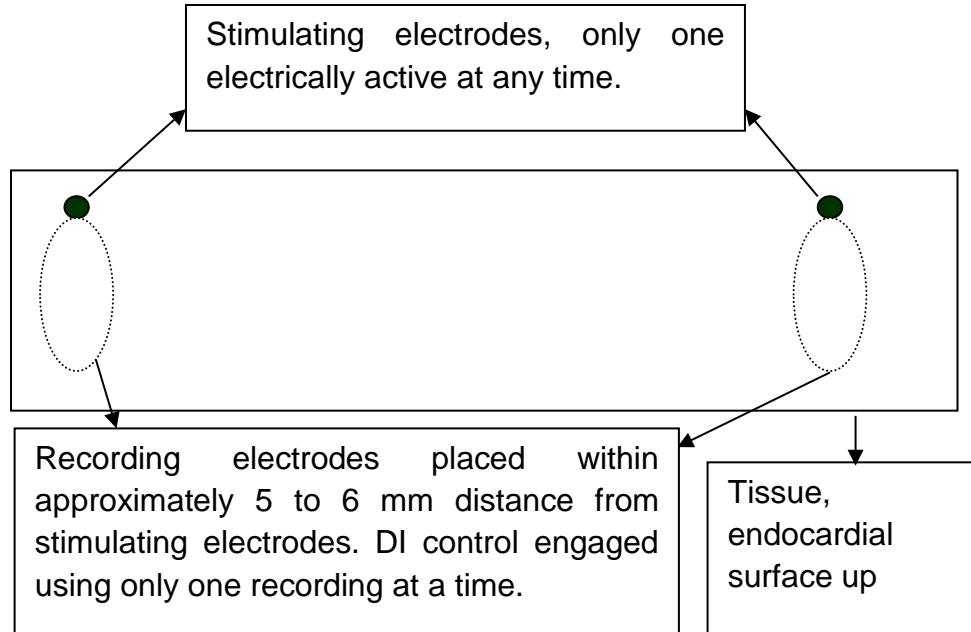
Figure 1: Schematic of a linear strand of tissue showing the arrangement of stimulating and recording electrodes.

RESULTS

Figure 2, shows an example of TMPs recorded from two ends of tissue. The TMPs show that the DI was controlled for successive beats at the pacing site. The figure shows that while at the pacing site the DIs preceding each action potential were nearly invariant, at the distal site; the oscillations in DI were large. The amplitude of alternans of APD at the pacing site was small compared to that at the distal site indicating increased DI dependent contribution of restitution.

To determine contribution of DI dependent restitution at the pacing and the distal sites we computed instantaneous slopes, i.e. ratios of beat-by-beat changes in APD divided by changes in preceding DI. Effective DI control was considered when absolute change in beat by beat DI was less than 4 msec for 10 or more successive beats. Similarly, an absolute change greater than 4 msec in amplitude of APDs for 10 or more successive beats was considered as occurrence of APD alternans. It is technically difficult to explicitly control short DIs for large number of beats; therefore, we selected sections of 10 or more successive beats meeting the above criteria in any trial to compute alternans amplitudes and instantaneous slopes. Results were first averaged from multiple trials within each animal, which includes pacing from either end, and then were averaged across the 3 animals.

Transmembrane potential trace
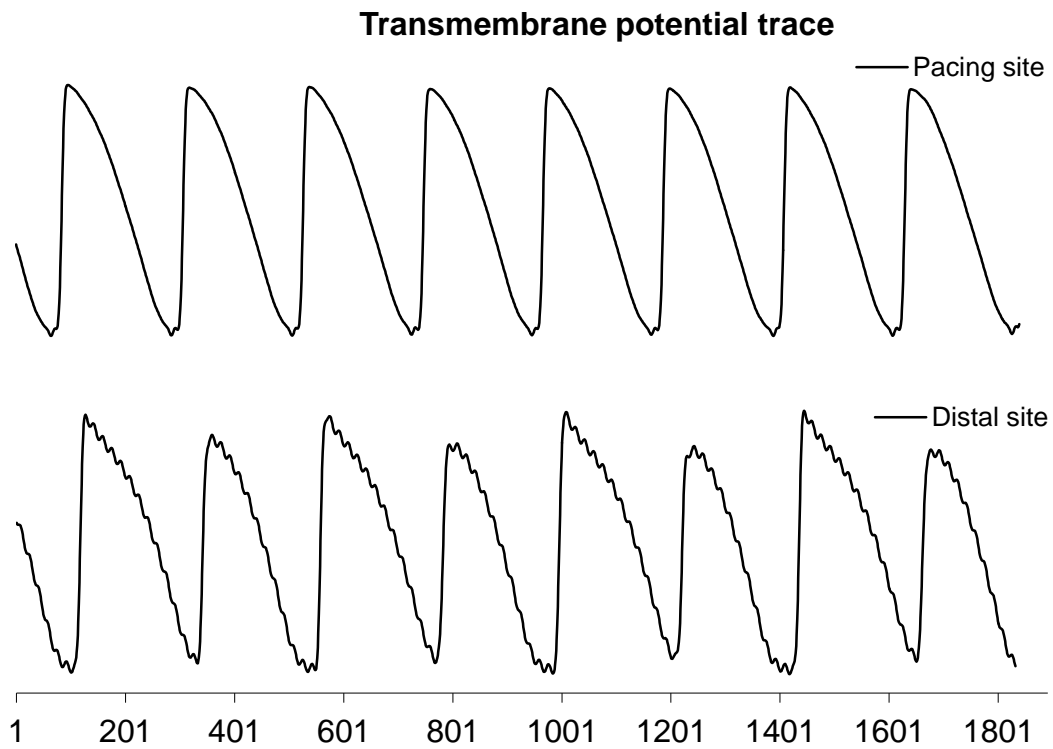
Figure 2: Example of TMP recorded from the two ends of a linear strand of tissue. The DI was made nearly invariant for successive beats at the pacing site. Alternans of larger amplitude are clearly seen at the distal site.

Figure 3 shows histograms of instantaneous slopes (ΔAPD/ΔDI) computed from the TMPs recorded at the pacing and the distal sites. When computing slopes, if the change in DI was numerically zero we set those slopes equal to the maximum range used in computing these histograms, which was $\pm$ 10. The figure shows that the slopes at the distal end were all concentrated in the bin with a center value of 1, very similar to the situation observed during constant cycle length pacing. The slopes at the pacing end were more widely distributed which reflects the fact that contribution from restitution was effectively abolished at this end, as expected. The peaks in the histograms within the two bins with center values of $\pm$ 1 are a result of ratios of two similar small numbers, i.e., a small change in APD divided by a nearly equal small change in DI.
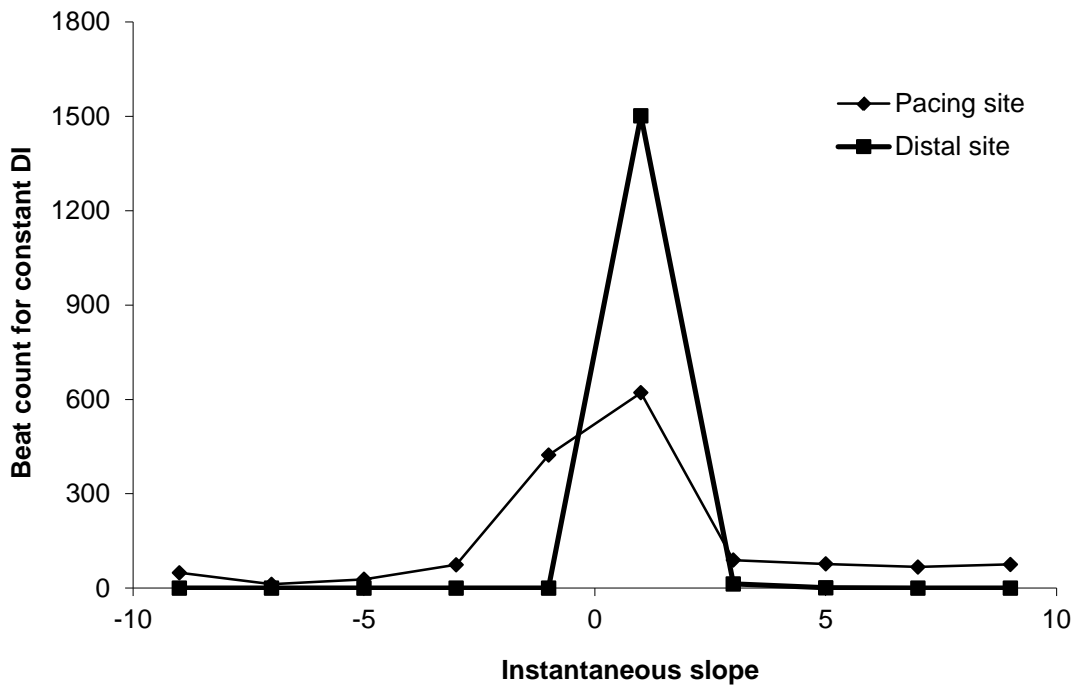
Figure 3: Histogram of instantaneous restitution slopes. The data points are plotted at the central value of each bin. At the pacing site, the instantaneous slopes were distributed over a wide range whereas at the distal site, the slopes were distributed over a much narrower range centered at 1.)

The average difference in alternans amplitude between the paced and the distal ends was 11.99, 25.49, and 39.37 msec for the three animals. The approximate distances between the impalements were 33, 15 and 35 mm. Assuming a linear change in alternans, we computed the rates of change in alternans amplitude as a function of distance to be 0.36, 1.69 and 0.97 msec/mm, with an average value of 1.01 msec/mm.

CONCLUSIONS

Restitution of APD contributes to alternans of APD, i.e. to the period doubling bifurcation. Although the presence of restitution independent component suggests it may not be possible to completely eliminate alternans by flattening restitution, it may be possible to minimize its amplitude. In order to determine how much decrease is likely to result from altering restitution, it becomes important to determine how much restitution contributes to alternans. We posit that the rate of change of alternans amplitude as a function of distance may provide such an estimate. While further studies are required to determine whether this rate of change does provide contribution of restitution, our results suggest that it may do so and show that the approach is feasible. The change in alternans amplitude as a function of distance has been previously reported by Fox et al (8) using constant cycle length pacing. It is possible to obtain rate of change of amplitude using constant cycle length pacing also, an advantage of the proposed approach is that it also provides an estimate of the non-restitution dependent contribution to alternans. In constant cycle length pacing approach, there are nodes along the distance where alternans of APD (and thus of DI) are eliminated i.e. amplitude of alternans increases and decreases along the distance. If these nodes are stationary in time and space, then it may be possible to obtain rates of change similar to the proposed approach. Because we just had two impalements, it is not possible to determine which phase of the alternans change the recordings were made, which may have contributed to the differences in the slopes (msec/mm) that we estimated. Obtaining more TMP

measurements along the tissue will be needed to fully address this issue. However, the marked difference in the histograms of slopes at the two ends suggest that the rate of change of alternans amplitude has the potential to be useful in determining contribution of restitution and thus may be helpful in evaluating potential therapeutic approaches.

REFERENCES

1. Narayan SM, Franz MR, Lalani G, Kim J, Sastry A. T-wave alternans, restitution of human action potential duration, and outcome. J Am Coll Cardiol 2007; 50(25):2385-2392.
2. Gilmour RF, Jr. A novel approach to identifying antiarrhythmic drug targets. Drug Discov Today 2003; 8(4):162-167.
3. Koller ML, Riccio ML, Gilmour RF, Jr. Dynamic restitution of action potential duration during electrical alternans and ventricular fibrillation. Am J Physiol 1998; 275(5 Pt 2):H1635-1642.
4. Kalb SS, Dobrovolny HM, Tolkacheva EG, Idriss SF, Krassowska W, Gauthier DJ. The restitution portrait: a new method for investigating rate-dependent restitution. J Cardiovasc Electrophysiol 2004; 15(6):698-709.
5. Wu R, Patwardhan A. Mechanism of repolarization alternans has restitution of action potential duration dependent and independent components. J Cardiovasc Electrophysiol 2006; 17(1):87-93.
6. Patwardhan A, Moghe S. Novel feedback based stimulation protocol shows hysteresis in cardiac action potential duration restitution. Biomed Sci Instrum 2001; 37:505-510.
7. Wu R, Patwardhan A. Restitution of action potential duration during sequential changes in diastolic intervals shows multimodal behavior. Circ Res 2004; 94(5):634-641.
8. Fox JJ, Riccio ML, Hua F, Bodenschatz E, Gilmour RF, Jr. Spatiotemporal transition to conduction block in canine ventricle. Circ Res 2002; 90(3):289-296.

APPENDIX C

Phase Relationship between Alternans of Early and Late Phases of Ventricular Action Potentials

Anuj Agarwal[ᵗ], Linyuan Jing[ᵗ], Sonam Chourasia and Abhijit Patwardhan

[ᵗ] Anuj Agarwal and Linyuan Jing have contributed equally to this work.

ABSTRACT

Alternans of early phase and of duration of action potential (AP) critically affect dispersion of refractoriness through their influence on conduction and repolarization. We investigated the phase relationship between the two alternans and its effect on conduction. Transmembrane potentials recorded from ventricles of eight swine and three canines during paced activation intervals of ≤300 ms were used to quantify alternans of maximum rate of depolarization ($|dv/dt|_{max}$) and of action potential duration (APD). Incidence of APD alternans was 62 and 76% in swine and canines. Alter- nans of APD was frequently accompanied with alternans of $|dv/dt|_{max}$. Of these, 4 and 26% were out of phase in swine and canines, i.e., low $|dv/dt|_{max}$ preceded long APD. Computer simulations show that out of phase alternans attenuate variation of wavelength and thus minimize formation of spatially discordant alternans. The spontaneous switching of phase relationship between alternans of depolarization and repolarization suggests that mechanisms underlying these alternans may operate independent of each other. The phase between these alternans can critically impact spatial dispersion of refractoriness and thus stability of conduction, with the in phase relation promoting transition from concord to discord while out of phase preventing formation of discord.

INTRODUCTION

Beat-to-beat variation in action potential (AP) morphology is termed as alternans. Several studies suggest that alternans of repolarization, i.e., of action potential duration (APD), play an important role in mechanisms of ventricular fibrillation (VF; Koller et al., 1998; Fox et al., 2002; Banville et al., 2004). Spatial dis- cord in alternans of APD is particularly conducive to initiation of arrhythmia (Qu et al., 2000), presumably, because of the increase in dispersion of repolarization. Transition of concord (where the alternating pattern is same everywhere) to discord is partly influenced by conduction (de Diego et al., 2008; Mironov et al., 2008). More recently, supernormal conduction (SNC), i.e., where a wave with shorter wavelength has faster velocity, has been shown to promote concordant alternans (de Diego et al., 2008; de Lange and Kucera, 2010). SNC is characterized by a negative slope of conduction velocity (CV) restitution, which is typically obtained using a S1S2 protocol. In addition to the cell to cell coupling, conduction is critically affected by maximum rate of depolarization ($|dv/dt|_{max}$). Consequentially, there has been a renewed interest in alternans of the early phase of an AP, i.e., of depolarization (Karagueuzian et al., 1993; Lalani et al., 2008). Our objective in this study was to investigate the phase relationship between alternans of repolarization and of depolarization, and to determine how this phase relationship may affect formation of concord and discord. The ionic mechanisms governing early and later parts of an AP are distinct but interlinked. We hypothesized, therefore, that alternans in early and late parts of an AP, i.e., alternans of $|dv/dt|_{max}$ and of APD, although correlated most of the time, could operate independently. Further, because of the interplay between the speed of a conducted AP (CV) and recovery from previous activation, the phase relationship between the two will impact conduction of APs importantly. Our results show that while these two alternans are frequently correlated, the phase relationship between the two does change. Simulations show a mechanism by which the phase relationship between the two affects generation of spatial discord in repolarization. These results suggest that the phase relationship between

alternans of early phase of AP and of APD plays an important role in stability of activation.

MATERIALS AND METHODS

All animal studies were approved by the Institutional Animal Care and Use Committee (IACUC) at the University of Kentucky. Data were collected from eight farm pigs (18–21 kg) and three dogs. For swine, animals were anesthetized using a combination of telazol (4–8 mg/kg), ketamine (2–4 mg/kg), and xylazine (2– 4 mg/kg), followed by thiopental sodium (Pentothal, 10–11 mg/kg, IV). After anesthesia, the hearts were rapidly excised and placed in cold Tyrode's solution. A small piece of ventricular tissue, approximately 20 mm × 10 mm × 5 mm, was isolated and pinned in a plastic chamber and superfused with warmed (36 ± 1˚C) Tyrode's solution bubbled with a mixture of 95% O_2 and 5% CO_2. Composition of the Tyrode's solution was (in mmol/L): 0.5 $MgCl_2$, 0.9 NaH_2PO_4, 2.0 $CaCl_2$, 137.0 NaCl, 4.0 KCl, and 5.5 glucose. To this solution, $NaHCO_3$ was added until the pH was between 7.3 ± 0.05. Tissue samples were obtained from the mid to apical anterior-lateral region of right ventricular free wall. Transmembrane potentials (TMP) were recorded from the endocardial side. Samples were equilibrated for about 60 min while being paced at a cycle length (CL) of 500 ms using 3 ms wide biphasic stimuli with intensities three to four times the diastolic threshold. Glass microelectrodes, filled with 3 M KCl solution, were used to record TMP. Non-alternans related data collected from six swine have been reported previously (Jing et al., 2010). Data from only those trials where APs observed during the preceding 500 ms CL pacing did not display obvious signs of ischemia, i.e., were not of triangular shape, were used for further analyses. For canines, we analyzed data collected as a part of a previous study (Wu and Patwardhan, 2006). Details of the experimental proto- col used for canines are provided elsewhere (Wu and Patwardhan, 2006), however, they were similar to that described above for the swine, i.e., TMPs were recorded using microelectrodes from endocardial side of superfused right ventricular tissues. Not

76

all TMP recordings from canines that we analyzed for the present study were used in the results reported previously (Wu and Patwardhan, 2006).

The TMP were digitized using a commercial data acquisition system at a rate of 10,000 samples/s and were analyzed offline using custom developed code in Matlab (MathWorks, Natick, MA, USA). In two pigs, we collected data at 50,000 samples/s to verify that the computed $|dv/dt\,|_{max}$ values were not affected by sampling rates. In order to quantify frequency of incidence of alternans we analyzed data from trials where the average activation intervals (i.e., the sum of diastolic interval, DI, and preceding APD) were ≤300 ms. A trial, in this context, refers to one continuous recording of TMP from the beginning to the end of a pacing protocol. The pacing stimuli were delivered either with fixed CL, i.e., the activation intervals were constant, or with fixed DI, i.e., the DIs preceding each AP were held constant by using a feed-back based pacing proto- col as described before (Wu and Patwardhan, 2006). Although for the purposes of the present study, control of DI was not germane, a difference between fixed CL and fixed DI is noteworthy: under fixed DI pacing, alternans of APD lead to alternans of CL; likewise, during fixed CL, alternans of APD lead to alternans of DIs.

All analyses were conducted offline: TMPs were lowpass filtered (cutoff 1000 Hz) and start of each AP was determined using the slope of lowpass filtered TMP as the instant at which the slope became positive. End of an AP was determined when the TMP repolarized to 90%. During analysis, these markings were identified by color coded symbols and were manually inspected for each AP. A change of alternating sign between successive differences in APD ≥4 ms for at least five consecutive beats was considered as occurrence of APD alternans. The threshold of 4 ms change is consistent with that used previously by others (Pruvot et al., 2004).

The $|dv/dt\,|_{max}$ was computed when APD alternans occurred. To minimize high frequency amplification during differentiation, we used a 10 point combined lowpass and differentiation fil- ter implemented using the "smooth_diff.m" function in Matlab. Because of the "built-in" filtering, the smoothed differentiation was

77

computed from non-lowpass filtered TMPs. Alternans of $|dv/dt|_{max}$ was considered out of phase with APD alternans if large $|dv/dt|_{max}$ was associated with short APD and in phase if large $|dv/dt|_{max}$ was associated with long APD.

We note that statistical analysis, i.e., estimating odds of an event happening by chance, of the results that we obtained was not necessary to meet the objectives of our study, which were to determine the frequency of occurrence of an event, e.g., out of phase relationship, and to determine what impact it may have on conduction of an impulse.

We simulated the effects of phase relationship on conduction in a linear strand of 1000 cells using the canine ventricular myocyte (CVM) mathematical model, developed by Fox et al. (2002), with parameters as given in reference (Hua and Gilmour, 2004) to simulate discordant alternans. Custom code developed in Fortran was used to implement the model. The simulated cells had a cell length of 200 μm and membrane capacitance of 1 μF/cm2. Cell to cell coupling was modeled using diffusion (diffusion coefficient = 0.0007 cm2/ms). No-flux boundary conditions were used on the ends.

The strand was paced at one end (cell 5) with a CL of 169 ms for 90 beats to obtain steady state. Each simulation was run for additional 90 beats following the steady state obtained as described above. Our objective was to determine the effects of the change in phase, therefore, to simulate phase change, we increased the sodium current I_{Na} for all cells based on a "one step ahead" pre-diction of APD for each cell. That is, a change in APD from two previous activations was used to predict whether the "about to begin" AP was going to have a long or short duration. The default relation between APD and $|dv/dt|_{max}$ at CL of 169 ms is in phase, therefore, no current change was applied to produce the in phase relationship. To simulate out of phase, we increased I_{Na} of the short AP by 80%. We chose this magnitude of change in I_{Na} because this change produced alternans of comparable magnitude at the paced cell (cell 5) between the in and out of phase trials. Traces of TMPs and of I_{Na} from different sites in the linear strand were analyzed to confirm that the imposed current change was as

expected. From simulations, APD and $|dv/dt|_{max}$ were computed using the same approach as that used for experimental data.

In order to quantify the oscillation of wavelength, we used a threshold method to compute the wavelength as follows: the membrane potentials of all cells for 90 beats were stored in a 2-D matrix V (i, j), where i represents spatial distance (or cell number) and j represents time (ms). Threshold V 0 was defined as the voltage at 90% repolarization. The potential matrix V was then converted to an index matrix I with ones [if an element V (i, j) ≥ V 0] and zeros [if V (i, j) < V 0], and the spatial derivative of index matrix I, i.e., matrix D was created. At any given time instance t, the wavefront anywhere was defined when D (i, t) = −1, and the wave end as D (i, t) = 1. Therefore, wavelength was computed as the distance (in number of cells) between the wavefront and wave end. Mean wavelength and coefficient of variation (COV), defined as standard deviation divided by mean wavelength, was computed for each wave and the average of these for all waves was used as an estimate of wavelength oscillation in a given simulation.

RESULTS

ALTERNANS OF $|dv/dt|_{MAX}$ AND APD IN CANINES

In 56 trials (n = 3), all with CL ≤300 ms, incidence of APD alternans was 76% and they were always accompanied with alternans of $|dv/dt|_{max}$. Figure 1B shows an example of the relationship between $|dv/dt|_{max}$ and CL obtained using stepwise decreasing CL pacing. As CL decreased, $|dv/dt|_{max}$ also decreased. An example from a trial of the in phase relationship between $|dv/dt|_{max}$ and APD alternans is shown in Figure 2 (closed diamonds), and an example of out of phase relationship is shown by the open circles in Figure 2, i.e., long APD was associated with slower rate of depolarization and short APD was associated with faster rate of depolarization. The incidence of out of phase $|dv/dt|_{max}$ alternans was 26% with 74% in phase. The average amplitude of $|dv/dt|_{max}$ alternans was

79

10%. Figure 3 shows an example of a continuous 20 AP sequence of in phase (Figures 3A–C) and out of phase (Figures 3D–F) relationship between alternans of APD and $|dv/dt|_{max}$. Both APD (Figures 3A, D) and $|dv/dt|_{max}$ (Figures 3B, E) traces show a beat-to-beat alternating pattern. The overlay of APD and $|dv/dt|_{max}$ (Figures 3C,F) clearly show that, during in phase, a change in APD is accompanied by change of $|dv/dt|_{max}$ in the same direction, while for out of phase, these two change in opposite directions for the same AP. We note that these are conducted APs in tissue and that the shapes of APs change remarkably at faster activation rates compared to what is seen during slower activation. As has also been previously reported by others (Omichi et al., 2000; Rubart et al., 2000; Huang et al., 2004, 2007), at faster activation rates (note the very short activation intervals in the figure), the upstroke velocity was decreased, the peak and the notch was blunted due to loss of I_{to}, the plateau phase nearly disappeared and the APs generally displayed a triangular-like shape. These changes in shapes of APs are an expected effect of faster activation rates.
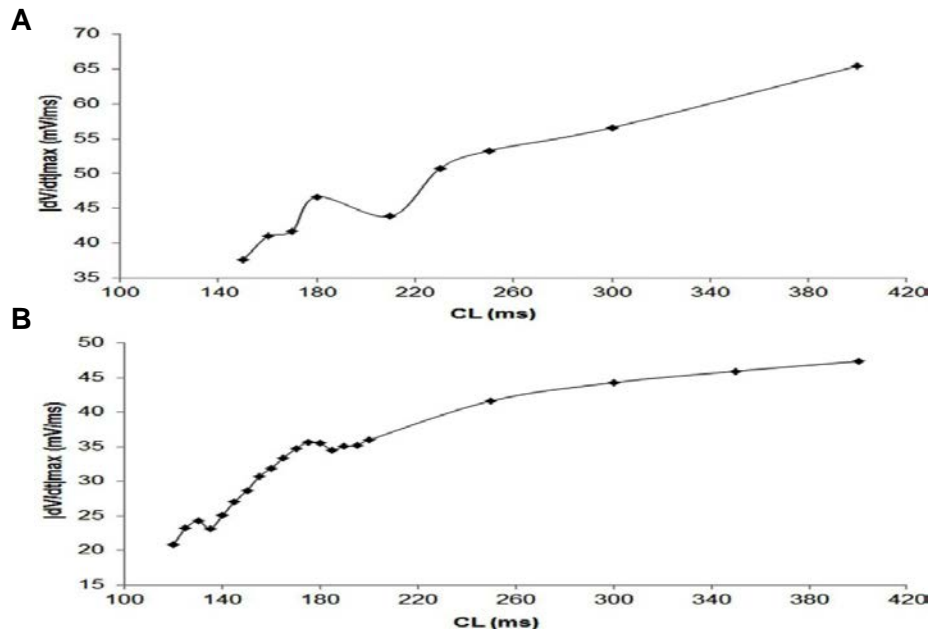
Figure 1: Dependence of $|dv/dt|_{max}$ on CL during a trial in swine (A) and canine (B) obtained using stepwise decreasing CL pacing.
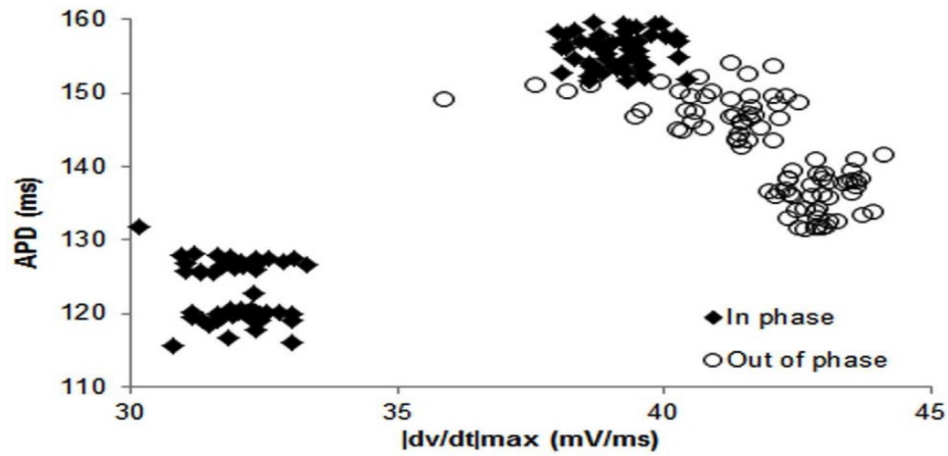
Figure 2: Examples of data from a trial in canines showing in phase (closed diamonds) and out of phase (open circles) relationship between APD and its preceding $|dv/dt|_{max}$, i.e., APD and $|dv/dt|_{max}$ for the same beat. These data were obtained using constant CL pacing.

ALTERNANS OF $|dv/dt|_{MAX}$ AND APD ALTERNANS IN THE SWINE

In 27 trials (n = 8), all with activation intervals ≤300 ms, we observed that the incidence of APD alternans was 62%. Alternans of $|dv/dt|_{max}$ occurred for all APs when APD alternans occurred. Figure 1A shows an example of the relationship between $|dv/dt|_{max}$ and CL. As expected, $|dv/dt|_{max}$ decreased as the activation intervals decreased, i.e., the CL decreased. Similar decrease in $|dv/dt|_{max}$ as a function of decreasing CL has also been reported in the swine by Huang et al., 2007 (their Figure 2). When APD alternans occurred, incidence of out of phase $|dv/dt|_{max}$ was 4%, with 96% in phase. The average amplitude of $|dv/dt|_{max}$ alternans was 13%. Figure 4 shows an example of continuous recording of in phase (Figures 4A–C) and out of phase (Figures 4D–F) APD alternans with $|dv/dt|_{max}$ alternans, similar to that in canines (Figure 3).

81
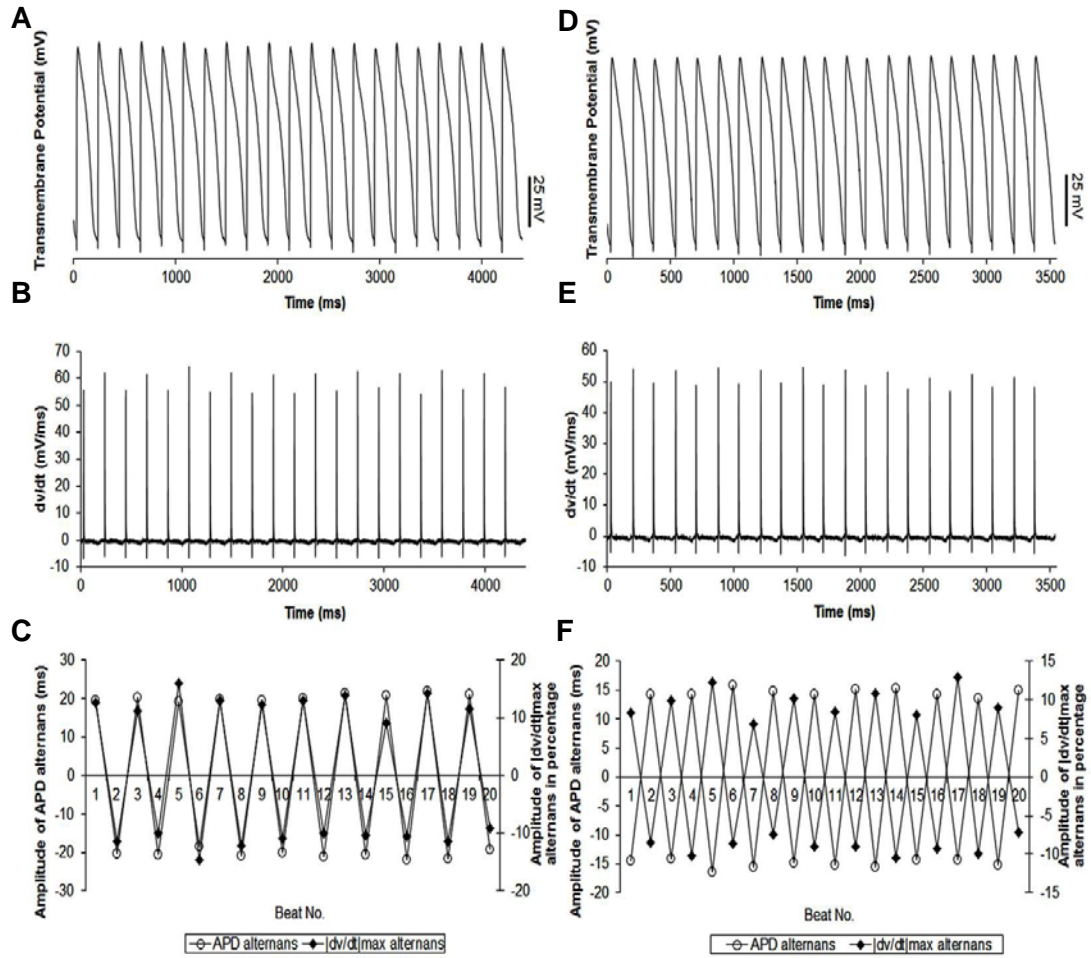
Figure 3: Example of continuous recordings, during constant CL pacing, showing in phase (A–C) and out of phase (D–F) relationship between APD and $|dv/dt|_{max}$ alternans in canines. Both APD (A, D) and $|dv/dt|_{max}$ (B, E) traces display beat-to-beat alternating patterns. (C, F) Show overlays of APD alternans (open circle) and alternans of $|dv/dt|_{max}$ (closed diamonds). In this example, average amplitudes of APD alternans were 20.4 ms for in phase (C) and 14.8 ms for out of phase (F). Average amplitudes of $|dv/dt|_{max}$ alternans were 11.9% (C) and 9.3% (F) respectively.
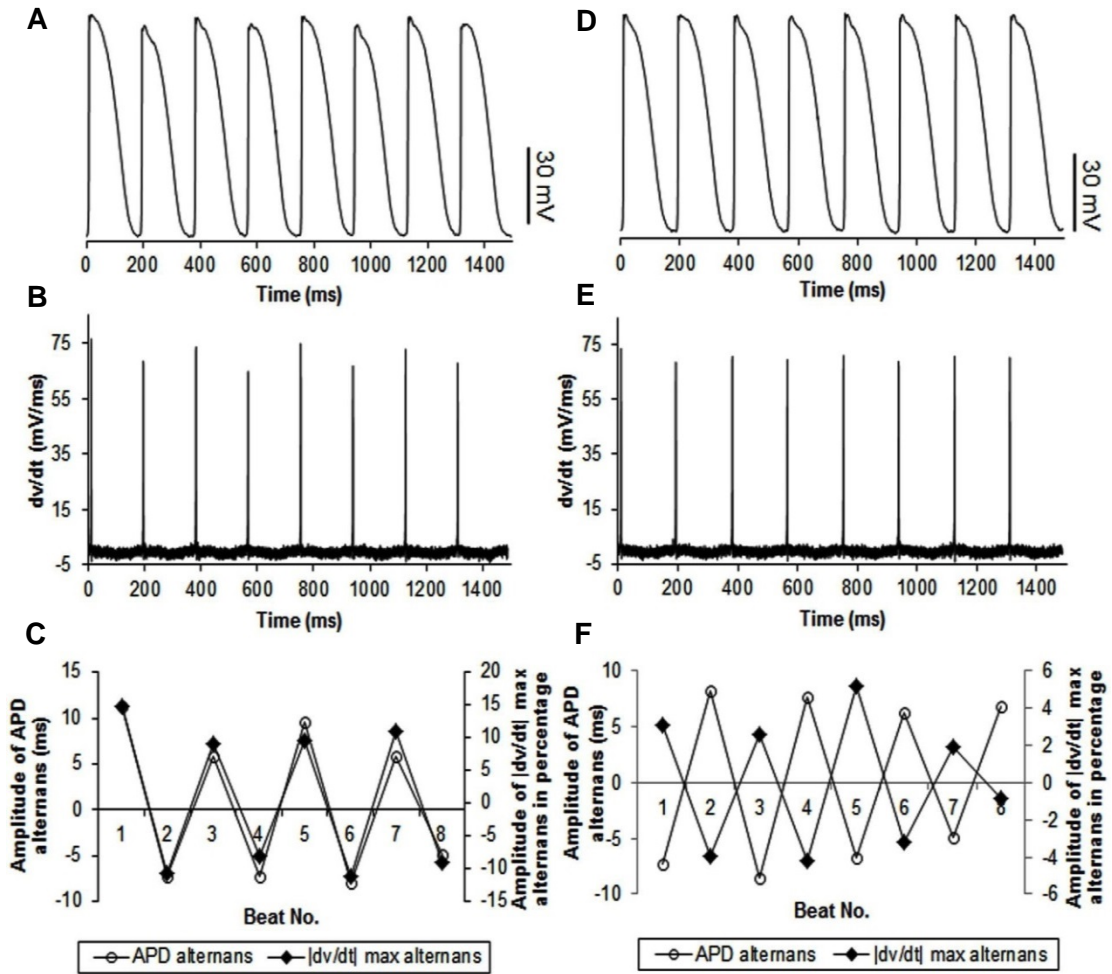
Figure 4: Example of continuous recordings, during constant CL pacing, showing in phase (A–C) and out of phase (D–F) relationship between APD and |dv/dt|$_{max}$ alternans in swine. The format is the same as in Figure 3. Note that the stimulus artifact for each action potential was blanked to better show |dv/dt|$_{max}$ alternans.

SIMULATED ACTIVATION IN A LINEAR STRAND OF CELLS

To explore possible effects of phase change between alternans of $|dv/dt|_{max}$ and APD alternans on conduction of an impulse, we simulated activation in a linear strand of 1000 cells. Before starting the imposed current change, we ran the simulation for 90 beats to reach a steady state, which produced discordant alternans at the chosen CL (169 ms). The simulation was continued for another 90 beats with (without) I_{Na} change to produce and compare the effects of out of phase (in phase) on conduction. Figure 5 shows the time-space plots for the last 90 beats of simulation during in phase (Figures 5A–C) and out of phase (Figures 5D–F) relationship between alternans of APD and $|dv/dt|_{max}$. Each panel successively represents data from 30 beats of simulation. When alternans of $|dv/dt|_{max}$ was in phase with APD alternans (Figures 5A–C), APD alternans transitioned into discord after about 100 cells, and several nodes were formed along the length of the tissue. Vertical lines drawn on the time-space plots (Figures 5C, F) show that the wavelength, which is the product of APD and CV, oscillated along the length of the strand. However, with a similar amplitude of APD alternans at the paced cell (64.4 ms for in phase vs 63.2 ms for out of phase, Table 1), during out of phase (Figures 5D–F), the originally formed discordant alternans were gradually eliminated by the out of phase relationship and totally disappeared after about 50 beats. After that, APD alternans remained concordant throughout, and there were no oscillations of wavelength. Results of simulation are summarized in Table 1. These time-space plots are similar to those reported by Echebarria et al., 2011 (their Figure 3) with SNC, suggesting that the supernormal CV observed by them and the out of phase $|dv/dt|_{max}$ alternans may share similar mechanistic pathways.

In Phase

Out of Phase

A

B

C

D

E

F

G In phase

25 mV

200 ms

Ito (pA/pF)

H Out of phase

25 mV

200 ms

Ito (pA/pF)

85
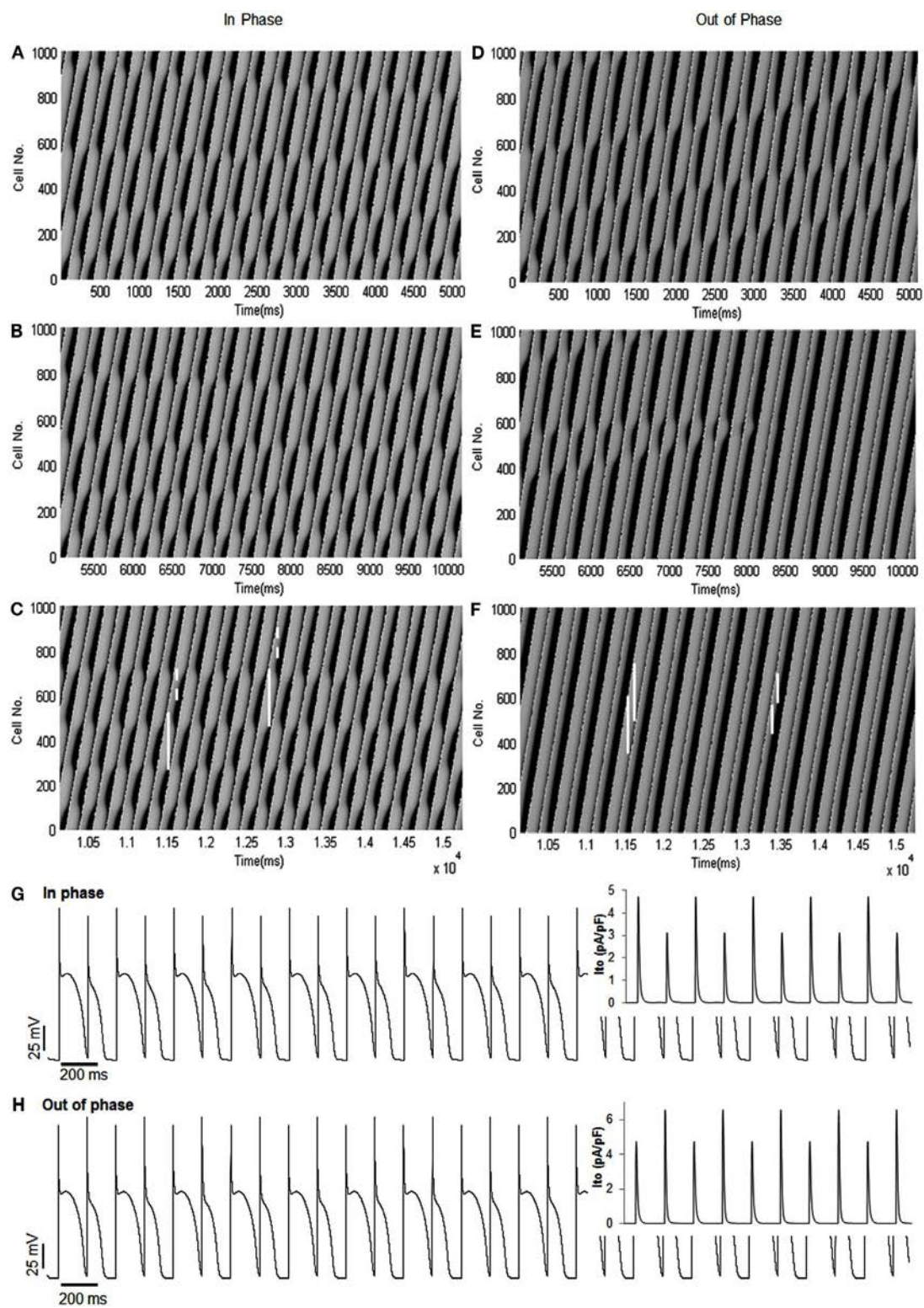
Figure 5: Time-space plots of simulated in phase and out of phase relationship between APD alternans and alternans of $|dv/dt|_{max}$. (A–C) Ninety beats of in phase $|dv/dt|_{max}$ with APD alternans, shown in three sections (30 beats for each panel). The figure shows that the transition between concordant and discordant alternans occurred several times. The vertical white lines (solid and dashed) show wavelengths (long and short, respectively) at different time instances. Note the pronounced spatial oscillation in wavelength. (D–F) Ninety beats of out of phase $|dv/dt|_{max}$ with APD alternans. The figure shows that the discordant alternans produced by the initial conditions were removed progressively by the out of phase relationship, and concordant alternans persisted along the tissue afterward. Compared to (A–C), the change in wavelength was minimal. (G, H) Show the TMP traces at the paced cell (cell 5) for the last 30 beats, corresponding to (C, F), respectively. In [(G,H); inset] are traces of Ito current for the last 10 APs which show that, as expected, Ito mimics changes in $|dv/dt|_{max}$.

Table 1: Summary of results of simulated activations

Phase relationship			Cell 5	Cell 100	Cell 200	Cell 400	Cell 600	Cell 800	Cell 980
In phase APD vs |dv/dt|max	APD (ms)	Odd beat	155.8	125.9	93.6	154.7	97.5	155.7	149.5
		Even beat	91.4	137.5	155.6	97.8	155	94.4	117.4
	ΔAPD (ms)		64.4	−11.6	−62	56.9	−57.5	61.3	32.1
	|dv/dt|max	Odd beat	184.5	126.4	114	128.8	116.2	129.6	129.3
	(mV/ms)	Even beat	170.9	129.3	129	117.3	129.4	114	125.9
	Δ|dv/dt|max		7.96	−2.24	−11.63	9.80	−10.20	13.68	2.70
Out of phase APD vs |dv/dt|max	APD (ms)	Odd beat	155	157.4	158.1	158.2	157.8	158	156.9
		Even beat	91.8	86	80.5	80.3	80.2	80.1	82.7
	ΔAPD (ms)		63.2	71.4	77.6	77.9	77.6	77.9	74.2
	|dv/dt|max	Odd beat	184.5	128	129.8	130	128	128.8	128.6
	(mV/ms)	Even beat	197.4	135.8	120	117.9	118.5	118.6	124.9
	Δ|dv/dt|max		−6.99	−6.09	7.55	10.26	8.02	8.60	2.88

APD and |dv/dt|max values at different cells were computed as the average of the last 10 beats of the simulation for both in phase and out of phase relationship. ΔAPD was computed as the difference between the APDs of odd beats and even beats; the sign +/− represents concordant/discordant alternans. Δ|dv/dt|max was computed as the percent difference between odd and even beats, the sign +/− represents in phase/out of phase relationship with APD alternans.

Table 2: Mean wavelength (WL) and coefficient of variation (COV) computed for in phase and out of phase relationship.

Phase relationship			All beats	Beat 1–30	Beat 31–60	Beat 61–90
In phase	All beats	Mean WL	235.5	238.7	235.7	234.8
		COV	0.21	0.21	0.21	0.21
	Odd beats	Mean WL	244.0	247.3	245.8	238.9
		COV	0.21	0.21	0.21	0.21
	Even beats	Mean WL	227.3	225.6	225.5	230.7
		COV	0.21	0.23	0.20	0.20
Out of phase	All beats	Mean WL	254.8	268.1	253.2	245.0
		COV	0.12	0.22	0.11	0.02
	Odd beats	Mean WL	203.3	246.2	193.6	170.3
		COV	0.16	0.23	0.17	0.05
	Even beats	Mean WL	305.1	282.5	312.9	319.8
		COV	0.09	0.21	0.07	0.00

Mean WL (in number of cells) and COV was computed for each beat, and then the average was calculated for all beats, for odd and even beats separately, and over different sections (beats 1–30, 31–60, and 61–90).

In order to quantify the wavelength variation, we computed the wavelength at different time instances for each wave. The values of mean wavelength and COV for different waves are summarized in Table 2. The table shows that the COV was markedly reduced during out of phase (0.12) as compared to in phase (0.21). To better explore how the out of phase relationship progressively minimizes discord, the 90 beats of simulation were segmented into three 30 beat sections. As the discord decreased, the COV decreased from 0.22 (first 30 beats) to 0.02 (last 30 beats). Compared to in phase, the difference in mean wavelengths (in number of cells) between long and short beats for out of phase was more prominent, i.e., 244 and 227 vs 203 and 305, this difference was especially noteworthy during the last 30 beats (beats 61–90) when all discord was absent (238 and 230 vs 170 and 319) because of the reduced variation of wavelength during the out of phase (0.12 overall and 0.02 for the last 30 beats). Figure 6 shows the distribution of wavelength during the in phase and out of phase relationship. The overall distribution (Figures 6A, E) shows that the wavelengths for in phase were more widely distributed while during out of phase, they were more concentrated in two bins centered at 176 and 326 (cell numbers). As discordant alternans reduced with time, the distribution became more concentrated for out of phase (Figures 6F–H), how- ever, for in phase (Figures 6B–D), the distribution pattern nearly stayed the same throughout the simulation.
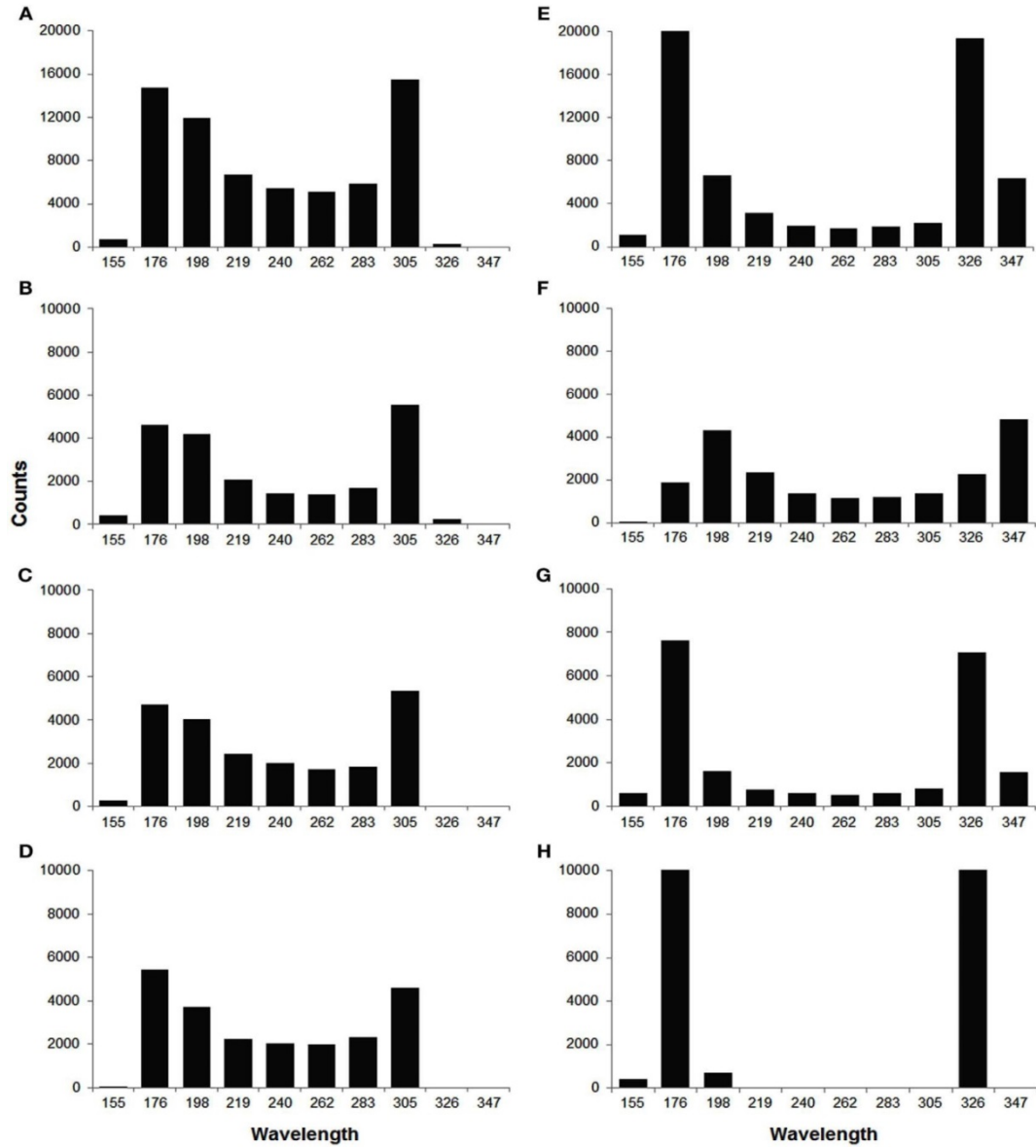
Figure 6: Histograms of wavelength distribution for in phase (A–D) and out of phase (E–H) relationship. (A, E) Show the overall wavelength distribution for all 90 beats. (B–D, F–H) Show the distribution in different sections (beat 1–30, 31–60, 61–90, from top to bottom), with 30 beats in each section. During in phase, the wavelength was more widely distributed between 150 and 350 (in number of cells), while during out of phase, it was more concentrated in two bins centered at 176 and 326, especially in the last section (H).

DISCUSSION

The primary results of our study show that the phase relationship between alternans in early and late phases of an AP is not invariant and that variations in the phase can have an important effect on conduction. Therefore, the phase relation may play a critical role in formation of discordant alternans and in dispersion of repolarization.

In the context of clinical utility of alternans, T wave alternans (the so called micro-volt TWA) is seen at high activation rates, i.e., at high heart rates. Likewise, APD alternans is also observed at high activation rates, which is why we focused only on TMP recordings made during high activation rates (CL ≤300 ms). We note again that the shape of an AP changes considerably as a function of increasing activation rates. Rubart et al. (2000) reported that during high activation rates, the transient outward potassium current I_{to}, which plays a dominant role in early phase of repolarization, is remarkably reduced. This expected decrease in I_{to} is the reason for the lack of distinct shape of phase 1 in our TMP traces all of which were obtained at high activation rates. The micro- electrode recordings of TMPs from swine, reported by Huang et al., 2007 (in their Figure 2) during fast pacing, also show rounded APs with a marked change in their shape. Similar changes have also been observed by others (Omichi et al., 2000, 2002; Banville et al., 2004; Huang et al., 2004). Therefore, the shapes of APs that we observed at short activation intervals are a consequence of fast activation rates. Further confirmation that the change in shape of APs was a result of fast pacing rate was provided by our observation that the shapes of APs recorded at a slower rate of 500 ms CL displayed sharp upstrokes, a notch and higher values of $|dv/dt|_{max}$ similar to those also reported at slower rates by Huang et al. (2007).

Huang et al. (2007) observed that during VF, $|dv/dt|_{max}$ was a dominant predictor of APD, but the regression coefficients between them were low. In the context of our results, the low coefficients observed by them suggest that the phase relation- ship between $|dv/dt|_{max}$ and APD may also be variable during VF. These results illustrate the role of depolarization phase in electrical instability along with

90

the repolarization phase. More directly, Gordon et al. (2010) showed that depolarization alternans along with repolarization alternans were important in predicting VF in an ischemic canine heart model.

Our rationale for investigating the phase relationships was twofold: (i) as shown by previous studies related to the initial rise of an AP upstroke (Fast et al., 1996; Spach et al., 1998; Kleber, 2005), the morphology of the early part of an AP, which is locally dictated by the recovery of sodium channels from inactivation (i.e., closed but available to open), contributes to the availability of depolarization charge in a connected tissue, and thus importantly affects conduction of an impulse and wavelength as also seen in our simulations. (ii) If the relationship between these alternans was invariant, then it is possible that a same mechanism underlies all facets of AP alternans, however, if the relationship was variable, that would suggest that different mechanisms may contribute to alternans of different phases of an AP. Although alternans of $|dv/dt|_{max}$ was mostly in phase with alternans of APD, the incidence of out of phase was not negligible. The percent incidence was low, however, considering the clinical observation of very low probability of any one activation degenerating into re-entry (compared to the total number of activations), the incidence of out of phase behavior is substantial. The critical impact of $|dv/dt|_{max}$ on CV, and CV being key in the transition from concordant to discordant alternans (Qu et al., 2000), provided rationale for investigating effects of the phase between $|dv/dt|_{max}$ and APD on dynamics of conduction. Results of simulations, in Figures 5 and 6 and in Tables 1 and 2, show that an out of phase relationship between these alternans minimizes the oscillations in wavelength and thus prevents discordant alternans. Assuming a cell length of about 200 μm, the length of the strand that we simulated is about 20 cm. Therefore, we consider that these results provide a global view of the effects of phase on the fate of a conducted impulse. We also note that the amplitudes of $|dv/dt|_{max}$ alternans that we simulated ranged from 2 to 14% and 3 to 10% (Table 1), similar to the amplitudes of experimentally observed alternans of $|dv/dt|_{max}$, which, when averaged over all occurrences of $|dv/dt|_{max}$ alternans in all animals, were 13 and 10% (swine and canines).

Mechanisms for discordant alternans have been linked to restitution of APD and of CV by several investigations (Qu et al., 2000; Weiss et al., 2000; de Diego et al., 2008; Mironov et al., 2008; de Lange and Kucera, 2010) and have been theoretically explained by Echebarria and Karma (2002, 2007) using amplitude equation approach. Alternating APD causes alternating I_{Na} amplitude and therefore (in phase) alternans of $|dv/dt|_{max}$. In case of in phase relationship, observed majority of the time, but not always, large $|dv/dt|_{max}$ associated with long APD results in faster conduction. The resulting decrease in preceding DI, in turn shortens the long APD, and slows propagation. Opposite process happens for the short APD, resulting in a spatial oscillation in wavelength and thus increase in the dispersion of refractoriness. On the other hand, for out of phase relationship, the long APD has a smaller leading $|dv/dt|_{max}$, therefore, the decrease in preceding DI does not occur due to slower (compared to the in phase situation) conduction, which suppresses oscillation of wavelength as shown in Figure 5 and Table 2. These observations are very similar to the results reported by Echebarria et al. (2011) in a recent study focused on SNC, where they observed that the transition to discordant alternans only happened in the case of normal conduction while during SNC, APD alternans always remains concordant. Their findings are consistent with our simulation results, whereby the in phase relationship between APD and $|dv/dt|_{max}$ alternans promoted discord while the out of phase relationship prevented it, suggesting a potential similarity between the effects of out of phase behavior and of SNC. Since $|dv/dt|_{max}$ is a primary cellular level variable that determines CV (in the absence of changes in gap junctional coupling) we consider that the out of phase behavior probably is the underlying mechanism of SNC in situations where SNC is observed to eliminate discord because of the following: during alternans, the out of phase behavior is caused due to an unexpected increase in sodium recovery (from inactivation) before the short AP, which leads to a higher rate of depolarization and thus faster conduction for the short AP as compared to the long AP. Faster conduction for the shorter AP (at faster rates, the AP resulting from S2 is shorter than the preceding AP from the last S1) then manifests into a negative slope for

the CV restitution. If the mechanism discussed above about suppression of discordant alternans holds, then slow conduction for a longer APD can lead to a continued increase in duration for the already long APD thus continued shortening of the short APD. However, all things being equal, as shown in Figure 5, for a length of simulated tissue that is of a size longer than a fiber that would span the ventricle, out of phase relationship minimizes wavelength oscillations. In a study by de Lange and Kucera (2010), SNC was shown to amplify the amplitude of APD alternans distal to the pacing site during alternant CL pacing, which is comparable to our results of the out of phase simulation (Table 1). As discussed in their paper, it is possible that the amplification of APD alternans could lead to a conduction block at a distal site. We also observed a similar increase; however, as discussed above, if a block were to happen, it would be at a site distal to the fiber length of 20 cm that we simulated. This length is longer than the dimension of the entire ventricle therefore, we hypothesize that the absence of discord resulting from out of phase behavior may be a stabilizing factor.

Table 1 shows that during out of phase simulations, the phase relationship that resulted between $|dv/dt|_{max}$ and APD was in phase for cell 200 and distal cells. Although seemingly in contrast to the imposed out of phase behavior, the reason for this switch was that even though we did increase the I_{Na} for the short AP, the decrease in preceding DI for the shorter AP resulted in a decreased availability of recovered I_{Na} and thus the decrease in I_{Na} was actually larger than the imposed increase of 80%. An opposite situation resulted in a spatially rapid increase in preceding DI (and thus of subsequent APD) for the longer APs during out of phase simulation because of decreased CV (the rapid change in APD from cell 1 to cell 200 followed by a much slower continued increase in APD). Once the DIs shortened sufficiently for the short AP, $|dv/dt|_{max}$ decreased (due to reduced I_{Na} for the short AP despite of the imposed 80% increase) which slowed conduction and thus slowed the decrease in DI and APD. However, it was interesting to observe that even though the out of phase behavior "switched" to in phase behavior for cells 200 and beyond, once the initial spatial oscillation was

prevented in the first 200 cells, then the rest of the wavelength changes were monotonic. The simulations show that it may not be necessary for the phase to change in entire tissue mass, a change in even smaller areas may alter spatial dynamics of repolarization.

The incidence of alternans (and out of phase) observed in the current study was much higher in canines compared to that in swines. Although several known (and unknown) differences in ionic currents could be the cause of the different incidence between these two species, we consider that differences in I_{to} is a likely candidate. Previous studies (Li et al., 2003) have shown that both I_{to1} and I_{to2} are present in CVM (Tseng and Hoffman, 1989) while only I_{to2} is present in swine. As I_{to} current plays an important role in phase 1 repolarization and generation of APD alternans, less expression of I_{to} current in swine provides a possible explanation of the less frequent alternans observed in this species.

In conclusion, our study shows that in two species widely used to study alternans and related phenomenon, swine and canines, APD alternans are frequently accompanied by alternans of $|dv/dt|_{max}$, and although mostly in phase with each other, they can spontaneously become out of phase in both species. Out of phase relationship can amplify amplitude of APD alternans; however, it also stabilizes concordant alternans and prevents the transition from concord to discord. We consider that absence of spatial discord is suggestive of a less arrhythmic substrate and therefore out of phase relationship may have a stabilizing effect on conduction of impulses.

LIMITATIONS

Ventricular myocytes are known to have different ion channel expression in different regions of the heart. Our observations are limited to the alternans in the endocardial region of the right ventricles. The phase change that we imposed in our simulation was phenomenological, because our primary aim was to determine the potential effects of phase change on conduction and not what causes the phase change per se. Although anomalous recovery of I_{Na} is the likely cause of out of phase behavior, the mechanisms behind what causes this anomaly and importantly, what causes the spontaneous phase change remain unclear.

ACKNOWLEDGMENTS

REFERENCES

- Banville I., Chattipakorn N., and Gray R.A. (2004). Restitution dynamics during pacing and arrhythmias in isolated pig hearts. J. Cardiovasc. Electrophysiol. 15, 455–463.
- de Diego, C., Pai R.K., Dave A.S., Lynch A., Thu M., Chen, F., Xie L.H., Weiss J.N., and Valderrabano M. (2008). Spatially discordant alternans in cardiomyocyte monolayers. Am. J. Physiol. Heart Circ. Physiol. 294, H1417–H1425.
- de Lange E., and Kucera J.P. (2010). Alternans resonance and propagation block during supernormal conduction in cardiac tissue with decreased [K(+)](o). Biophys. J. 98, 1129–1138.
- Echebarria B., and Karma A. (2002). Instability and spatiotemporal dynamics of alternans in paced cardiac tissue. Phys. Rev. Lett. 88,208101.

- Echebarria B., and Karma A. (2007). Amplitude equation approach to spatiotemporal dynamics of cardiac alternans. Phys. Rev. E Stat. Nonlin. Soft Matter Phys. 76, 51911.

- Echebarria B., RoderG., Engel H., Davidsen J., and Bar M. (2011). Supernormal conduction in cardiac tissue promotes concordant alternans and action potential bunching. Phys. Rev. E Stat. Nonlin. Soft Matter Phys. 83, 040902.

- Fast V.G., Darrow B.J., SaffitzJ.E., and Kleber A.G. (1996). Anisotropic activation spread in heart cell monolayers assessed by high-resolution optical mapping. Role of tissue discontinuities. *Circ. Res.* 79, 115–127.

- Fox J.J., McHarg J.L., and Gilmour R.F .Jr. (2002). Ionic mechanism of electrical alternans. *Am. J. Physiol. Heart Circ. Physiol.* 282, H516–H530.

- Gordon D., Kadish A.H., Koolish D., Taneja T., Ulphani J., Goldberger J.J., and Ng J. (2010). High-resolution electrical mapping of depolarization and repolarization alternans in an ischemic dog model. *Am. J. Physiol. Heart Circ. Physiol.* 298, H352–H359.

- Hua F., and Gilmour R.F. Jr. (2004). Contribution of I_{Kr} to rate-dependent action potential dynamics in canine endocardium. *Circ. Res.* 94, 810–819.

- Huang J., Cheng K.A., Dosdall D.J., Smith W.M., and Ideker R.E. (2007). Role of maximum rate of depolarization in predicting action potential duration during ventricular fibrillation. *Am. J. Physiol. Heart Circ. Physiol.* 293, H2530–H2536.

- Huang J., Zhou X., Smith W.M., and Ideker R.E. (2004). Restitution properties during ventricular fibrillation in the in situ swine heart. *Circulation* 110, 3161–3167.

- Jing L., Chourasia S., and Patwardhan A. (2010). Heterogeneous memory in restitution of action potential duration in pig ventricles. *J. Electro-cardiol.* 43, 425–432.

- Karagueuzian H.S., Khan S.S., Hong K., Kobayashi Y., Denton T., Mandel W.J., and Diamond G.A. (1993). Action-potential alternans and irregular

dynamics in quinidine-intoxicated ventricular muscle-cells: implications for ventricular proarrhythmia. *Circulation* 87, 1661–1672.

- Kleber A.G. (2005). The shape of the electrical action-potential upstroke: a new aspect from optical measurements on the surface of the heart. *Circ.Res.* 97, 204–206.

- Koller M.L., Riccio M.L., and Gilmour R.F .Jr. (1998). Dynamic restitution of action potential duration during electrical alternans and ventricular fibrillation. *Am. J. Physiol.* 275, H1635–H1642.

- Lalani G.G., Bayer J., Trayanova N.A., and Narayan S.M. (2008). Action potential dynamics explain arrhythmic susceptibility in systolic heart failure. *J. Card. Fail.* 14, S8.

- Li G.R., Du X.L., Siow Y.L., O K., Tse H.F., and Lau C.P. (2003). Calcium-activated transient outward chloride current and phase1 repolarization of swine ventricular action potential. *Cardiovasc. Res.* 58, 89–98.

- Mironov S., Jalife J., and Tolkacheva E.G. (2008). Role of conduction velocity restitution and short-term memory in the development of action potential duration alternans in isolated rabbit hearts. *Circulation* 118, 17–25.

- Omichi C., Lee M.H., Ohara T., Naik A.M., Wang N.C., Karagueuzian H.S., and Chen P.S. (2000). Comparing cardiac action potentials recorded with metal and glass microelectrodes. *Am. J. Physiol. Heart Circ. Physiol.* 279, H3113–H3117.

- Omichi C., Zhou S., Lee M.H., Naik A., Chang C.M., Garfinkel A., Weiss J.N., Lin S.F., Karagueuzian H.S., and Chen P.S. (2002). Effects of amiodarone on wavefront dynamics during ventricular fibrillation in isolated swine right ventricle. *Am. J. Physiol. Heart Circ. Physiol.* 282, H1063–H1070.

- Pruvot E.J., Katra R.P., Rosenbaum D.S., and Laurita K.R. (2004). Role of calcium cycling versus restitution in the mechanism of repolarization alternans. *Circ. Res.* 94, 1083–1090.

- Qu Z., Garfinkel A., Chen P.S., and Weiss J.N. (2000). Mechanisms of discordant alternans and induction of reentry in simulated cardiac tissue. *Circulation* 102, 1664–1670.

- Rubart M., Lopshire J.C., Fineberg N.S., and Zipes D.P. (2000). Changes in left ventricular repolarization and ion channel currents following a transient rate increase superimposed on bradycardia in anesthetized dogs. *J. Cardiovasc. Electro-physiol.* 11, 652–664.

- Spach M.S., Heidlage J.F., Dolber P.C., and Barr R.C. (1998). Extracellular discontinuities in cardiac muscle: evidence for capillary effects on the action potential foot. *Circ. Res.* 83, 1144–1164.

- Tseng G.N., and Hoffman B.F. (1989). Two components of transient outward current in canine ventricular myocytes. *Circ. Res.* 64, 633–647.

- Weiss J.N., Chen P.S., Qu Z., Karagueuzian H.S., and Garfinkel A. (2000). Ventricular fibrillation: how do we stop the waves from breaking? *Circ. Res.* 87, 1103–1107.

- Wu R.Z., and Patwardhan A. (2006). Mechanism of repolarization alternans has restitution of action potential duration dependent and independent components. *J. Cardiovasc. Electrophysiol.* 17, 87–93.

REFERENCES

[1] A. Agarwal and A. Patwardhan, "A new approach to measure the contribution of restitution to repolarization alternans," *Conference proceedings : Annual International Conference of the IEEE Engineering in Medicine and Biology Society. IEEE Engineering in Medicine and Biology Society. Conference,* vol. 2009, pp. 4516-8, 2009.

[2] L. Jing, A. Agarwal, S. Chourasia, and A. Patwardhan, "Phase Relationship between Alternans of Early and Late Phases of Ventricular Action Potentials," *Frontiers in physiology,* vol. 3, p. 190, 2012.

[3] L. National Heart, and Blood Institute. *Arrhythmia.* Available: http://www.nhlbi.nih.gov/health/health-topics/topics/arr/

[4] C. f. D. C. a. Prevention. Available: http://www.cdc.gov/heartdisease/facts.htm

[5] C. f. D. C. a. Prevention, "Out-of-Hospital Cardiac Arrest Surveillance --- Cardiac Arrest Registry to Enhance Survival (CARES)," 2011.

[6] FARLEX. *THE FREE DICTIONARY.* Available: http://www.thefreedictionary.com/restitution

[7] Y. Yamanouchi, S. Jaalouk, A. A. Shehadeh, F. Jaeger, H. Goren, and F. M. Fouad-Tarazi, "Changes in left ventricular volume during head-up tilt in patients with vasovagal syncope: an echocardiographic study," *American heart journal,* vol. 131, pp. 73-80, Jan 1996.

[8] J. M. Cao, Z. Qu, Y. H. Kim, T. J. Wu, A. Garfinkel, J. N. Weiss, H. S. Karagueuzian, and P. S. Chen, "Spatiotemporal heterogeneity in the induction of ventricular fibrillation by rapid pacing: importance of cardiac restitution properties," *Circulation research,* vol. 84, pp. 1318-31, Jun 11 1999.

[9] R. F. Gilmour, Jr., "A novel approach to identifying antiarrhythmic drug targets," *Drug discovery today,* vol. 8, pp. 162-7, Feb 15 2003.

[10] Z. Qu, A. Garfinkel, P. S. Chen, and J. N. Weiss, "Mechanisms of discordant alternans and induction of reentry in simulated cardiac tissue," *Circulation,* vol. 102, pp. 1664-70, Oct 3 2000.

[11] Z. Qu, J. N. Weiss, and A. Garfinkel, "Cardiac electrical restitution properties and stability of reentrant spiral waves: a simulation study," *The American journal of physiology,* vol. 276, pp. H269-83, Jan 1999.

[12] M. Swissa, Z. Qu, T. Ohara, M. H. Lee, S. F. Lin, A. Garfinkel, H. S. Karagueuzian, J. N. Weiss, and P. S. Chen, "Action potential duration restitution and ventricular fibrillation due to rapid focal excitation," *American journal of physiology. Heart and circulatory physiology,* vol. 282, pp. H1915-23, May 2002.

[13] J. N. Weiss, A. Garfinkel, H. S. Karagueuzian, Z. Qu, and P. S. Chen, "Chaos and the transition to ventricular fibrillation: a new approach to antiarrhythmic drug evaluation," *Circulation,* vol. 99, pp. 2819-26, Jun 1 1999.

[14] T. J. Wu, S. F. Lin, J. N. Weiss, C. T. Ting, and P. S. Chen, "Two types of ventricular fibrillation in isolated rabbit hearts: importance of excitability and action potential duration restitution," *Circulation,* vol. 106, pp. 1859-66, Oct 1 2002.

[15] F. Xie, Z. Qu, A. Garfinkel, and J. N. Weiss, "Electrophysiological heterogeneity and stability of reentry in simulated cardiac tissue," *American journal of physiology. Heart and circulatory physiology,* vol. 280, pp. H535-45, Feb 2001.

[16] M. L. Koller, M. L. Riccio, and R. F. Gilmour, Jr., "Effects of [K(+)](o) on electrical restitution and activation dynamics during ventricular fibrillation," *American journal of physiology. Heart and circulatory physiology,* vol. 279, pp. H2665-72, Dec 2000.

[17] E. M. Cherry and F. H. Fenton, "Suppression of alternans and conduction blocks despite steep APD restitution: electrotonic, memory, and conduction velocity restitution effects," *American journal of physiology. Heart and circulatory physiology,* vol. 286, pp. H2332-41, Jun 2004.

[18] J. Huang, X. Zhou, W. M. Smith, and R. E. Ideker, "Restitution properties during ventricular fibrillation in the in situ swine heart," *Circulation,* vol. 110, pp. 3161-7, Nov 16 2004.

[19] R. Wu and A. Patwardhan, "Restitution of action potential duration during sequential changes in diastolic intervals shows multimodal behavior," *Circulation research,* vol. 94, pp. 634-41, Mar 19 2004.

[20] K. M. Guzman, L. Jing, and A. Patwardhan, "Effects of changes in the L-type calcium current on hysteresis in restitution of action potential duration," *Pacing and clinical electrophysiology : PACE,* vol. 33, pp. 451-9, Apr 2010.

[21] D. R. Chialvo, D. C. Michaels, and J. Jalife, "Supernormal excitability as a mechanism of chaotic dynamics of activation in cardiac Purkinje fibers," *Circulation research,* vol. 66, pp. 525-45, Feb 1990.

[22] H. V. Huikuri, A. Castellanos, and R. J. Myerburg, "Medical progress: Sudden death due to cardiac arrhythmias," *New England Journal of Medicine,* vol. 345, pp. 1473-1482, Nov 15 2001.

[23] H. J. J. Wellens, A. P. Gorgels, and H. de Munter, "Cardiac arrest outside of a hospital - How can we improve results of resuscitation?," *Circulation,* vol. 107, pp. 1948-1950, Apr 22 2003.

[24] A. K. Gehi, R. H. Stein, L. D. Metz, and J. A. Gomes, "Microvolt T-wave alternans for the risk stratification of ventricular tachyarrhythmic events: a meta-analysis," *Journal of the American College of Cardiology,* vol. 46, pp. 75-82, Jul 5 2005.

[25] A. A. Armoundas, S. H. Hohnloser, T. Ikeda, and R. J. Cohen, "Can microvolt T-wave alternans testing reduce unnecessary defibrillator implantation?," *Nature Clinical Practice Cardiovascular Medicine,* vol. 2, pp. 522-528, Oct 2005.

[26] D. B. Mark, K. J. Anstrom, J. L. Sun, N. E. Clapp-Channing, A. A. Tsiatis, L. Davidson-Ray, K. L. Lee, G. H. Bardy, and S. C. D. H. Failure, "Quality of life with defibrillator therapy or amiodarone in heart failure," *New England Journal of Medicine,* vol. 359, pp. 999-1008, Sep 4 2008.

[27] L. A. Prudente, "Phantom shock in a patient with an implantable cardioverter defibrillator: Case report," *American Journal of Critical Care,* vol. 12, pp. 144-146, Mar 2003.

[28] J. B. van Rees, C. J. Borleffs, M. K. de Bie, T. Stijnen, L. van Erven, J. J. Bax, and M. J. Schalij, "Inappropriate implantable cardioverter-defibrillator shocks: incidence, predictors, and impact on mortality," *Journal of the American College of Cardiology,* vol. 57, pp. 556-62, Feb 1 2011.

[29] R. Wu and A. Patwardhan, "Mechanism of repolarization alternans has restitution of action potential duration dependent and independent components," *Journal of cardiovascular electrophysiology,* vol. 17, pp. 87-93, Jan 2006.

[30] S. S. Kalb, H. M. Dobrovolny, E. G. Tolkacheva, S. F. Idriss, W. Krassowska, and D. J. Gauthier, "The restitution portrait: a new method for investigating rate-dependent restitution," *Journal of cardiovascular electrophysiology,* vol. 15, pp. 698-709, Jun 2004.

[31] A. Patwardhan and S. Moghe, "Novel feedback based stimulation protocol shows hysteresis in cardiac action potential duration restitution," *Biomedical sciences instrumentation,* vol. 37, pp. 505-10, 2001.

[32] R. Wu and A. Patwardhan, "Effects of rapid and slow potassium repolarization currents and calcium dynamics on hysteresis in restitution of action potential duration," *Journal of electrocardiology,* vol. 40, pp. 188-99, Apr 2007.

[33] J. P. Piccini, D. J. Whellan, B. R. Berridge, J. K. Finkle, S. D. Pettit, N. Stockbridge, J. P. Valentin, H. M. Vargas, and M. W. Krucoff, "Current challenges in the evaluation of cardiac safety during drug development: translational medicine meets the Critical Path Initiative," *American heart journal,* vol. 158, pp. 317-26, Sep 2009.

[34] A. J. Moss, P. J. Schwartz, R. S. Crampton, D. Tzivoni, E. H. Locati, J. MacCluer, W. J. Hall, L. Weitkamp, G. M. Vincent, A. Garson, Jr., and et al., "The long QT syndrome. Prospective longitudinal study of 328 families," *Circulation,* vol. 84, pp. 1136-44, Sep 1991.

[35] A. C. Guyton, A. W. Lindsey, and B. N. Kaufmann, "Effect of mean circulatory filling pressure and other peripheral circulatory factors on

cardiac output," *The American journal of physiology,* vol. 180, pp. 463-8, Mar 1955.

[36] S. Steen, Q. M. Liao, L. Pierre, A. Paskevicius, and T. Sjoberg, "The critical importance of minimal delay between chest compressions and subsequent defibrillation: a haemodynamic explanation," *Resuscitation,* vol. 58, pp. 249-258, Sep 2003.

[37] R. A. Berg, V. L. Sorrell, K. B. Kern, R. W. Hilwig, M. I. Altbach, M. M. Hayes, K. A. Bates, and G. A. Ewy, "Magnetic resonance imaging during untreated ventricular fibrillation reveals prompt right ventricular overdistention without left ventricular volume loss," *Circulation,* vol. 111, pp. 1136-40, Mar 8 2005.

[38] D. Engelstein and C. Servadio, "Treatment options for localized cancer of the prostate," *Israel journal of medical sciences,* vol. 31, pp. 133-6, Feb-Mar 1995.

[39] M. H. Raitt, G. Johnson, G. L. Dolack, J. E. Poole, P. J. Kudenchuk, and G. H. Bardy, "Clinical predictors of the defibrillation threshold with the unipolar implantable defibrillation system," *Journal of the American College of Cardiology,* vol. 25, pp. 1576-83, Jun 1995.

[40] P. Ott and M. J. Reiter, "Effect of ventricular dilatation on defibrillation threshold in the isolated perfused rabbit heart," *Journal of cardiovascular electrophysiology,* vol. 8, pp. 1013-9, Sep 1997.

[41] A. G. Vigh, J. Lowder, and H. J. Deantonio, "Does acute volume overloading in the setting of left ventricular dysfunction and pulmonary hypertension affect the defibrillation threshold?," *Pace-Pacing and Clinical Electrophysiology,* vol. 22, pp. 759-764, May 1999.

[42] S. F. Idriss, M. P. Anstadt, G. L. Anstadt, and R. E. Ideker, "The Effect of Cardiac Compression on Defibrillation Efficacy and the Upper Limit of Vulnerability," *Journal of cardiovascular electrophysiology,* vol. 6, pp. 368-378, May 1995.

[43] J. S. Strobel, G. N. Kay, G. P. Walcott, W. M. Smith, and R. E. Ideker, "Defibrillation efficacy with endocardial electrodes is influenced by

reductions in cardiac preload," *Journal of interventional cardiac electrophysiology : an international journal of arrhythmias and pacing,* vol. 1, pp. 95-102, Sep 1997.

[44]   N. Trayanova, W. Li, J. Eason, and P. Kohl, "Effect of stretch-activated channels on defibrillation efficacy," *Heart rhythm : the official journal of the Heart Rhythm Society,* vol. 1, pp. 67-77, May 2004.

[45]   M. R. Franz, "Mechano-electrical feedback," *Cardiovascular research,* vol. 45, pp. 263-6, Jan 14 2000.

[46]   W. Li, V. Gurev, A. D. McCulloch, and N. A. Trayanova, "The role of mechanoelectric feedback in vulnerability to electric shock," *Progress in biophysics and molecular biology,* vol. 97, pp. 461-78, Jun-Jul 2008.

[47]   M. J. Lab, "Contraction-excitation feedback in myocardium. Physiological basis and clinical relevance," *Circulation research,* vol. 50, pp. 757-66, Jun 1982.

[48]   M. Zabel, S. Portnoy, and M. R. Franz, "Effect of sustained load on dispersion of ventricular repolarization and conduction time in the isolated intact rabbit heart," *Journal of cardiovascular electrophysiology,* vol. 7, pp. 9-16, Jan 1996.

[49]   D. Sung, R. W. Mills, J. Schettler, S. M. Narayan, J. H. Omens, and A. D. McCulloch, "Ventricular filling slows epicardial conduction and increases action potential duration in an optical mapping study of the isolated rabbit heart," *Journal of cardiovascular electrophysiology,* vol. 14, pp. 739-49, Jul 2003.

[50]   G. Dominguez and H. A. Fozzard, "Effect of Stretch on Conduction-Velocity and Cable Properties of Cardiac Purkinje-Fibers," *American Journal of Physiology,* vol. 237, pp. C119-C124, 1979.

[51]   M. J. Reiter, M. Landers, Z. Zetelaki, C. J. Kirchhof, and M. A. Allessie, "Electrophysiological effects of acute dilatation in the isolated rabbit heart: cycle length-dependent effects on ventricular refractoriness and conduction velocity," *Circulation,* vol. 96, pp. 4050-6, Dec 2 1997.

[52] Z. J. Penefsky and B. F. Hoffman, "Effects of Stretch on Mechanical and Electrical Properties of Cardiac Muscle," *American Journal of Physiology,* vol. 204, pp. 433-&, 1963.

[53] I. Banville and R. A. Gray, "Effect of action potential duration and conduction velocity restitution and their spatial dispersion on alternans and the stability of arrhythmias," *Journal of cardiovascular electrophysiology,* vol. 13, pp. 1141-9, Nov 2002.

[54] F. Extramiana and C. Antzelevitch, "Amplified transmural dispersion of repolarization as the basis for arrhythmogenesis in a canine ventricular-wedge model of short-QT syndrome," *Circulation,* vol. 110, pp. 3661-6, Dec 14 2004.

[55] L. Jing, S. Chourasia, and A. Patwardhan, "Heterogeneous memory in restitution of action potential duration in pig ventricles," *Journal of electrocardiology,* vol. 43, pp. 425-32, Sep-Oct 2010.

[56] F. Guharay and F. Sachs, "Stretch-activated single ion channel currents in tissue-cultured embryonic chick skeletal muscle," *The Journal of physiology,* vol. 352, pp. 685-701, Jul 1984.

[57] J. Sadoshima, L. Jahn, T. Takahashi, T. J. Kulik, and S. Izumo, "Molecular characterization of the stretch-induced adaptation of cultured cardiac cells. An in vitro model of load-induced cardiac hypertrophy," *The Journal of biological chemistry,* vol. 267, pp. 10551-60, May 25 1992.

[58] J. Sadoshima, T. Takahashi, L. Jahn, and S. Izumo, "Roles of mechano-sensitive ion channels, cytoskeleton, and contractile activity in stretch-induced immediate-early gene expression and hypertrophy of cardiac myocytes," *Proceedings of the National Academy of Sciences of the United States of America,* vol. 89, pp. 9905-9, Oct 15 1992.

[59] A. Elvan, A. Adiyaman, R. J. Beukema, H. T. Sie, and M. A. Allessie, "Electrophysiological effects of acute atrial stretch on persistent atrial fibrillation in patients undergoing open heart surgery," *Heart rhythm : the official journal of the Heart Rhythm Society,* vol. 10, pp. 322-30, Mar 2013.

[60] M. R. Franz, D. Burkhoff, D. T. Yue, and K. Sagawa, "Mechanically induced action potential changes and arrhythmia in isolated and in situ canine hearts," *Cardiovascular research,* vol. 23, pp. 213-23, Mar 1989.

[61] P. Meghji, S. A. Nazir, D. J. Dick, M. E. S. Bailey, K. J. Johnson, and M. J. Lab, "Regional workload induced changes in electrophysiology and immediate early gene expression in intact in situ porcine heart," *Journal of Molecular and Cellular Cardiology,* vol. 29, pp. 3147-3155, Nov 1997.

[62] M. J. Lab, "Mechanically dependent changes in action potentials recorded from the intact frog ventricle," *Circulation research,* vol. 42, pp. 519-28, Apr 1978.

[63] M. L. Koller, M. L. Riccio, and R. F. Gilmour, Jr., "Dynamic restitution of action potential duration during electrical alternans and ventricular fibrillation," *The American journal of physiology,* vol. 275, pp. H1635-42, Nov 1998.

[64] E. J. Pruvot, R. P. Katra, D. S. Rosenbaum, and K. R. Laurita, "Role of calcium cycling versus restitution in the mechanism of repolarization alternans," *Circulation research,* vol. 94, pp. 1083-90, Apr 30 2004.

[65] M. Kowalski, T. Kukulski, F. Jamal, J. D'Hooge, F. Weidemann, F. Rademakers, B. Bijnens, L. Hatle, and G. R. Sutherland, "Can natural strain and strain rate quantify regional myocardial deformation? A study in healthy subjects," *Ultrasound in Medicine and Biology,* vol. 27, pp. 1087-1097, Aug 2001.

[66] C. Soeller and M. B. Cannell, "Examination of the transverse tubular system in living cardiac rat myocytes by 2-photon microscopy and digital image-processing techniques," *Circulation research,* vol. 84, pp. 266-75, Feb 19 1999.

[67] A. F. Dulhunty and C. Franzini-Armstrong, "The relative contributions of the folds and caveolae to the surface membrane of frog skeletal muscle fibres at different sarcomere lengths," *The Journal of physiology,* vol. 250, pp. 513-39, Sep 1975.

[68] M.-L. Ward and D. G. Allen, "Stretch-Activated Channels in the Heart: Contribution to Cardiac performance," in *Mechanosensitivity of the heart*, A. Kamkin and I. Kiseleva, Eds., ed: Springer, 2010, pp. 141-168.

[69] T. Zeng, G. C. Bett, and F. Sachs, "Stretch-activated whole cell currents in adult rat cardiac myocytes," *American journal of physiology. Heart and circulatory physiology,* vol. 278, pp. H548-57, Feb 2000.

[70] C. F. Murphy, M. J. Lab, S. M. Horner, D. J. Dick, and F. G. Harrison, "Regional electromechanical alternans in anesthetized pig hearts: modulation by mechanoelectric feedback," *The American journal of physiology,* vol. 267, pp. H1726-35, Nov 1994.

[71] I. Banville, N. Chattipakorn, and R. A. Gray, "Restitution dynamics during pacing and arrhythmias in isolated pig hearts," *Journal of cardiovascular electrophysiology,* vol. 15, pp. 455-63, Apr 2004.

[72] J. J. Fox, E. Bodenschatz, and R. F. Gilmour, Jr., "Period-doubling instability and memory in cardiac tissue," *Physical review letters,* vol. 89, p. 138101, Sep 23 2002.

[73] R. Carrick, L. Ge, L. C. Lee, Z. Zhang, R. Mishra, L. Axel, J. M. Guccione, E. A. Grossi, and M. B. Ratcliffe, "Patient-specific finite element-based analysis of ventricular myofiber stress after Coapsys: importance of residual stress," *The Annals of thoracic surgery,* vol. 93, pp. 1964-71, Jun 2012.

[74] Z. Zhang, K. Sun, D. A. Saloner, A. W. Wallace, L. Ge, A. J. Baker, J. M. Guccione, and M. B. Ratcliffe, "The benefit of enhanced contractility in the infarct borderzone: a virtual experiment," *Frontiers in physiology,* vol. 3, p. 86, 2012.

[75] H. G. Pouleur, M. A. Konstam, J. E. Udelson, and M. F. Rousseau, "Changes in ventricular volume, wall thickness and wall stress during progression of left ventricular dysfunction. The SOLVD Investigators," *Journal of the American College of Cardiology,* vol. 22, pp. 43A-48A, Oct 1993.

VITA

Author's Name: Anuj Agarwal

Birthplace: Indore, India

Education:

B.E. in Biomedical Engineering, R.G.P.V. University, India   June 2006

Publications:

1. Linyuan Jing*, Anuj Agarwal*, Sonam Chourasia, Abhijit Patwardhan. Phase relationship between alternans of early and late phases of ventricular action potentials. *Frontiers in Physiology. 3:190, 2012*
   * Both authors contributed equally to this work

2. Anuj Agarwal, Linyuan Jing, Abhijit Patwardhan. Effect of rapid delayed rectifier current on hysteresis in restitution of action potential duration in swine. Conference Proceedings of the International Conference of IEEE Engineering in Medicine and Biology Society. *2012:673-6*

3. Anuj Agarwal, Abhijit Patwardhan. A new approach to measure the contribution of restitution to repolarization alternans. Conference Proceedings of the International Conference of IEEE Engineering in Medicine and Biology Society. 2009:4516-8

4. Anuj Agarwal, Abhijit Patwardhan. Role of restitution in mechanism of electrical instability in the heart. *24th Southern Biomedical Engineering Conference, 2008, Texas*

5. Ye Chen-Izu, Ling Chen, Tamás Bányász, Stacey L. McCulle, Byron Norton, Steven M. Scharf, Anuj Agarwal, Abhijit Patwardhan, Leighton T. Izu, and C. William Balke. Hypertension-induced remodeling of cardiac excitation-contraction coupling in ventricular myocytes occurs prior to hypertrophy development. *AJP- Heart and Circulatory Physiology 293: H3301-H3310, 2007*